An Analysis of Incomplete Contacts in Partial Slip



Thesis submitted to the Department of Engineering Science of the University of Oxford in partial fulfilment of the requirements for the degree of Doctor of Philosophy

Rangarajan Ramesh

St Hugh's College

An Analysis of Incomplete Contacts in Partial Slip

Rangarajan Ramesh, St Hugh's College

Doctor of Philosophy in Engineering Science

Trinity Term 2018

Abstract

Fretting fatigue is often the cause of failure in many engineering components. It is of importance in safety critical components subject to extreme loads such as in dovetail joints in jet engines. In order to accurately estimate the life of these components, accurate knowledge of the shear traction and differential strains at the contact interface is required. The loading that these components are subjected to is often complicated (varying normal load, bulk tension and shear force) and needs to be simplified, to ignore the variation in either the bulk tension or the normal load.

The aim of this thesis is to develop a method which estimates the extent and magnitude of slip in incomplete contact problems where the normal load, shear force and bulk tension vary with time.

Three new methods are first presented to solve incomplete contact problems in partial slip. One of these methods - using a dislocation correction to the fully stuck solution - is used to study problems where the normal load is held constant. Then, the problem of a varying normal load and bulk tension is studied in detail using the existing method of a traction correction to the sliding solution. Finally, the distributed dislocation method is used to solve the most general problem involving an incomplete problem with a varying normal load, bulk tension and shear force.

Acknowledgments

I would like to thank my supervisor Professor David Hills for his guidance. I would also like to thank Professor James Barber for his help on numerous technical problems and for hosting me in Ann Arbor in the summer of 2016. Finally, I would like to thank Dr Matthew Moore for his help with the integral inversion in Chapter 3.

Preface

This thesis is a collection of research performed by the author in the Department of Engineering Science at the University of Oxford under the supervision of Professor David Hills. This work is original and no part of it has been submitted for a degree at this university or elsewhere. Some of the work described in this thesis has been published in the following papers:

1. D. A Hills, **R. Ramesh** and J. R. Barber, Half-plane partial slip contact problems with a varying normal load in partial slip, In preparation.

2. D. A Hills, **R. Ramesh**, J. R. Barber and M. R. Moore, Methods to solve half-plane partial slip contact problems, International Journal of Solids and Structures, Accepted, 2018.

3. M. R. Moore, **R. Ramesh**, D. A. Hills and J. R. Barber, Half-plane partial slip contact problems with a constant normal load subject to a shear force and differential bulk tension, Journal of the Mechanics and Physics of Solids, 118: 245 - 253, 2018.

4. Z. Clark, **R. Ramesh** and D. A. Hills, Edge slip zone size of misaligned common edge contacts, Journal of Strain Analysis for Engineering Design, 52(7): 450 - 454, 2017.

5. **R. Ramesh**, J. R. Barber and D. A. Hills, Plane incomplete contact problems subject to bulk stress with a varying normal load, International Journal of Mechanical Sciences, 122: 228 - 234, 2017.

6. R. M. N. Fleury, D. A. Hills, **R. Ramesh** and J. R. Barber, Incomplete contacts in

partial slip subject to varying normal and shear loading, and their representation by asymptotes, Journal of the Mechanics and Physics of Solids, 99: 178 - 191, 2017.

7. D. A. Hills, **R. Ramesh**, R. M. N. Fleury and K. Parel, A unified approach fore representing fretting and damage at the edges of incomplete and receding contacts, Tribology International, 108: 16 - 22, 2017.

8. **R. Ramesh** and D. A. Hills, Sharp notch roots subject to in-plane and anti-plane loading: An alternative normalisation of the eigenfields & their application to example problems, Theoretical and Applied Fracture Mechanics, 86: 301 - 308, 2016.

Some of the work described in this thesis has been presented at conferences:

1. **R. Ramesh** and D. A. Hills, Half-plane elastic contact problems in partial slip with a varying normal load, Society of Engineering Science, Boston 2017.

2. **R. Ramesh** and D. A. Hills, An asymptotic solution to the incomplete contact problem in partial slip, TriboUK, London 2017.

3. **R. Ramesh** and D. A. Hills, Characteristics of the process zone at sharp notch roots subject to in-plane and anti-plane loading, International Conference on Multiaxial Fatigue & Fracture, Seville 2016.

Contents

1 Introduction **10**

1.1 Motivation 10

1.2 Contact mechanics 12

1.3 Types of contact 14

1.4 Half-plane theory 21

1.5 Assumptions 24

1.6 Summary of research chapters 27

2 Methods for solving incomplete contact problems in partial slip **29**

2.1 Introduction 29

2.2 Traction correction to the sliding solution (1) 32

2.3 Dislocation correction to the fully stuck solution (4) 34

2.4 Traction correction to the fully stuck solution (2) 37

2.5 Dislocation correction to the sliding solution (3) 38

2.6 Summary 39

3 Constant normal load **40**

3.1 Introduction 40

3.2 Mathematical framework 41

3.3 Constant normal load 42

3.4 Application to a Hertzian contact 45

3.5 Problems without closed form results 47

3.6 Asymptotic approximation 48

3.7 Summary 51

4 Varying normal load and bulk tension 53

4.1 Introduction 53

4.2 Condition for full stick 54

4.3 General loading solution procedure 54

4.4 Specialisation to a Hertzian contact 56

4.5 Periodic loading 59

4.6 Transient cycle 61

4.7 The second cycle 65

4.8 The permanent stick zone 67

4.9 Example 67

4.10 Summary 68

5 Varying normal load with a shear force and bulk tension 70

5.1 Introduction 70

5.2 Normal load and shear force 71

5.3 General loading loop 78

5.4 Example problem 83

5.5 Numerical challenges 86

5.6 Summary 87

6 Conclusions 88

6.1 Methods to solve incomplete contact problems in partial slip 88

6.2 Varying normal load and bulk tension 89

6.3 Varying normal load, bulk tension and shear force 89

7 Further work 91

Bibliography 93

A An alternative normalisation of sharp notch roots **102**

A.1 Introduction 102

A.2 Formulation 103

A.3 Mode I and III loading 107

A.4 Mode II and III loading 109

A.5 General loading 112

A.6 Finite example problems 114

A.7 Summary 120

B Analytical inversion of singular integral equations **121**

C Dislocations between partially bonded half-planes **123**

C.1 Bounded distribution of dislocations 124

D Side condition - bulk tension **125**

E Incomplete contact problems with a constant normal load **126**

E.1 Inversion of the integral equation 126

E.2 Integral evaluation for fully a fully stuck contact with a constant normal load 128

F Elliptic integrals **130**

G Williams' eigenvectors & mode III **131**

Notation

a	Contact half-width
b	Stick zone half-width
b_1	Stick zone size of the right edge of the contact
b_2	Stick zone size of the left edge of the contact
b_x	Displacement vector
$B_x(x)$	Dislocation density
c	Depth of notch
d	Length of the slip zone
D	Diameter of cylinder
d_0	Characteristic length scale in sharp notches
E	Young's modulus
E^*	$\frac{E}{2(1-\nu^2)}$
f	Coefficient of friction
f_{ij}^k	Mode k Williams' eigenvector
G_0	Magnitude of loading in a sharp notch
h_0	Profile of the contacting body
J_2	Second deviatoric stress invariant
k	Yield stress in pure shear
K_k	Mode k stress intensity factor
K_N	Generalised normal stress intensity factor
K_T	Generalised shear stress intensity factor
L	Length of cylinder
M	Moment load
$p(x)$	Normal traction at the contact interface
p_0	Peak contact pressure
P	Normal force per unit depth
$q(x)$	Shear traction at the contact interface

$q_c(x)$	Corrective shear traction at the contact interface
$q_{c1}(x)$	First of two corrections to the shear traction at the contact interface
$q_{c2}(x)$	Second of two corrections to the shear traction at the contact interface
$q_S(x)$	Shear traction in the stick zone
$q_{sl}(x)$	Sliding shear traction at the contact interface
$q_{st}(x)$	Fully stuck shear traction at the contact interface
r	Polar length co-ordinate
r_p	Plastic radius
R	Relative radius of curvature of cylinders
T	Torque load
u	Displacement in the x-direction
x	Tangential co-ordinate
z	Tangential co-ordinate from the edge of the contact
α	Half-angle of a semi-infinite wedge
β	Dundurs' constant
ϵ	Strain
θ	Polar angle co-ordinate
κ	$3 - 4\nu$
λ_k	Mode k Williams' eigenvalue
μ	Modulus of rigidity
ν	Poisson's ratio
ϕ	Angle between the interface and surface normal
σ	Differential bulk tension
σ_0	Stress due to an axial load
τ_T	Shear stress induced by a torque
τ_0	Shear stress induced by a shear force
ψ	Polar angle co-ordinate

1 Introduction

This thesis aims to develop a solution to incomplete contact problems in partial slip where the normal load, shear force and bulk tension vary with time. This chapter provides the motivation, the industrial context, a study of the background literature, and a detailed review of half-plane theory. Finally, it provides a summary of the subsequent research chapters.

1.1 Motivation

Incomplete contact problems - where an increase in normal load leads to an increase in contact size - are found in jet engines, gas turbines and many other engineering applications. When these contacts are subjected to service loads, they often enter a state called partial slip, when some particles in the contact interface move relative to the other body. These movements cause surface damage and the high stresses near the contact interface aid the nucleation of cracks which eventually leads to component failure.

1.1.1 Industrial context

There are only two ways of transferring forces into bodies: through body forces (gravitational, electromagnetic, etc.) and through contact with other bodies. Therefore, in most engineering mechanisms, a contact is unavoidable. Contacts act as stress concentrators, raising the stress state local to the contact interface (sometimes to a singular state). The raising of the stress state often means that failure begins at the contact interface. This means contacts are of great importance in industrial design.

Failure is of concern in the dovetail joints of fan blades in both jet engines and gas turbines [1]. Figure 1.1 shows the slot where the fan blades are inserted in the disk. Figure 1.2 shows a dovetail joint test specimen which has nucleated and propagated a crack from the contact interface. Understanding the state of stress and differential strain at the contact interface will lead to improved experimental design to estimate more accurately the life of these components.



Figure 1.1: Jet engine disk [2]



Figure 1.2: Dovetail joint - found in jet engines [1]

Currently a mix of the finite element method and other numerical procedures are used to find the shear traction. The contact algorithms (Lagrange, penalty etc.) used in commercial finite element packages are computationally intensive. Many of the important

details are found at the edges, where numerical methods give poor resolution due to the discontinuous nature of contacts.

The advantage of an analytical approach is that it allows general principles to be deduced without solving each individual problem. An example of a general principle is that the normal traction always falls to zero at the edge of an incomplete contact, which we cannot say from any number of numerical solutions. Analytical results also give a solution of much higher resolution compared to numerical methods, so there is no a loss of detail, especially at the edges. A third benefit of analytical methods is that they offer a check for numerical methods. When testing a new numerical scheme, first solving a known problem with it and comparing it with the analytical result helps validate the method.

Unfortunately, current analytical and semi-analytical methods have to simplify the loading cycles as they cannot handle a variation in the normal load, shear force and bulk tension with time. In this thesis, a new method is proposed which does not require any simplification of the loading cycle. This method gives a more accurate estimate of the shear traction and the extent of slip and therefore failure.

1.2 Contact mechanics

Contact mechanics is a broad field. In this thesis, the focus is on the effect of external loads on the contact interface, specifically slip. Slip leads to surface damage and eventual failure. When a contact is subject to tangential loads, there are three possible states the interface may be in:

1. None of the particles moves tangentially relative to the other body - the contact is fully stuck.

2. All of the particles move relative to the other body - the contact is sliding.

3. Some of the particles move relative to the other body - the contact is in partial slip.

There are a number of different failure mechanisms. Wear is the gradual removal of material from the contact interface, which leads to failure [3]. Wear can be seen in many

instances, such as gear teeth and brake pads.

If the contact is in partial slip, the damage mechanism is called fretting fatigue. When particles move relative to the other body, the surface is damaged. This damage leads to the nucleation of cracks which grow until the component fails, such as in a dovetail joint. This is the failure mechanism of interest in this thesis.

1.2.1 Fretting fatigue

Fretting fatigue occurs when there is sustained small amplitude differential motion of two bodies in contact [4]. There are two distinct stages to failure by fretting fatigue: the first is the nucleation of a crack from a defect; the second is the propagation of the crack. The most likely region to nucleate a crack is at the contact interface, due to the surface damage caused by the relative movement of particles. An example of the surface damage and the subsequent crack nucleation is shown in Figure 1.3.

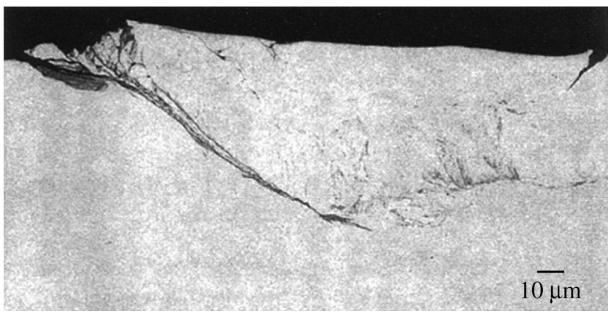


Figure 1.3: Scanning Electron Microscope image of fretting damage [5]

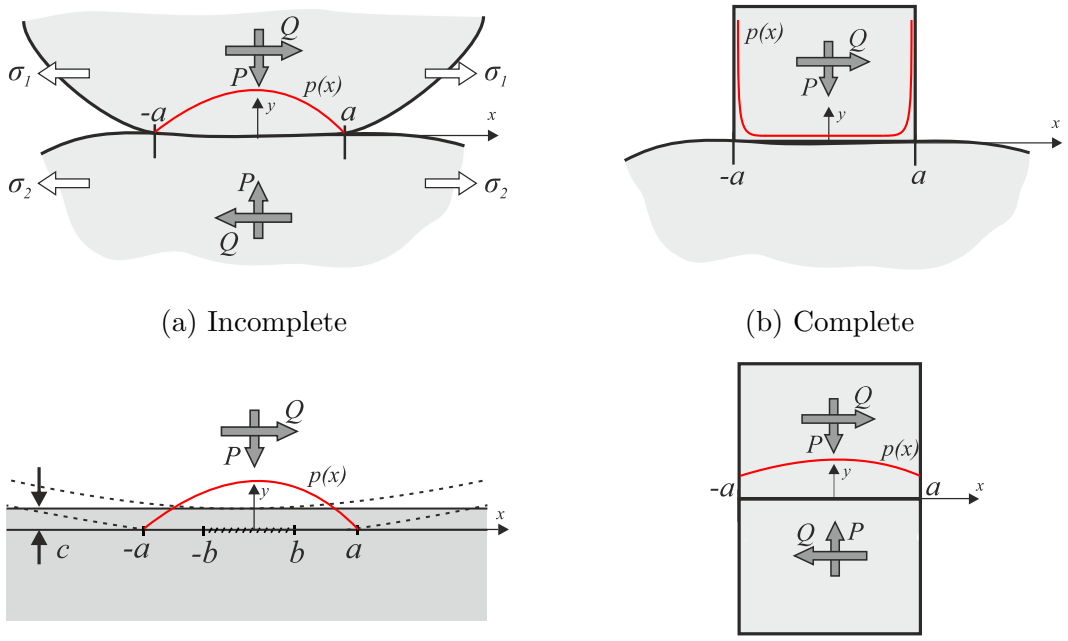
In safety critical components, the manufacturing process is designed to eliminate defects; the life of a component is determined by both the nucleation and propagation of a crack. Once the crack is initiated and developing, the contact stress field merely augments any other loading present, and standard methods of crack propagation (such as Paris' law [6]) may be applied. The challenge lies in estimating when and where nucleation occurs for a given contact geometry and loading.

Therefore, there is a great deal of interest in the crack nucleation phase [7]. It is investigated experimentally [8], with tests carried out for complete (with fixed contact size) and incomplete contacts [9]. A more mathematical approach taken by Hills et al. [10]

shows that the fatigue life has a good correlation with the peak energy dissipated over the contact interface. In order to find the peak energy dissipated, the shear traction and slip displacement over the contact interface is required. The methods required to find this varies depending on the type of contact.

1.3 Types of contact

In general, contacts may be categorised into one of four types (or some combination of them) as shown in Figure 1.4. While the focus of this thesis is on incomplete contacts, with Appendix A included on complete contacts, an introduction to the other types of contact is given here for completeness.



(a) Incomplete

(b) Complete

(c) Receding

(d) Common edge

Figure 1.4: Types of contact

1.3.1 Incomplete contacts

In incomplete contact problems, the higher the normal load, P, the bigger the contact patch. Incomplete contacts may be subdivided into conformal and non-conformal contacts. A conformal contact is one where the two bodies have curvatures in the same direction

- an example is the outer contact formed by the bearing and ring in Figure 1.5. In this thesis, only non-conformal contacts are considered, with the consequence that each body may be represented as a half-plane (e.g., the inner contact in the roller bearing).

Incomplete contacts invariably display a contact pressure distribution which falls smoothly to zero at the contact edges. If the Dundurs [11] parameter $\beta = 0$ (a measure of the coupling between two materials), or the contact is lubricated so that no shear traction arises, the contact pressure falls to zero in a locally square root bounded manner. One of the main features of this class of problem is that the contact problem itself may be studied in isolation - there is no need to know what the geometry looks like remote from the contact. A railway wheel/rail solution is equivalent to that in, for example, a shallow groove ball bearing.



Figure 1.5: Roller bearing - example incomplete contact [12]

Figure 1.4a shows a schematic of an incomplete contact, exemplified by a Hertzian contact (in two dimensions - this is two cylinders of different radii). Hertz first solved this problem (for solids whose local curvature can be described by a general second order surface) in the 1880s by representing the bodies as half-planes. Hertz was able to find closed form solutions for the contact law (the relation between the applied load and contact size) and the contact pressure distribution. Reviews of this kind of problem (Deresiewicz [13]) reflected the steady development of the solution to include the effects of elastic mismatch (a study pioneered by Spence [14]) and contacts in partial slip (original article by Cattaneo [15]; further cases studied by Mindlin [16, 17]). Other convex bodies can, in principle, be treated in this way, including shallow wedges. The majority of solutions employ formulations

based on half-planes [17].

Figure 1.6 shows a schematic of a dovetail joint along with the applied loads. It may be modeled as an incomplete contact. It is obvious that there is geometric coupling, as the applied loads give rise to some combination of a normal load, shear force and bulk tension in local coordinates.

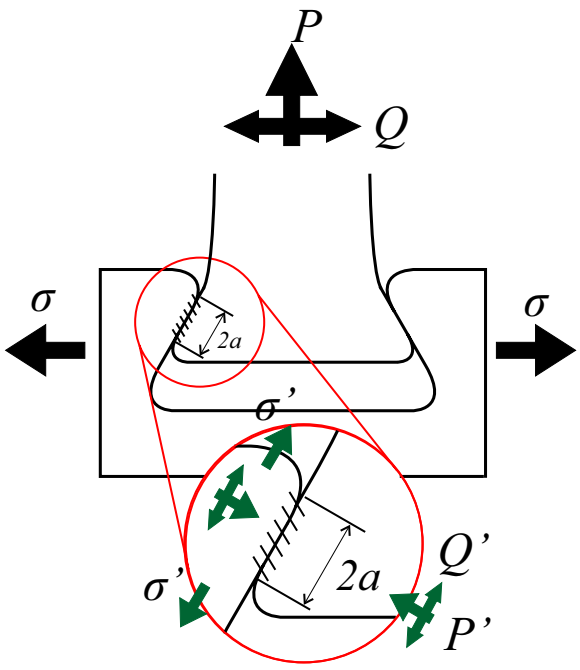


Figure 1.6: Schematic of a dovetail joint

In order to represent better these loads, there has been a drive to solve contact problems with mixed loading regimes. The biggest challenges have been with a varying normal load and most analytical solutions have been limited to Hertzian contacts.

An approximate way of solving these contact problems is to use an asymptotic solution at each edge [18, 19]. This allows more complex geometries and loading cases to be studied. Since each edge of the contact is considered in isolation, symmetry in the geometry is not required and the inclusion of a moment is allowed. However, this is an approximate method and comparisons with the exact solution (where possible) show that it is limited to cases where the slip zone is roughly 10% of the contact width [20].

1.3.2 Complete contacts

Figure 1.4b shows the simplest possible complete contact: an elastic square block, of side $2a$, pressed onto an elastically similar half-plane, by a normal load. This deceptively simple problem cannot be solved analytically - a numerical approach such as the finite element or boundary element method must be employed to determine the resulting contact pressure distribution. The presence of singularities at the edges of the contact in both the shear and normal traction causes difficulties for numerical procedures.

The edge can be studied closely by zooming into a single edge and modelling it as a sharp notch. This allows the Williams solution to be used to estimate the stress singularities. Appendix A shows a different way of expressing the stress state that shows which mode of loading is dominant.

Unlike incomplete contacts, a change in the normal load does not change the size of the contact. The contact size is determined wholly by the geometry, independent of the loading. In an incomplete contact, even if the contacting bodies have differing curvatures, provided only that they are elastically similar, surface particles tend to move laterally by the same amount. Therefore, no surface shearing traction arises with the application of a normal load. In contrast, with complete contacts, where the free surfaces forming the sides of the contact must be traction-free so only friction prevents material from moving sideways. This is referred to as coupling. Resistance is in the form of friction and this is controlled by the coefficient of friction, f. If the friction is insufficient, both corners tend to spread outwards in a manner referred to as 'leading edge'. Hills and Dini [21] showed that for a block with vertical edges, $f > 0.543$ is the condition to ensure there isn't a spread outwards.

There have been many studies carried out to better understand complete contacts. A complete contact subject to an oscillatory shear force was studied by Churchman and Hills [22, 23]. The contact in a state of partial slip and sliding was studied by Karupunan et al. [24, 25] using a mix of the finite element method and asymptotes. Flicek et al. [26] went on to study the transition from normal loading to sliding. Figure 1.7 shows how different the behaviour of the contact is if the coefficient of friction is above or below

0.543.

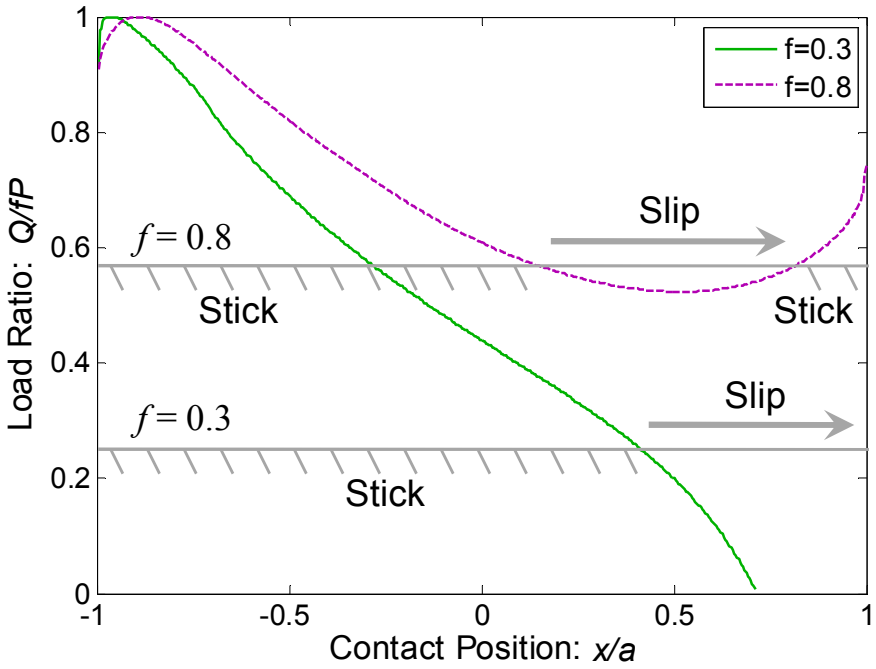


Figure 1.7: Evolution of contact behaviour for $f = 0.3, 0.8$

An application of complete contacts is studying spline joints found in jet engines. It is also useful for the analysis of rounded punches, which are common in engineering applications, as carried out by Fleury et al. [27, 28].

1.3.3 Receding contacts

Receding contacts, as a class, were identified and first analysed in the early 1970s. A typical problem is shown in Figure 1.4c where an elastic layer rests on an elastically similar half-plane.

An interesting feature of a layer resting on a half-plane is that, upon the application of an infinitesimal normal load (at a point), the layer lifts off, to leave a small contact length, which subsequently remains unchanged. The problem then becomes linear: the displacements (including the lift off angle) and state of stress are proportional to the applied load. Initial contributions to this class of problem include papers by Keer and Dundurs [30, 31]. The latter defined a receding contact as one which either remains a fixed length or becomes smaller as a greater load is applied [32]. A recent study looked



Figure 1.8: Flanged joint - example receding contact [29]

at the effect of a point load on the surface of a layer resting on an elastically similar half-plane [33], and the effects of cyclic loading [34].

Receding contacts are not merely a curiosity: they frequently arise in bolted joints of the 'high strength friction grip' variety often encountered in structural steel work. An example can be seen in the flanged joint shown in Figure 1.8. Civil engineering design codes do not take into account the way the connection functions, and more work is required to be able to understand the contact behaviour in the case of cyclic excitation (vibration).

There is still much to discover in contacts of this class and it would be very useful to know whether a particular contact will remain complete or will recede and become incomplete. There will always be fretting fatigue damage in the latter case but unlikely in the former. Recent investigations of receding contacts have used distributed dislocations [35]. The work by Hills et al.[1] [36] shows the similarities between incomplete and receding contacts. The methods in this thesis carry over the use of dislocations to incomplete contacts and show that they are more effective than the classical integral equation methods.

1.3.4 Common edge contacts

A contact can be formed by two components, of the same size, clamped together as shown in Figure 1.4d. The contact size is defined by both bodies. For example, two blocks of the same size may be fastened with a bolt through their middle. If the blocks are thin compared with their width, the contact edges will almost certainly separate and

the problem will fall into the receding category described above. However, if the blocks are thick they will remain in contact up to their edge. Whether slip begins at the edge or centre depends on the loading and coefficient of friction. An engineering example is that of a connecting rod as given in Figure 1.9.

General results are hard to find due to the geometry dependence of the solution in contacts of this class. One problem that has been studied is two semi-infinite strips of the same width pressed together and subject to shear [37]. The results show (in accordance with the standard methods of elementary beam theory) that the mid point slips first, and the edges are the last points to slip [37] . On the other hand, when two circular rods of equal radius are pressed end-to-end and subjected to a torque, the edge is the first point to slip. Ramesh and Hills[1] [38] explore the case when the rods are subject to both a torsion and shear force. They go on to look at instances where the interface is not perpendicular to the free surface and the effect this has on the first point of slip.



Figure 1.9: Connecting rod - example common edge contact [39]

To study in-plane forms of loading without being too specific about the geometry, a semi-infinite wedge is studied as shown in Figure 1.10. It is subjected to a normal load and shear force, with an interface line drawn normal to the wedge bisector. A moment is applied to ensure the line of action of the shear force is through the contact interface. The minimum coefficient of friction to inhibit edge slip is found when the interface line is not normal to the free surface. It is shown that edge slip is avoided provided that $f > \tan\phi$, where ϕ is the angle between the interface and the surface normal [40].

[1]The author of this thesis contributed to this article, but details are not included as it is not central

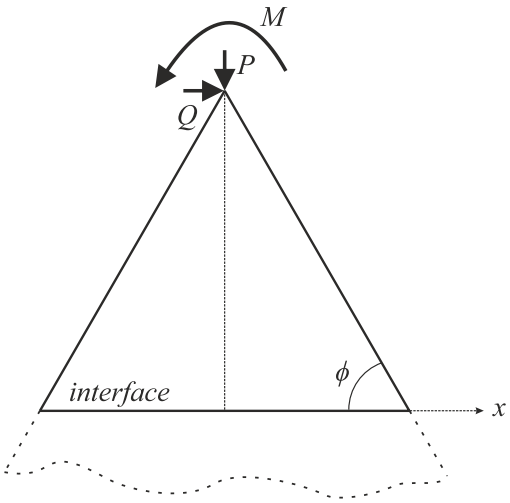


Figure 1.10: Common edge contact: semi-infinite wedge

Unlike the other forms of contact, slight rigid body shifts in one of the bodies causes a large change in behaviour. An initial study on the impact of a small misalignment has been carried out by Clark et al.[2] [41].

1.4 Half-plane theory

If the dimensions of the contact are small compared to the two bodies, it is known that the shape of the bodies distant to the contact do not have a strong influence on the contact. Therefore, each body is considered as a semi-infinite elastic solid bounded by a plane surface, also known as an elastic half-plane. This allows the use of elasticity theory developed for half-planes in contact problems.

The use of half-planes in solid mechanics has a long history. It began with Flamant [42] who found the stress and displacement caused by a point load. This can then be integrated to find the stress and displacement due to a distributed load. This is the solution to the inverse problem where the displacement is known but the applied traction is unknown. Since the profile of the contacting body is known, h_0, the required displacement for a

to the subject of the thesis.

[2]The author of this thesis contributed to this article, but details are not included as it is not central to the subject of the thesis.

contact to be formed whilst still obeying continuity of material is known. This leads to the integral equation,

$$E^* \frac{dh_0}{dx} = \frac{1}{\pi} \text{⨍}_{-a}^{a} \frac{p(\xi)}{\xi - x} d\xi; \quad |x| \leq a. \tag{1.1}$$

where the primary unknown is the normal traction, $p(x)$. A dash through the integral sign indicates that the integral is evaluated in a Cauchy Principal Value sense. The displacement gradient (gradient of the contact profile) is given by dh_0/dx and the integral extends over the whole contact interface.

For the geometry of two cylinders (Hertzian contact), given the normal load; the size of the contact, a, and the normal traction, $p(x)$ may be found. It is possible to find analogous solutions for a few other geometries, such as the shallow wedge [43] and a flat but rounded punch [44]. In many instances, numerical methods have been used to solve the underlying integral equation.

Once the normal contact problem has been resolved, it is natural to study the effect of tangential loads. This includes a shear force acting across the contact interface and differential bulk tensions. It is important to note that Coulomb friction is assumed and so the sliding shear traction is equal to $fp(x)$ (slip zones of the same sign) for a shear force and $\pm fp(x)$ for differential bulk tension (slip zones of opposite sign). Note that differential bulk tension alone never gives rise to rigid body motion.

A monotonically increasing shearing force, less than that needed to cause sliding, was studied by Cattaneo [15], and re-examined ten years or so later by Mindlin [16]. All solutions to date start off with a shear traction between the bodies which corresponds to sliding. A corrective shear traction distribution is applied over a central part of the contact, the stick zone b, to ensure the surface strains in the two bodies are equal in that region,

$$\frac{du}{dx} = \text{⨍}_{-a}^{a} \frac{fp(\xi)}{\xi - x} d\xi + \text{⨍}_{-b}^{b} \frac{q_c(\xi)}{\xi - x} d\xi = 0; \quad |x| \leq b. \tag{1.2}$$

Cattaneo and Mindlin noticed that, for a Hertzian contact, the corrective traction was

similar to that induced by the sliding contact but scaled. Ciavarella [45] and Jäger [46] later noted that this similarity argument would apply whatever the contacting profile.

The Ciavarella-Jäger theorem applies in the case of a shear force only; it cannot be extended to problems where the shear traction is induced by differential bulk tension. Nowell and Hills [47] showed that analytical results may be obtained when the slip zones have slip in the same direction for a Hertzian contact. Ciavarella and Macina [48] derived an analytical result for the analogous problem with bulk tension by inverting the integral equation. Here the slip zones are still of the same size but have slip in opposite directions. This was built on by Vázquez [49] to solve the case where the slip zones are of different size and the slip is in opposite directions.

All of these methods use a traction correction to the sliding solution. This method ensures that the shear traction in the slip zone is correct but requires a corrective term to ensure the correct strain in the stick zone.

1.4.1 Varying normal load

A major step to solving problems with a varying normal load was studied by Barber [50] who noted that the Ciavarella-Jäger theorem continues to apply in problems where the normal load is varying. He devised a simple graphical method to solve problems where the normal load, $P(t)$ and shear force, $Q(t)$ (with t denoting the sequence of events) vary together. The problem of a varying normal load with bulk tension was solved by Ramesh et al. [51], using a similar graphical method for establishing the extent of the slip zones. It cannot be extended to include a shear force. Again the restriction applies that the contact must be symmetrical so that the slip zones on each side of the contact must be of equal extent.

To remove this restriction and consider more general problems, a new approach has been developed using a displacement correction to the fully stuck solution. The fully stuck shear traction is straightforward in problems where no tangential loads are applied during normal loading. Figure 1.11 shows that the particles in both bodies move by the same amount. The application of tangential loads during the normal loading means that relative

displacements will be locked into the contact.

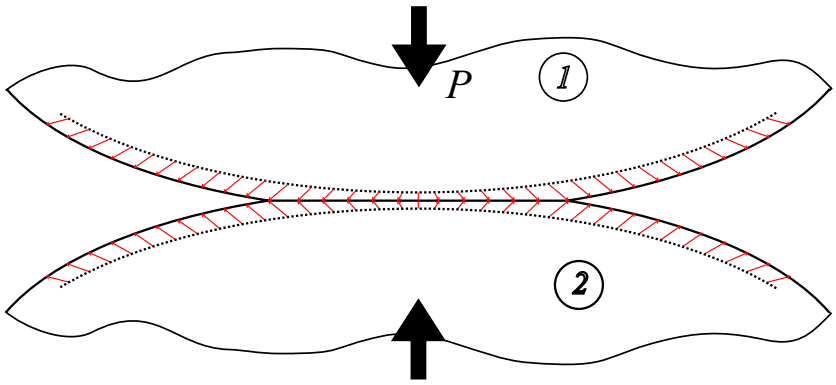


Figure 1.11: Lateral movement of particles - normal load

Hills et al. [52] developed the Mossakovski method to find the fully stuck traction and strains for contacts with an increasing normal load. This allows the fully stuck shear traction and shear strain to be calculated over a general loading cycle. Dislocations [53] may then be applied to unzip the contact and allow slip.

1.4.2 Dislocations

Slip can be modeled by distributing strain nuclei (dislocations) into an otherwise perfect body. This is an exploitation of Bueckner's theorem [53]: the stress state in the body is a superposition of the stresses in the perfect body (here conformal half planes) due to the loads and in the unloaded body due to the imperfection. This is a technique which is widely used to model cracks and can easily be used to model the effects of slip in a contact. This is a mathematical device which can be visualised as making a cut and slipping the material by the burgers vector before rejoining the material.

1.5 Assumptions

Contact mechanics is a rich field and is applied in a variety of areas from biological joints to the impact of projectiles. Since the application of interest is to dovetail joints, a number of simplifying assumptions are made to aid the analysis. These are outlined below:

1.5.1 Quasi-static

It is assumed that the movement of contacting bodies is slow, such that any inertial forces may be ignored. This allows the simplification of the problem by ignoring any dynamic effects.

This is not a major restriction to the methods proposed as most applications do not have loads that change at a rate comparable to the wave propagation speed of the material. However if dynamic effects do need to be considered, it would not be a straightforward extension.

1.5.2 Linear elastic

First, it is assumed that the materials are a continuum - so they fill entirely the space they occupy. The presence of atoms is ignored and this proves highly accurate for length scales much greater than inter atomic distances. Secondly, deformations are thought to be small, so the strains are infinitesimal. Further to this, it is assumed that there is a linear relationship between stress and strain. The final assumption is that the stress states present do not cause yielding. These assumptions allow the use of a Hookean constitutive law and ignore the effects of plasticity. In reality, there may be plasticity, contained in a small region. When this region is much less than the smallest length scale in the problem it is considered as small scale yielding and linear elasticity continues to apply [54]. Also, displacements are small and rotations are negligible.

1.5.3 Uncoupled

The two contacting bodies are either made from the same elastic material or one is rigid and the other incompressible. Both of these scenarios give rise to a Dundurs parameter [11] of $\beta = 0$. The consequence is that the contacts are uncoupled, a normal load does not give rise to a change in the shear traction and a shear force does not give rise to a change in the normal traction. It does not hold for the other classes of contact (or combination of elastic constants).

The restriction that the contact must be uncoupled is a significant limitation of the method. It only provides the solution for a subset of engineering problems. In many real contacts, the two bodies are made of different materials and so there is coupling present. Fortunately, it is possible to extend the methods proposed in this thesis to coupled problems by accounting for the contribution of the tangential forces to the normal traction and the contribution of the normal force to the shear traction. It is no longer possible to treat the normal problem as solved; here too a corrective term is required. Climb dislocations may be used for this new corrective term. Although the complexity of the solution would increase, there is no physical reason that the formulation cannot be extended to handle this more general class of problem.

1.5.4 Homogeneous & Isotropic

Although the analysis is material independent, a key requirement is that the material is of uniform composition - it cannot be mechanically separated into different materials. It must also exhibit identical properties in all directions.

1.5.5 Coulomb friction

Since the materials of interest are primarily metals, it is reasonable to assume that Coulomb's friction law applies. Thus, the frictional force is independent of the area in contact and opposes the applied loading. Coulomb friction is applied in a pointwise sense.

1.5.6 Surface smoothness

It is assumed that the surfaces of the two bodies in contact are perfectly smooth [55] and exhibit a constant coefficient of friction both in space and time. There is evidence to suggest the friction increases with time [56]. The work by Gorbatikh et al. [57] shows that the effect is minimised with larger shear forces.

It is known that real contact surfaces are rough at a micro scale but are treated as smooth at a macro level. The application of the methods proposed in this thesis are to problems

that will have many thousands of load cycles. Over the load cycles, the smoothing of the surface is the cause of the change in the coefficient of friction. This is currently not taken into account but it would not be challenging to do so, the coefficient could be changed with every loading loop or the steady state value could be used.

1.5.7 Plane strain

All of the contacts considered are assumed to have a depth much bigger than the largest length scale in the problem and so can be treated as plane strain problems.

1.6 Summary of research chapters

The primary contribution of this thesis is a new method of solving partial slip problems. This new method allows for the study of complex loading trajectories which better represent that experienced in real engineering problems. A new way to normalise the stress state near sharp notches to quantify mode dominance is also presented in the appendix.

1.6.1 Methods for solving incomplete contact problems in partial slip

The limits of the Ciavarella [45] - Jäger [46] theorem are discussed before three new methods to solve incomplete contact problems in partial slip are presented. It is shown that using distributed dislocations to introduce slip in a fully stuck contact is useful when presented with complex loading trajectories.

1.6.2 Constant normal load

The method of inserting dislocations into a fully stuck contact is applied to problems where both a shear force and bulk tension is present, with the normal load held constant. An approximate method using asymptotes is developed for this class of problem and the limits of its validity are shown.

1.6.3 Varying normal and bulk tension

The solution to a problem where the normal load and bulk tension are varying with time is found (with no applied shear force). In an example loading trajectory, the shear traction and slip-stick boundary is found.

1.6.4 Varying normal with a shear force and bulk tension

The method of inserting dislocations into a fully stuck contact is applied to problems where the normal load, shear force and bulk tension are varying with time. The slip-stick boundaries are found for an example loading trajectory.

1.6.5 An alternative normalisation of sharp notch roots

A new set of variables is used to describe the state of stress near sharp notch roots. These variables bring out internal length scales which indicate regions of single mode dominance.

2 Methods for solving incomplete contact problems in partial slip

An incomplete contact formed between elastic components subject to time-varying loads is prone to slip, even when the shear force is less than that needed to cause rigid body motion (sliding). In this chapter, four methods of solving partial slip contact problems are presented.

2.1 Introduction

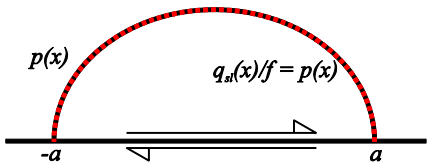
Starting from a sliding solution, a correction can be introduced where the kernel represents the effect of shear traction on the half-plane surfaces. This approach may be extended to problems where the surface shear traction is induced by differential bulk tension (direction of slip is opposite at one end of the contact from the other) [47, 48, 49].

This is not the only way to formulate the problem; Table A shows four different formulations. The numbers given in parenthesis show the solution form summarised in Table A.

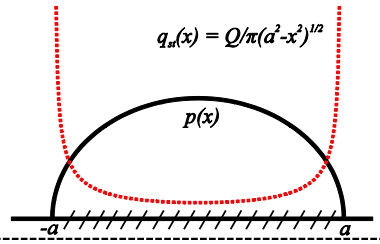
The half-width of the contact is denoted by a, similarly the half-width of the stick zone is given by b. The shear force is given by Q and the plane strain elastic modulus $E^* = \frac{E}{2(1-\nu^2))}$. The subscripts c, st and sl refer to the corrective, stuck and sliding solutions. $p(x)$ and $q(x)$ denote the normal and shear traction at the contact interface. Similarly the tangential displacement is given by u, with b_x denoting the Burgers vector of a dislocation and $B_x(x) = \frac{db_x}{dx}$ giving the dislocation density function.

Historically, solutions have always begun with the sliding solution, which automatically

Sliding

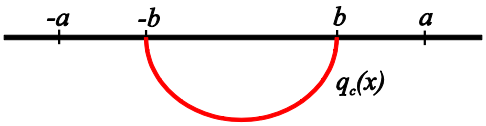


Fully stuck



Corrective tractions

1



The displacement must be zero in the stick zone. A corrective traction is required only in the stick zone as the tractions in the slip zone are already correct,

$$\left.\frac{du}{dx}\right|_{sl} + \left.\frac{du}{dx}\right|_{c} = 0; \quad |x| \le b.$$

The strain difference due to the sliding solution may be found from:

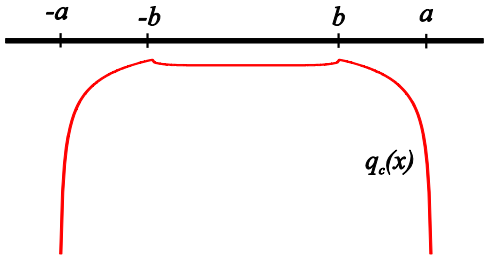
$$\left.\frac{du}{dx}\right|_{sl} = \frac{2f}{\pi E^*}\int_{-a}^{a}\frac{p(\xi)d\xi}{\xi - x}.$$

The corrective term produces the strain,

$$\left.\frac{du}{dx}\right|_{c} = \frac{2}{\pi E^*}\int_{-b}^{b}\frac{q_c(\xi)d\xi}{\xi - x}.$$

It is found that $q_c(x) = -fp_c(x)$, a scaled normal traction.

2



A corrective traction is required in the slip zone, so $q(x) = fp(x)$,

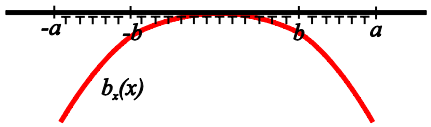
$$q_{c1} = fp(x) - \frac{Q}{\pi\sqrt{a^2 - x^2}}; \quad b \le |x| \le a.$$

This will cause a non zero displacement in the stick zone. A corrective traction is required in the stick zone to ensure the displacement is zero in the stick zone,

$$\frac{du}{dx} = \frac{2}{\pi E^*}\left(\int_{-b}^{b}\frac{fp(\xi)d\xi}{\xi - x} + \int_{-b}^{b}\frac{q_{c2}(\xi)d\xi}{\xi - x}\right) = 0; \quad |x| \le b.$$

Corrective displacements (dislocations)

3



Find the strains in the stick zone due to the ***sliding solution***. Dislocations are introduced to bring the surface strain to zero in the stick region,

$$B_x(x) = -\left.\frac{du}{dx}\right|_{sl}; \quad |x| \le b.$$

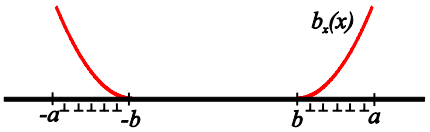
The tractions due to these dislocations are given by,

$$q_{c1}(x) = \frac{E^*\sqrt{b^2 - x^2}}{2\pi}\int_{-b}^{b}\frac{B_x(\xi)d\xi}{\sqrt{b^2 - \xi^2}(\xi - x)}.$$

A corrective strain in the slip zone is required such that,

$$q_{c1}(x) + q_{c2}(x) = 0; \quad b \le |x| \le a.$$

4



The tractions in the slip zone must be corrected whilst keeping the stick zone displacement at zero,

$$q_{st} + q_c = fp(x); \quad b \le |x| \le a.$$

Dislocations are introduced in the slip zones which gives rise to a corrective traction

$$q_c(x) = \frac{E^*}{2\pi\sqrt{b^2 - x^2}}\left(\int_{-a}^{-b} + \int_{b}^{a}\right)\frac{\sqrt{a^2 - \xi^2}B_x(\xi)d\xi}{\xi - x}.$$

Table A: An incomplete contact subject to a shear force in partial slip - solution techniques

satisfies the first condition for a partial slip solution (Equation 2.1), and requires a correction to satisfy the second condition (Equation 2.2). Method (1) is the application of the Ciavarella - Jäger theorem; it begins with a sliding solution and introduces a corrective shear traction over the central stick zone. Method (3) also begins with a sliding solution, but the correction is made in the form of a displacement over the entire contact interface. It is equally valid to begin with the fully stuck solution, which automatically satisfies the second equation but not the first. Method (2) begins with the fully stuck solution and introduces a corrective traction over the entire contact interface. Finally, method (4) starts with the fully stuck traction and introduces a corrective displacement in the slip zones. This method is of interest as it ensures the automatic preservation of any strains locked into the stick zone. This makes solving problems with a varying normal load much more straightforward as the information about the loading trajectory is locked in by the differential strains in the contact. A further advantage is that the primary output is the slip displacement - a key ingredient in finding the energy dissipated.

2.1.1 Conditions for partial slip

For incomplete symmetrical contact problems (subject to a shear force only), it is expected that there is a central stick zone and slip zones of equal extent at both edges of the contact. The following two conditions must be satisfied by the partial slip solution. The shear traction,

$$q(x) = fp(x); \quad b \leq |x| \leq a, \tag{2.1}$$

and the slip displacement gradient (initial loading is normal load only),

$$\frac{du}{dx} = 0; \quad |x| \leq b. \tag{2.2}$$

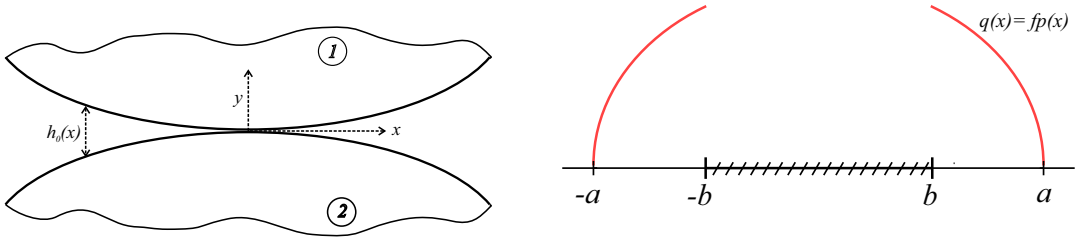
2.2 Traction correction to the sliding solution (1)

Figure 2.1a shows two symmetrical, undeformed elastic bodies, made of the same material on the point of being brought into contact, and with a gap function $h_0(x)$. The integral equation defining the contact pressure distribution, $p(x)$, as the contact is formed, is

$$E^* \frac{dh_0}{dx} = \frac{2}{\pi} \fint_{-a}^{a} \frac{p(\xi)\, d\xi}{\xi - x}; \quad |x| \leq a, \tag{2.3}$$

and, from normal equilibrium, the corresponding normal load, P is,

$$P = \int_{-a}^{a} p(x)\, dx. \tag{2.4}$$



(a) (b)

Figure 2.1: (a) Convex contact; (b) Conditions for partial slip

During the formation of the contact, equal surface strains will develop in each body, but no shear traction will arise because $\epsilon_{xx1}(x) = \epsilon_{xx2}(x)$. Once the contact has been formed, a monotonically increasing shear force causes edge slip (as the contact pressure goes smoothly to zero and is unable to sustain sufficient shearing traction to preserve stick) while the central part of the contact ($|x| \leq b$) remains stuck.

Figure 2.1b shows the conditions visually: the shear traction in the slip zone is equal to the sliding solution and the strains are zero in the stick zone. The shear traction may be written as the sum of the sliding distribution, $fp(x)$ and a corrective term, $q_c(x)$ over the stick interval. The integral giving the relationship between the difference in surface strains, $\frac{du}{dx} = \epsilon_{xx1}(x) - \epsilon_{xx2}(x)$ and the shear traction present is,

$$E^* \frac{du}{dx} = \frac{2f}{\pi} \int_{-a}^{a} \frac{p\,(\xi)\,d\xi}{\xi - x} + \frac{2}{\pi} \int_{-b}^{b} \frac{q_c(\xi) d\xi}{\xi - x}. \tag{2.5}$$

To turn this into an integral equation, the requirement that the strain difference is preserved (at zero) in the stick zone is imposed (Equation 2.2), i.e.,

$$\frac{du}{dx} = 0; \quad |x| \leq b, \tag{2.6}$$

and, as $a \geq b$, substituting Equation 2.3,

$$f E^* \frac{dh_0}{dx} = -\frac{2}{\pi} \int_{-b}^{b} \frac{q_c(\xi) d\xi}{\xi - x}; \quad |x| \leq b. \tag{2.7}$$

A comparison of Equations 2.3 and 2.7 shows that the corrective shear traction, $q_c(x) = -f p_c\,(x)$ may be obtained by solving the normal load contact equation, at a reduced load, P_c. If the shear force exerted at this point is Q, tangential equilibrium requires that $Q = f\,(P - P_c)$, giving the value of P_c.

2.2.1 Application to a Hertzian contact

In a Hertzian contact with a relative radius of curvature, R, between the contacting bodies, the gradient of the contact profile is given by $dh_0/dx = -2x/R$. If this is substituted into Equation 2.3 and a bounded both ends solution is sought, the resulting pressure distribution is elliptical and given by,

$$p\,(x) = p_0 \sqrt{1 - \left(\frac{x}{a}\right)^2}; \quad |x| \leq a, \tag{2.8}$$

where the peak contact pressure, p_0, is given by $p_0 = \frac{2P}{\pi a} = \sqrt{\frac{PE^*}{\pi R}}$. Normal equilibrium gives the half-width of the contact as, $a = \sqrt{\frac{4PR}{\pi E^*}}$. Similarly, the corrective term may be written with P replaced by P_c and the half-width of the contact, a replaced by the half-width of the stick zone, b. Explicitly, the shear traction distribution in partial slip is given by,

$$\frac{q\,(x)}{f} = p_0 \left[\sqrt{1 - \left(\frac{x}{a}\right)^2} - \frac{b}{a}\sqrt{1 - \left(\frac{x}{b}\right)^2} \right], \tag{2.9}$$

where the second term is included only if $|x| \leq b$ and,

$$\frac{b}{a} = \sqrt{1 - \frac{Q}{fP}}. \tag{2.10}$$

2.3 Dislocation correction to the fully stuck solution (4)

An alternative approach is to take the solution for a fully stuck contact subject to shear, and then to permit slip to develop in the regions where the frictional stick condition, $|q(x)| < fp(x)$, is violated. In a fully stuck contact, the relative tangential displacement is a constant, therefore,

$$\int_{-a}^{a} \frac{q(\xi)}{\xi - x} d\xi = \frac{du}{dx} = 0; \quad |x| \leq a. \tag{2.11}$$

Inverting this integral equation using the procedure given in Appendix B, assuming a singular both ends solution, gives rise to the required form of the fully stuck traction. Horizontal equilibrium can be applied to find the value of the constant (when a shear force, Q is applied),

$$q_{st}(x) = \frac{Q}{\pi\sqrt{a^2 - x^2}}; \quad |x| \leq a, \tag{2.12}$$

and is independent of geometry. The appropriate strain nucleus, needed to permit slip, is a glide dislocation, $b_x(x)$, located on the interface between two half-planes adhered over the interval $[-a\ , a]$. The surfaces of the half-planes are traction-free outside this interval. The shear traction distribution, due to a single dislocation, b_x at the point ξ, is

$$q(x) = \frac{E^* b_x(\xi)}{2\pi\sqrt{a^2 - x^2}} \frac{\sqrt{a^2 - \xi^2}}{\xi - x}; \quad |x| \leq a. \tag{2.13}$$

Appendix C gives the derivation for the shear traction distribution from both a single dislocation and a distribution. The dislocations are distributed over the two slip zones ($b < x \leq a$ & $-a \leq x < -b$), and the corresponding shear traction, $q_c(x)$ (not the same as that defined in Section 2.2) is given by,

$$q_c(x) = \frac{E^*}{2\pi\sqrt{a^2 - x^2}} \left[\int_b^a \frac{\sqrt{a^2 - \xi^2} B_x(\xi)}{\xi - x} d\xi + \int_{-a}^{-b} \frac{\sqrt{a^2 - \xi^2} B_x(\xi)}{\xi - x} d\xi \right], \tag{2.14}$$

where $B_x(x) = \frac{db_x}{dx}$ is the dislocation density. The integral equation defining the dislocation density is given by,

$$\begin{aligned} \frac{E^*}{2\pi\sqrt{a^2 - x^2}} \left[\int_b^a \frac{\sqrt{a^2 - \xi^2} B_x(\xi)}{\xi - x} d\xi + \int_{-a}^{-b} \frac{\sqrt{a^2 - \xi^2} B_x(\xi)}{\xi - x} d\xi \right] \\ = fp\,(x) - \frac{Q}{\pi\sqrt{a^2 - x^2}}; \quad b \leq |x| \leq a, \end{aligned} \tag{2.15}$$

where, the limits of the integral are the same as the slip zones. When the contact is symmetrical about $x = 0$, the contact pressure is also symmetrical, and when the shear tractions are induced by a shear force alone, the slip displacements themselves constitute an even function of x hence the dislocation density is odd. Therefore, $B_x(x) = -B_x(-x)$, giving,

$$q_c(x) = \frac{E^*}{\pi\sqrt{a^2 - x^2}} \int_b^a \left[\frac{\sqrt{a^2 - \xi^2} B_x(\xi) \xi}{x + \xi} \frac{1}{\xi - x} \right] d\xi; \quad b \leq |x| \leq a, \tag{2.16}$$

where,

$$q_c(x) = fp(x) - \frac{Q}{\pi\sqrt{a^2 - x^2}}; \quad b \leq |x| \leq a. \tag{2.17}$$

This is best illustrated by reference to an example geometry, and here a Hertzian contact is used.

2.3.1 Application to a Hertzian contact

It has been shown, in Section 2.1, that for this problem the contact pressure distribution is given by Equation 2.8 where a and P are related by the contact law, and hence Equation 2.16 becomes,

$$\int_b^a \left[\frac{\sqrt{a^2-\xi^2}B_x(\xi)\xi}{x^2-\xi^2}\right]d\xi = \frac{Q}{E^*} - \frac{2Pf(a^2-x^2)}{a^2E^*}; \quad b \le x \le a. \tag{2.18}$$

The kernel does not have a standard form, so the transformation,

$$g = a^2, \quad e = b^2, \quad y = x^2 \text{ and } \eta = \xi^2 \tag{2.19}$$

is required, so that,

$$\int_e^g \left[\frac{\sqrt{g-\eta}B_x(\eta)}{y-\eta}\right]d\eta = \frac{Q}{E^*} - \frac{2Pf}{E^*}\left(1-\frac{y}{g}\right); \quad e \le y \le g. \tag{2.20}$$

A bounded both ends solution is sought using the standard Riemann-Hilbert inversion [58] (Appendix B),

$$B(x) = \frac{-\sqrt{a^2-x^2}}{\pi}\int_{-a}^a \left[\frac{Q}{E^*} - \frac{2Pf}{E^*}\left(1-\frac{s}{g}\right)\right]\frac{ds}{\sqrt{a^2-s^2}(s-x)} \tag{2.21}$$

with the side condition,

$$\int_{-a}^a \left[\frac{Q}{E^*} - \frac{2Pf}{E^*}\left(1-\frac{s}{g}\right)\right]\frac{ds}{\sqrt{a^2-s^2}} = 0. \tag{2.22}$$

The side condition provides the size of the stick zone (Equation 2.10 but revealed by this different route) and the inversion gives,

$$B_x(x) = \frac{2fp_0}{E^*}\frac{x}{a}\sqrt{1-(b/x)^2}; \quad b \le |x| \le a. \tag{2.23}$$

A consistent slip displacement and stick interval are now known. Note that $B_x(\pm a)$ is finite.

2.3.2 Pure bulk tension

Attention is now restricted to the case when the shear traction is excited by a differential bulk tension alone. The differential bulk tension is defined as $\sigma = \sigma_1 - \sigma_2$ where σ_1 is the tension in the top body and σ_2 in the bottom body.

The shear traction when the contact is fully stuck is given by,

$$q_{st}(x) = \frac{\sigma x}{4\sqrt{a^2 - x^2}}; \quad |x| \leq a, \tag{2.24}$$

and is again independent of the contact geometry. The kernel for the dislocations is identical to the shear case. However, the displacements are now an odd function of x and so the dislocation density is an even function, $B_x(x) = B_x(-x)$. As before, the slip regions are of equal size, so that,

$$\frac{xE^*}{\pi\sqrt{a^2 - x^2}} \int_b^a \left[\frac{\sqrt{a^2 - \xi^2} B_x(\xi)}{x + \xi} \frac{1}{\xi - x} \right] d\xi = sgn(x) f p\,(x) - \frac{\sigma x}{4\sqrt{a^2 - x^2}}; \quad b \leq |x| \leq a. \tag{2.25}$$

The associated side condition gives the size of the stick zone, which for a Hertzian contact is found to be,

$$K\left(\sqrt{1 - \left(\frac{b}{a}\right)^2}\right) - E\left(\sqrt{1 - \left(\frac{b}{a}\right)^2}\right) = \frac{\sigma\pi}{8 f p_0}. \tag{2.26}$$

Further details are given in Appendix D. The same result can also be found by using a traction correction to the sliding solution. The slip displacement cannot be written in closed form.

2.4 Traction correction to the fully stuck solution (2)

A further method, with little physical interpretation, is to start with the fully stuck solution, and introduce a corrective shear traction, $q_c(x)$ to get the correct shear traction in the slip zone whilst ensuring that the displacements in the stick zone remain zero. The

correction must be carried out in two steps and over the entire contact patch. First, a corrective shear traction $q_{c1}(x)$ is imposed on the slip regions,

$$q_{c1}(x) = fp(x) - \frac{Q}{\pi\sqrt{a^2 - x^2}}; \quad b \leq |x| \leq a. \tag{2.27}$$

This has the consequence of developing displacements in the stick zone, which means a further corrective traction $q_{c2}(x)$ is required in the stick zone to return the displacements to zero in the stick zone,

$$\frac{du}{dx} = \frac{2}{\pi E^*}\int_{-b}^{b} \frac{q_{c2}(\xi)d\xi}{\xi - x} + \left.\frac{du}{dx}\right|_{c1} = 0; \quad |x| \leq b. \tag{2.28}$$

Inverting this integral equation (assuming bounded both ends) yields the second corrective traction. The associated side condition gives the size of the stick zone.

2.5 Dislocation correction to the sliding solution (3)

Starting with the sliding solution, the strain in the contact interface is given by,

$$\left.\frac{du}{dx}\right|_{sl} = \frac{2f}{\pi E^*}\int_{-a}^{a} \frac{p(\xi)d\xi}{\xi - x}. \tag{2.29}$$

The corrective term must return the strain in the stick region to zero. This may be done with the imposition of an equal and opposite correction term $\left.\frac{du}{dx}\right|_{c1}$. Such that,

$$B_{c1}(x) = -\left.\frac{du}{dx}\right|_{sl}; \quad |x| \leq b. \tag{2.30}$$

Unlike in method (4), the dislocations give rise to a bounded shear traction (derivation in Appendix C.1). The effect of the glide dislocations inserted in the stick zone is to induce a shear traction in the slip zone,

$$q_{c1}(x) = \frac{E^*\sqrt{b^2 - x^2}}{2\pi}\int_{-b}^{b} \frac{B_{c1}(\xi)d\xi}{\sqrt{b^2 - \xi^2}(\xi - x)}. \tag{2.31}$$

The shear traction in the slip zones has now been changed because of these dislocations.

Further glide dislocations must be introduced in the slip zones to ensure that $q(x) = fp(x)$ in the slip zones. This produces an integral equation,

$$q_{c2}(x) = \frac{E^*}{2\pi\sqrt{a^2 - x^2}} \left[\int_b^a \frac{\sqrt{a^2 - \xi^2} B_{c1}(\xi)}{\xi - x} d\xi + \int_{-a}^{-b} \frac{\sqrt{a^2 - \xi^2} B_{c1}(\xi)}{\xi - x} d\xi \right]. \tag{2.32}$$

The inversion will give the dislocation distribution required in the slip zones and the side condition will yield the size of the stick zone.

2.6 Summary

The four methods presented offer more options for solving half-plane contact problems in partial slip. Two of the procedures - applying a corrective shear to a sliding solution (1) the classical approach, and applying a corrective displacement to the stuck solution (4) are very attractive. Two further procedures, were also studied briefly: imposing a corrective shear on the stuck solution (2), and applying a corrective displacement to the sliding solution (3). The method of superimposing a corrective dislocation on the fully stuck solution is ideal for solving complicated loading trajectories because: (a) it automatically preserves locked in displacements and (b) it gives the displacements in the slip zone immediately, which can be used to calculate the energy dissipated.

Methods (1) and (4) are more attractive because they require a single correction to go from either the sliding or fully stuck solution to partial slip. The second benefit is that the correction only needs to be made in either the slip zone or stick zone. On the other hand, methods (2) and (3) require two sets of corrections which must be made over the entire contact interface.

3 Constant normal load

The previous chapter introduced four methods of solving incomplete contact problems in partial slip. The most promising method is using a dislocation correction to the fully stuck solution. In this chapter, that method is used to solve problems where the normal load is held constant and both a shear force and bulk tension are applied. Some of the work in this chapter was carried out by Dr Matthew Moore; this is indicated in the text.

3.1 Introduction

There are two methods by which surface shear tractions may be excited within the contact: one is through a shear force, the other is a differential bulk tension. The first solution for cyclically applied shear force and bulk tension to a Hertzian contact, was by Nowell and Hills [47]. They solved the partial slip problem numerically by forming an integral equation in terms of the 'corrective' shear traction needed to the slipping solution. Using the Ciavarella [45] - Jäger [46] theorem, Ciavarella and Macina [48] solved the problem of pure bulk tension analytically for a Hertzian contact. Building on this, Vázquez et al. [49] obtained an exact solution when both bulk tension and shear are present with slip zones of opposite sign, also for a Hertzian contact.

In this chapter, a method is developed that gives the solution to problems where the contact is formed and subject to both a shear force and bulk tension for a general half-plane contact geometry. Instead of a traction correction to the slipping solution, the method uses a displacement correction to the fully stuck solution. The mathematical framework for finding the corrective displacement and the slip stick boundary is given in the following section.

3.2 Mathematical framework

In contacts that may be modeled as half-planes, the normal traction falls to zero at the edges in a square root manner. Therefore, the edges are the first points to slip when subjected to a tangential shear force, Q, and/or differential bulk tension. The desired output is the size and location of the stick zone and the strains in the slip zone.

The method starts by inhibiting slip at all points on the contact interface and the corresponding shear traction is used as the starting solution. Dislocations are included to introduce slip in the regions where it is expected [53]. The dislocations induce a shear traction over the entire contact. In the areas which experience slip, this traction must equal the difference between the slipping, $q_{sl}(x)$, and fully stuck shear traction, $q_{st}(x)$,

$$q_c(x) = q_{sl}(x) - q_{st}(x); \quad x \in \textit{slip zones}. \tag{3.1}$$

A single dislocation b_x at a point c on the contact interface gives rise to,

$$q(x) = \frac{E^*}{2\pi} \frac{b_x(c)}{\sqrt{a^2 - x^2}} \frac{\sqrt{a^2 - c^2}}{c - x}. \tag{3.2}$$

The following integral equation can be formed from the introduction of a distribution of dislocations,

$$\frac{E^*}{2\pi\sqrt{a^2 - x^2}} \left[\int_{b_1}^{a} \frac{\sqrt{a^2 - \xi^2} B_x(\xi)}{\xi - x} d\xi + \int_{-a}^{-b_2} \frac{\sqrt{a^2 - \xi^2} B_x(\xi)}{\xi - x} d\xi \right] = q_c(x); \quad x \in \textit{slip zones}, \tag{3.3}$$

where the unknown function $B_x(x) = \frac{db_x}{dx}$ is the dislocation density, which is the same as the slip displacement gradient or relative surface strain. The slipping traction is, $q_{sl} = \pm fp(x)$. The size of the stick zone is given by b_1 and b_2. The integral equation may be inverted analytically (Appendix E), leading to the following solution,

$$B_x(x) = \frac{-2}{E^*\pi}\sqrt{(x-b_1)(x+b_2)}\left[\int_{b_1}^{a}\frac{q_c(\xi)d\xi}{\sqrt{(\xi-b_1)(\xi+b_2)}(\xi-x)} - \int_{-a}^{-b_2}\frac{q_c(\xi)d\xi}{\sqrt{(\xi-b_1)(\xi+b_2)}(\xi-x)}\right]; \quad b_1 \le x \le a \tag{3.4}$$

$$B_x(x) = \frac{2}{E^*\pi}\sqrt{(x-b_1)(x+b_2)}\left[\int_{b_1}^{a}\frac{q_c(\xi)d\xi}{\sqrt{(\xi-b_1)(\xi+b_2)}(\xi-x)} - \int_{-a}^{-b_2}\frac{q_c(\xi)d\xi}{\sqrt{(\xi-b_1)(\xi+b_2)}(\xi-x)}\right]; \quad -a \le x \le -b_2 \tag{3.5}$$

This inversion was carried out using contour integration by Dr Matthew Moore. The two side conditions generated from the inversion determine the slip-stick boundaries are,

$$\int_{-a}^{-b_2}\frac{q_c(s)ds}{\sqrt{(s-b_1)(s+b_2)}} - \int_{b_1}^{a}\frac{q_c(s)ds}{\sqrt{(s-b_1)(s+b_2)}} = 0, \tag{3.6}$$

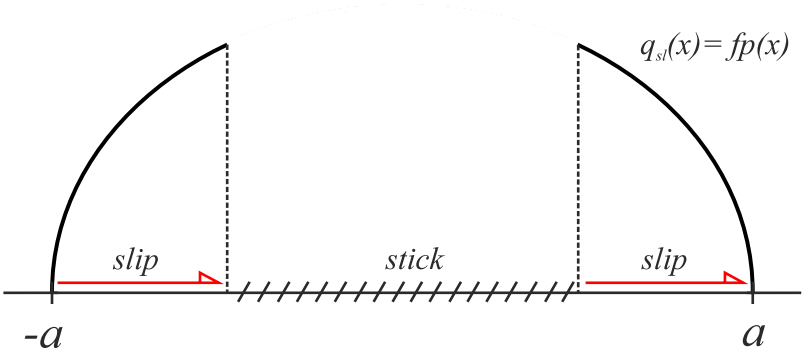
$$\int_{-a}^{-b_2}\frac{q_c(s)sds}{\sqrt{(s-b_1)(s+b_2)}} - \int_{b_1}^{a}\frac{q_c(s)sds}{\sqrt{(s-b_1)(s+b_2)}} = 0. \tag{3.7}$$

3.3 Constant normal load

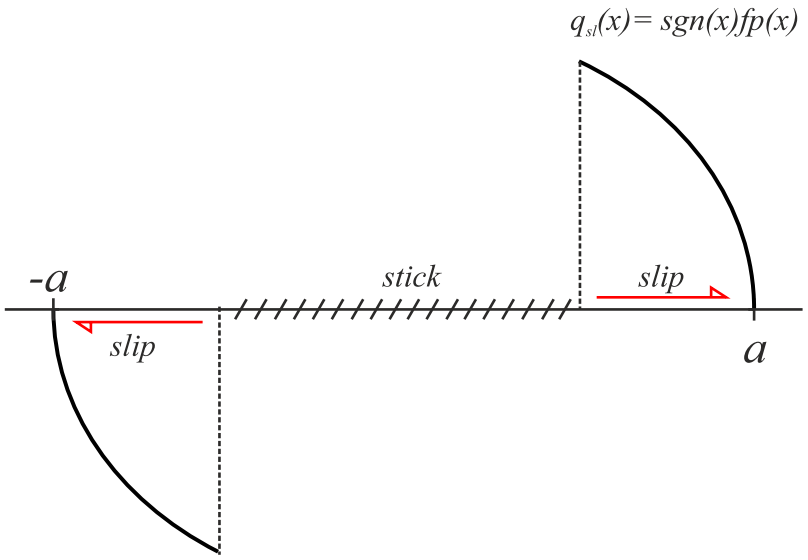
When the normal load is held constant, the size of the contact does not change and so the behaviour over a load cycle is easy to study. For fully stuck half-plane contacts, the shear traction is given by

$$q_{st}(x) = \frac{Q}{\pi\sqrt{a^2-x^2}} + \frac{\sigma x}{4\sqrt{a^2-x^2}}; \quad |x| \le a, \tag{3.8}$$

where the first term is from a transverse shear load ($|Q| < fP$) and the second term is from a differential bulk tension. If the contact is in partial slip, the direction of slip is dependent upon the relative mix of the tangential loading. Slip in the two edge zones will occur in the same direction if the shear force is dominant (Figure 3.1a), but in opposite directions if the differential bulk tension is dominant (Figure 3.1b).



(a)



(b)

Figure 3.1: (a) The sliding shear traction - slip zones of the same sign; (b) The sliding shear traction - slip zones of opposite sign (positive σ)

The fully stuck shear traction, $q_{st}(x)$ (Equation 3.8) and the pressure distribution, $p(x)$ are substituted into the integrals in Equations 3.4 and 3.5 to find the dislocation density. Further details are given in Appendix E.2. The solution now becomes,

$$B_x(x) = \frac{-2f}{E^*\pi}\sqrt{(x-b_1)(x+b_2)}\left[\fint_{b_1}^{a}\frac{p(\xi)d\xi}{\sqrt{(\xi-b_1)(\xi+b_2)}(\xi-x)} - \int_{-a}^{-b_2}\frac{\pm p(\xi)d\xi}{\sqrt{(\xi-b_1)(\xi+b_2)}(\xi-x)}\right]; \quad b_1 \le x \le a \tag{3.9}$$

$$B_x(x) = \frac{2f}{E^*\pi}\sqrt{(x-b_1)(x+b_2)}\left[\int_{b_1}^{a}\frac{p(\xi)d\xi}{\sqrt{(\xi-b_1)(\xi+b_2)}(\xi-x)} - \fint_{-a}^{-b_2}\frac{\pm p(\xi)d\xi}{\sqrt{(\xi-b_1)(\xi+b_2)}(\xi-x)}\right]; \quad -a \le x \le -b_2 \tag{3.10}$$

The fully stuck traction, $q_{st}(x)$, does not affect the dislocation density but does affect the size of the stick zone. The signs chosen depend on the signs and relative magnitudes of the shear force and differential bulk tension. The side conditions are given by,

$$\int_{-a}^{-b_2}\frac{\pm fp(s)ds}{\sqrt{(s-b_1)(s+b_2)}} - \int_{b_1}^{a}\frac{fp(s)ds}{\sqrt{(s-b_1)(s+b_2)}} = \pi\frac{\sigma}{4}, \tag{3.11}$$

$$\int_{-a}^{-b_2}\frac{\pm fp(s)sds}{\sqrt{(s-b_1)(s+b_2)}} - \int_{b_1}^{a}\frac{fp(s)sds}{\sqrt{(s-b_1)(s+b_2)}} = \frac{\pi\sigma(b_1-b_2)}{8} - Q. \tag{3.12}$$

3.3.1 Shear force only

A simple case where only one tangential load is applied is explored in detail here. In the absence of any bulk tension, a number of simplifications can be made. The slip zones at either end of the contact will be of the same size and slip is in the same direction, therefore $b_1 = b_2 = b$. This means,

$$q_c(x) = fp(x) - \frac{Q}{\pi\sqrt{a^2-x^2}}; \quad b \le |x| \le a. \tag{3.13}$$

The slip displacements are an even function of x, so the dislocation density is odd, and therefore $B_x(x) = -B_x(-x)$, giving,

$$B_x(x) = \frac{4f}{E^*\pi}\sqrt{x^2-b^2}\int_b^a \frac{\xi p(\xi)d\xi}{\sqrt{\xi^2-b^2}(\xi^2-x^2)}; \quad b \leq |x| \leq a \tag{3.14}$$

The first side condition (Equation 3.11) is automatically satisfied, the second may be written as,

$$\int_b^a \frac{sp(s)ds}{\sqrt{s^2-b^2}} = \frac{Q}{2f}. \tag{3.15}$$

3.3.2 Bulk tension only

Analogously, in the absence of a shear force, a number of simplifications can be made. The slip zones at either end of the contact will be of the same size but slip is in opposite directions and therefore, $b_1 = b_2 = b$. This allows the corrective traction to be written as,

$$q_c(x) = sgn(x)fp(x) - \frac{\sigma x}{4\sqrt{a^2-x^2}}; \quad b \leq |x| \leq a. \tag{3.16}$$

The slip displacements are an odd function of x, so the dislocation density is even, and therefore $B_x(x) = B_x(-x)$, giving,

$$B_x(x) = \frac{4f}{E^*\pi}\sqrt{x^2-b^2}\int_b^a \frac{xp(\xi)d\xi}{\sqrt{\xi^2-b^2}(\xi^2-x^2)}; \quad b \leq |x| \leq a \tag{3.17}$$

The first side condition is no longer automatically satisfied and demands that,

$$\int_b^a \frac{p(s)ds}{\sqrt{s^2-b^2}} = \frac{\sigma\pi}{8f}. \tag{3.18}$$

On the other hand, the second side condition is now automatically satisfied (Equation 3.12).

3.4 Application to a Hertzian contact

So far, the results have been geometry independent. A Hertzian contact is used to illustrate the proposed method and show that the results are consistent with the existing

theory. The normal traction distribution for a Hertzian contact is given by (see Appendix E.2),

$$p(x) = \frac{2P}{\pi a}\sqrt{1-\left(\frac{x}{a}\right)^2} = p_0\sqrt{1-\left(\frac{x}{a}\right)^2}. \tag{3.19}$$

This may be substituted into Equations 3.11 and 3.12 to find the extent of the stick zone in the general case of combined shear and bulk tension loading. If the slip directions are the same (positive Q and σ),

$$\frac{b_1}{a} = \sqrt{1-\frac{Q}{fP}} + \frac{\sigma}{4fp_0}, \quad \frac{b_2}{a} = \sqrt{1-\frac{Q}{fP}} - \frac{\sigma}{4fp_0}. \tag{3.20}$$

The strains developed in the slip regions can also be found by substitution of the contact pressure into Equation 3.9 and Equation 3.10,

$$B_x(x) = Sign(x)\frac{2fp_0}{aE^*}\sqrt{(x-b_1)(x+b_2)}; \quad x \in slip\ zones. \tag{3.21}$$

The limits of this solution can be found when the slip zone length becomes zero (either $b_2 \to -a$ or $b_1 \to a$). To ensure the slip zones are of the same sign,

$$\frac{\sigma}{fp_0} \leq 4(1-\sqrt{1-Q/fP}). \tag{3.22}$$

When this condition is violated, the slip zones are of opposite sign, and the following two conditions must be satisfied (positive Q and σ),

$$\begin{aligned}\frac{-2}{\sqrt{(1+\beta_1)(1+\beta_2)}}\Bigg[(1+\beta_1)(1+\beta_2)E\left(\frac{\sqrt{(1-\beta_1^2)(1-\beta_2^2)}}{(1+\beta_1)(1+\beta_2)}\right) + (1+\beta_2)\left(\frac{\beta_1-\beta_2}{2}+2\right)\\ K\left(\frac{\sqrt{(1-\beta_1^2)(1-\beta_2^2)}}{(1+\beta_1)(1+\beta_2)}\right) + (\beta_1-\beta_2)\Pi\left(\frac{\beta_2-1}{\beta_2+1}, \frac{\sqrt{(1-\beta_1^2)(1-\beta_2^2)}}{(1+\beta_1)(1+\beta_2)}\right)\\ -\frac{\beta_1^2-\beta_2^2}{2}\Pi\left(\frac{1-\beta_1}{1+\beta_2}, \frac{\sqrt{(1-\beta_1^2)(1-\beta_2^2)}}{(1+\beta_1)(1+\beta_2)}\right)\Bigg] = \frac{\pi\sigma}{4fp_0},\end{aligned} \tag{3.23}$$

where $\beta_1 = \frac{b_1}{a}$ and $\beta_2 = \frac{b_2}{a}$, and

$$\begin{aligned}\frac{-3a}{2\sqrt{(1+\beta_1)(1+\beta_2)}}\Bigg[&-(1+\beta_2)(1+\beta_1)(\beta_1-\beta_2)E\left(\frac{\sqrt{(1-\beta_1^2)(1-\beta_2^2)}}{(1+\beta_1)(1+\beta_2)}\right)\\&-(1+\beta_2)((\frac{\beta_1}{3}+2)\beta_2-\frac{\beta_2^2}{2}-\frac{\beta_1^2}{2}-\frac{2\beta_1}{3}-\frac{2}{3})K\left(\frac{\sqrt{(1-\beta_1^2)(1-\beta_2^2)}}{(1+\beta_1)(1+\beta_2)}\right)\\&-\left(\frac{\beta_1+\beta_2}{2}\right)\left(\beta_1^2-\frac{2\beta_1\beta_2}{3}+\beta_2^2-\frac{4}{3}\right)\Pi\left(\frac{1-\beta_1}{\beta_2+1},\frac{\sqrt{(1-\beta_1^2)(1-\beta_2^2)}}{(1+\beta_1)(1+\beta_2)}\right)\Bigg]\\&=\frac{\pi\sigma(b_1-b_2)}{8fp_0}-\frac{Q}{fp_0},\end{aligned} \tag{3.24}$$

where, $K(\gamma)$, $E(\gamma)$ and $\Pi(n,\gamma)$ are elliptic integrals of the first, second and third kind (explicit forms given in Appendix F). This result was derived by Dr Matthew Moore (see Appendix E.2). The results are shown in Figure 3.2 where the dotted lines give the boundary between shear and bulk dominated behaviour at either end of the contact. To find the corresponding values of b_2 the y-axis should be flipped, i.e. replace σ/fp_0 with $-\sigma/fp_0$.

3.5 Problems without closed form results

The examples given so far have been for a Hertzian contact but the method presented is not restricted to problems that have a pressure distribution that may be presented in closed form. The integrals in Equation 3.4 and Equation 3.5 and the corresponding side conditions may be evaluated numerically. The numerical representation of $p(x)$ can be used rather than the closed form result. The integration cannot be done using standard methods such as the trapezium rule as it contains singularities but may be carried out using the Gauss-Chebychev numerical scheme [59].

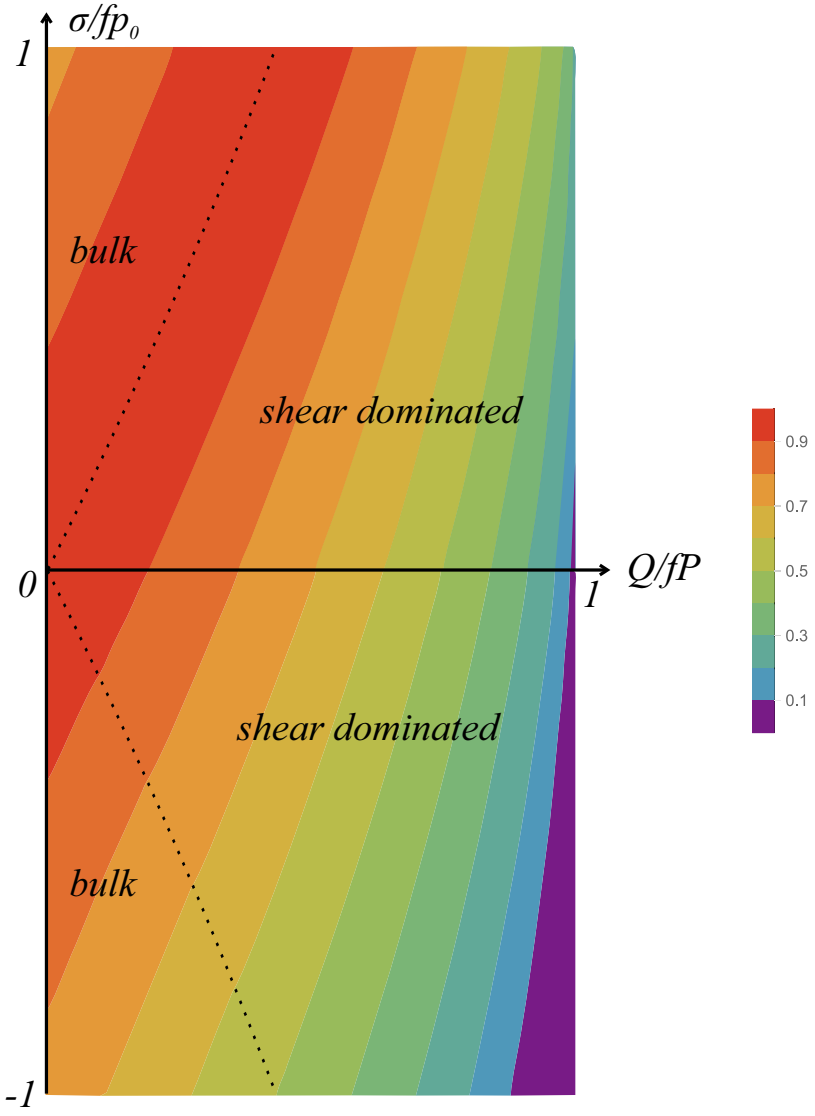


Figure 3.2: Contours of b_1/a

3.6 Asymptotic approximation

The method outlined in this chapter works well for geometries that have a pressure distribution and contact law in closed form. It is possible to solve the equations numerically if the geometry or the pressure distribution is complicated. However, if the region of interest is the edge of the contact then an asymptotic solution can give an estimate with a much lower calculation overhead.

The method works by zooming into one edge of the contact and ignoring all other geometric features. This has the effect of making the contact look similar to a crack and a single term approximation of the tractions can be used with multipliers representing the

magnitude of loading.

When it is not possible to solve the problem exactly, it is possible to get an approximate answer through the use of asymptotes. Attention is focused on the slip zone at one end of the contact and an asymptotic solution is introduced. The simplified geometry is shown in Figure 3.3, which is similar to a semi-infinite crack. However, the interface does not support a tension, and the symmetrical solution for loading (the contact pressure) falls smoothly to zero as the contact edge is approached.

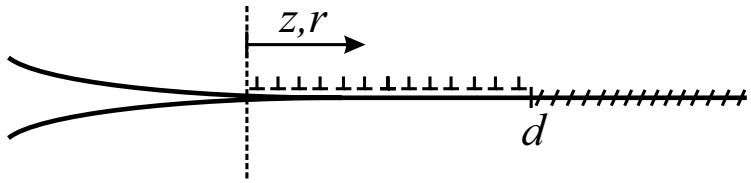


Figure 3.3: Dislocations at one edge of a half-plane contact

Consider only one edge of the contact, such that both a, $b \to \infty$ but $a - b = d$ remains finite. The resulting problem is to derive the shear traction due to a distribution of dislocations close to one edge of a fully stuck semi-infinite contact.

3.6.1 Dislocations on the centreline of a semi-infinite crack

The solution for a dislocation near the edge of a fully stuck semi-infinite contact is equivalent to a dislocation near the tip of a semi-infinite crack, and may therefore be found readily. By moving the origin to the left-hand contact edge and making the substitutions $x = -a+z$, $\xi = -a+r$ into Equation 3.3, a distribution of dislocations (of density $B_x(r)$) will produce the shear traction,

$$q(z) = \frac{E^*}{2\pi\sqrt{z}} \int_0^d \frac{\sqrt{r} B_x(r)}{r - z} dr, \tag{3.25}$$

where d is the extent of slip. The dislocations must provide a corrective traction such that the shear traction in the slip zone is equal to $fp(z)$, which leads to the following integral equation,

$$q_c(z) = \frac{E^*}{2\pi\sqrt{z}}\int_0^d \frac{\sqrt{r}B_x(r)}{r-z}dr = fp(z) - q_{st}(z); \quad 0 \le z \le d. \tag{3.26}$$

Now, a single term description of the near-edge traction is taken and the substitutions $p(z) = K_N\sqrt{z}$ and $q(z) = \frac{K_T}{\sqrt{z}}$ [20],

$$K_N = \frac{1}{\pi}\sqrt{\frac{2}{a}}\frac{dP}{da}, \quad K_T = \frac{\sigma}{4}\sqrt{\frac{a}{2}} \pm \frac{Q}{\pi\sqrt{2a}}. \tag{3.27}$$

where K_N and K_T are the generalised stress intensity factors. Equations 3.25, 3.26 and 3.27 then become,

$$fK_N z - K_T = \frac{E^*}{2\pi}\int_0^d \frac{\sqrt{r}B_x(r)}{r-z}dr; \quad 0 \le z \le d, \tag{3.28}$$

which may then be inverted, assuming that the solution is bounded both ends (Appendix B). It is found that the dislocation distribution and the size of the slip zone are given by

$$B_x(z) = \frac{fK_N}{E^*}\sqrt{d-z}, \quad d = \frac{2K_T}{fK_N}. \tag{3.29}$$

3.6.2 Limits of the approximation

The work done against friction estimated from the asymptotic procedure is compared, for a Hertzian contact, with the exact solution. For a given stick zone size, b/a, the work done is slightly different for the two problems because the slip displacements are greater when induced by bulk tension. For the case when the slip zone is 10% of the contact half width ($b/a = 0.9$), the work done against friction, $W(z/d)$ is shown in Figure 3.4. Also included is the work done calculated using the asymptotic approximation (Figure 3.4). It is apparent that the asymptotic approximation always yields an underestimate of the work done if the slip is induced by pure shear and, conversely, always yields an overestimate when induced by pure bulk tension. Any combination of shear and bulk loading will result in an energy dissipation that lies between the two extremes; thus the pure loading cases are the extremes of error between the finite solution and the asymptotic approximation.

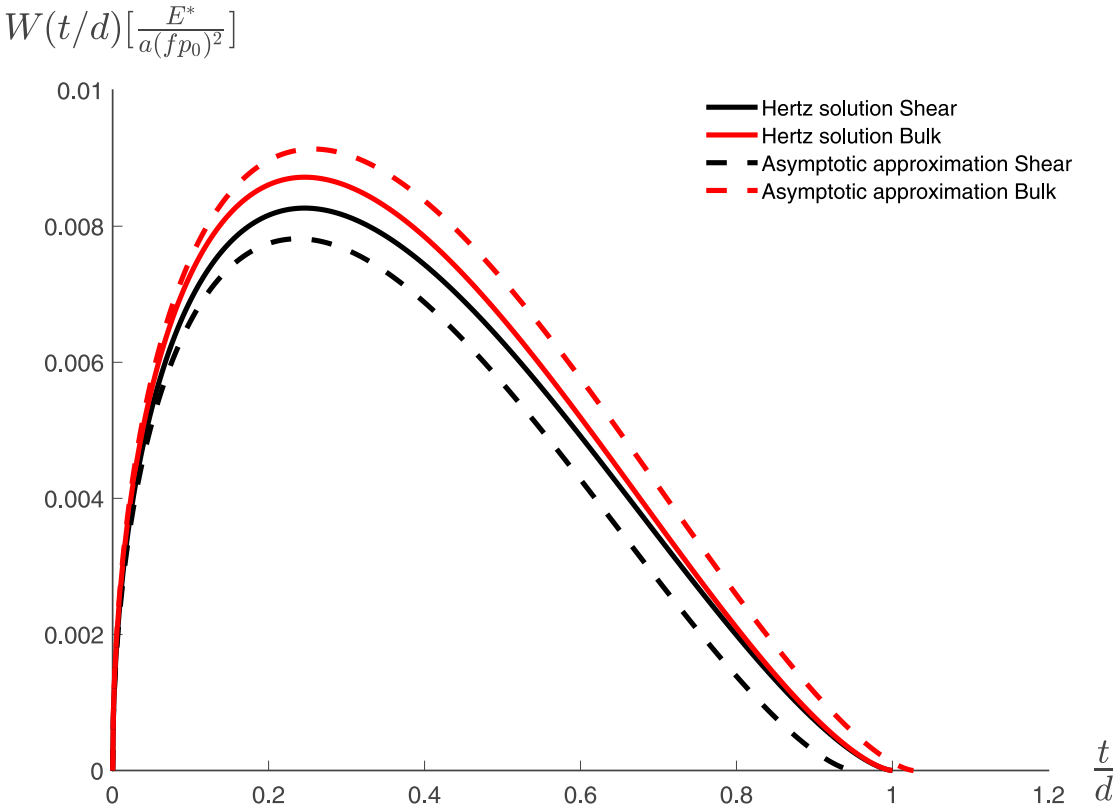


Figure 3.4: Energy dissipation at one edge of a Hertzian contact ($b/a = 0.9$, $d/a = 0.1$)

Figure 3.5 shows the fractional error in the total energy dissipated (the integral of $W(z/d)$ over the region $0 < z/d < 1$) in the slip zone. The error is calculated by comparing the asymptotic form with the full solution. The ratio $b/a = 0.9$ gives rise to a 10% error in the energy dissipated.

3.7 Summary

In this chapter, it has been shown that it is possible to treat any combination of shear force and bulk tension when the normal load is held constant. This is done by starting with the fully stuck solution, and then introducing a corrective displacement. It can be applied to any contact that may be idealised as two partially bonded half-planes. The advantage of the method is the automatic preservation of any locked in slip displacements, which makes it easier to solve problems where the stick zone is not at the centre of the

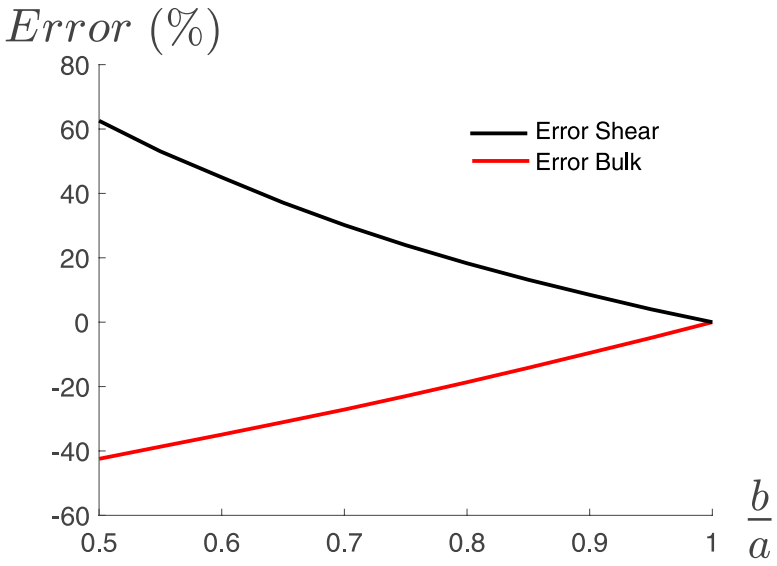


Figure 3.5: Fractional error in energy from the asymptotic form

contact. An asymptotic approximation is derived that is much simpler to use. It is clear that, when the slip zone is less than 10% of the overall contact size, the approximation gives a good estimate of the energy dissipation. When the slip zone is larger, the error is significant and the asymptotic solution is not usable.

4 Varying normal load and bulk tension

This chapter uses a traction correction to the sliding solution to solve the problem when both the normal load and bulk tension are varying with time.

4.1 Introduction

In many contacts, bulk tension acting parallel to the surfaces of contacting bodies may be present and vary with time, inducing a shear traction. Nowell and Hills [47] solved the problem of applying the normal load first, holding it constant, and then subjecting the contact to a combination of shear force and bulk tension with a numerical procedure. Ciavarella and Macina [48] later solved, in closed form, the problem of applying the normal load first then imposing bulk tension only.

In order to solve the problem of a partial slip incomplete contact subject to bulk tension and normal load varying in time, the solution for a constant normal load is required first.

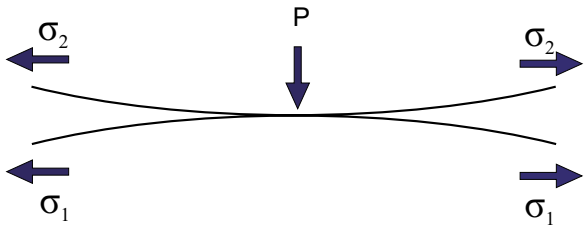


Figure 4.1: An incomplete contact subject to bulk tension

Figure 4.1 shows a formed incomplete contact where each body is subsequently subject

to bulk tension. The difference between the tensions ($\sigma = \sigma_1 - \sigma_2$) is responsible for inducing a shear traction. The starting point is to find the condition to keep the contact fully stuck.

4.2 Condition for full stick

The requirement for full stick of a contact idealised by two half-planes, subject to bulk tension, σ, is given by Hills et al. [52]. It depends on the change in normal load and bulk tension and is,

$$\frac{d\sigma}{dP} < \frac{4f}{\pi a}. \tag{4.1}$$

In the formulation developed, the contact half width, a, gives a cleaner measure of the normal load than P itself. Thus, the full stick condition may be re-written as,

$$\frac{d\sigma}{da} < \frac{4f}{\pi a}\frac{dP}{da}, \tag{4.2}$$

where dP/da represents the contact law. In the varying normal load and shear force ($P - Q$) problem considered by Barber et al. [50], the lines $Q = \pm fP$ set the bounds for gross sliding. In the case of bulk tension alone, there is no equivalent behaviour, since the slip is in opposite directions, the contact cannot slide.

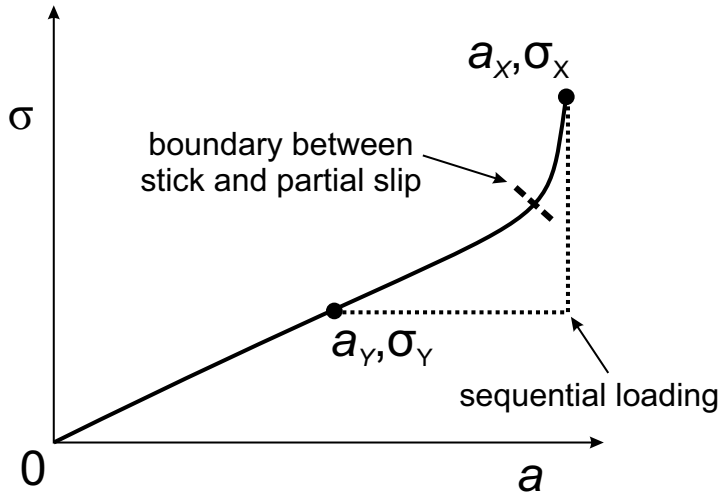
4.3 General loading solution procedure

Given the solution to the sequential loading problem, where the normal load is applied first, held constant, and a differential bulk tension is introduced, the general loading problem can be solved. The problem is considered in $a - \sigma$ space for simplicity of algebra. Consider a general point, a_X, σ_X where the contact is under a state of partial slip. The aim is to determine the size of the stick zone and the shear traction in the contact at this loading point. Only bulk tension is present and hence the interface is expected to have a central stick zone with slip zones of opposite sign at either edge of the contact. In the

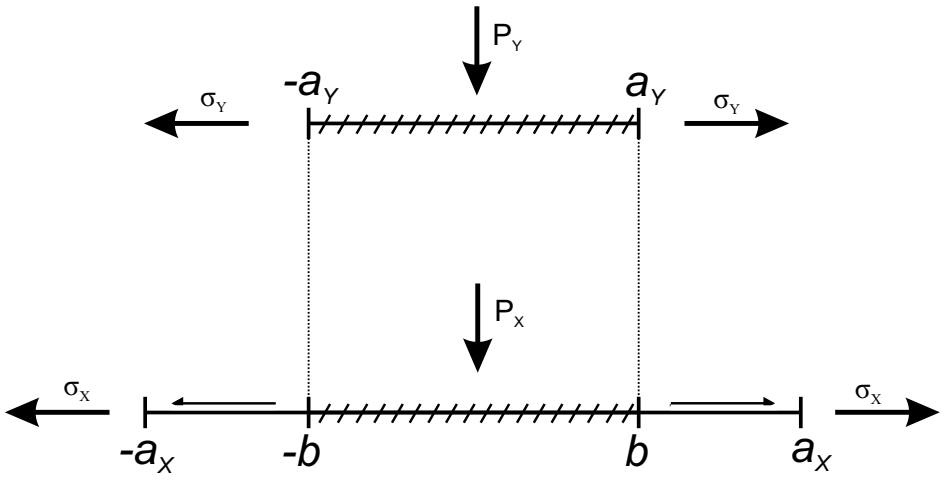
slip zones, the following traction distribution (positive σ) is expected,

$$q_X(x) = f p_X(x) sgn(x); \quad b \leq |x| \leq a_X, \tag{4.3}$$

where b is the half width of the stick zone. A shorthand notation, $p_X(x)$, is used to denote the contact pressure associated with the normal load, P_X, distributed over the interval $-a_X \leq x \leq a_X$. Consider a previous point in the load trajectory which is fully stuck, (a_Y, σ_Y). The point a_Y is chosen such that it is the size of the stick zone at X ($b = a_Y$). This may be seen graphically in Figure 4.2.



(a)



(b)

Figure 4.2: Transformation of the general loading problem

The problem can be considered as having two phases of loading. First, from no loading to, Y which is fully stuck, and the second phase from Y to X which is is replaced by sequential loading (as shown in Figure 4.2a). During the first phase strain differences are locked into the contact as material is laid down and subject to differential tensions at the same time. During the second phase, the strain difference already locked in is preserved despite additional tension being applied, so that

$$\left.\frac{\partial(u_1-u_2)}{\partial x}\right|_X = \left.\frac{\partial(u_1-u_2)}{\partial x}\right|_Y; \quad |x| \leq a_Y = b. \tag{4.4}$$

In order to preserve the strain difference between Y and X there is a condition on the shear traction change, within the stick zone, $q_X(x) - q_Y(x)$, from this phase, as derived in Nowell et al. [47],

$$\left.\frac{\partial(u_1-u_2)}{\partial x}\right|_{X-Y} = 0 = \frac{2}{\pi E^*}\int_{-a_X}^{a_X} \frac{q_X(\xi)-q_Y(\xi)}{\xi - x} d\xi - \frac{\sigma_X - \sigma_Y}{2E^*}; \quad |x| \leq a_Y. \tag{4.5}$$

The boundary conditions given by Equations 4.3 and 4.5 are the same as those in the bulk stress phase of the sequential loading problem.

4.4 Specialisation to a Hertzian contact

By writing the full stick condition in terms of $a(P)$ instead of P, the condition for full stick is independent of the position in the load space. The average load in the steady state does not affect the condition to initiate or terminate slip. Therefore, the steady state solution is independent of the mean load. For other geometries, the choice of parameter will be different to ensure the condition is independent of the mean load.

From this point onwards, the equations are specialised to a Hertzian contact. This is because for this particular class of contact, there exists a closed form solution for the sequential loading problem. The Hertzian contact law can be used to make explicit, the general equations given in previous sections. The contact law is,

$$P = \frac{\pi E^* a^2}{4R}, \tag{4.6}$$

where R is the radius of curvature, and P the applied normal contact load. Using the contact law, the condition for full stick (Equation 4.2) may be written as,

$$\left|\frac{d\bar{\sigma}}{d\bar{a}}\right| < f, \tag{4.7}$$

where,

$$\bar{\sigma} = \frac{\sigma}{E^*}, \quad \bar{a} = \frac{2a}{R}. \tag{4.8}$$

For convenience, in the remainder of this chapter, the bar is omitted.

4.4.1 Sequential application of the normal load and bulk tension

A Hertzian contact is formed, the normal force is held constant and a differential bulk tension is applied to the bodies, which results in the formation of slip zones of opposite sign attached to the contact edges. The derivation of the extent of the slip zone and the shear traction within the stick region is presented in Ciavarella et al. [48].

The underlying argument for the solution procedure used in [47, 48] is that, in an incomplete contact without bulk tension, equal surface strains ($\epsilon_{xx}(x)$) develop in each body, so that as points on the surface are brought into contact, they remain opposite each other. At this point the surface shear traction is zero everywhere. When remote tensions are imposed, the surface strains in the stick zones have (a) (equal) contributions from the normal load, together with further contributions from (b) the remote tensions applied, and (c) the (initially partly unknown) shear traction, so that,

$$F(x) \equiv \frac{\partial u_1}{\partial x} - \frac{\partial u_2}{\partial x} = \frac{2}{\pi E^*}\int_{-a}^{a} \frac{q(\xi)}{\xi - x} d\xi - \frac{\sigma}{2E^*}. \tag{4.9}$$

The strain difference is set to be zero within the stick region,

$$F(x) = 0; \quad |x| \leq b, \tag{4.10}$$

where b is the stick zone half width, and note that, in the slip zones,

$$q(x) = sgn(x) f p(x); \quad b \leq |x| \leq a. \tag{4.11}$$

Equations 4.10 and 4.11 define an integral equation of the first kind with a Cauchy kernel, in terms of the shear traction in the stick zone,

$$\frac{2}{\pi E^*} \int_{-b}^{b} \frac{q(\xi)}{\xi - x} d\xi = -\frac{2f}{\pi E^*} \int_{b}^{a} \frac{p(\xi)}{\xi - x} d\xi + \frac{2f}{\pi E^*} \int_{-a}^{-b} \frac{p(\xi)}{\xi - x} d\xi + \frac{\sigma}{2E^*}; \quad |x| \leq b. \tag{4.12}$$

The consistency condition due to the shear traction being bounded at both ends $x = \pm b$ of the stick zone which enables the value of b to be found. The solution is,

$$K(k) - E(k) = \frac{\pi \sigma}{8 f p_0}, \tag{4.13}$$

with,

$$\frac{b}{a} = \sqrt{1 - k^2}, \tag{4.14}$$

where $K(k)$, $E(k)$ are, respectively, the complete elliptic integrals of the first and second kind. A full definition of elliptic integrals and some useful relations are given in Appendix F. The peak pressure in the contact is given by $p_0 = \frac{2P}{\pi a}$. Figure 4.3 shows the size of the stick zone for a given magnitude of bulk tension. Note that an infinite tension is required to achieve a zero stick zone size. The shear traction distribution within the stuck region, $q_S(x; a, b)$, from Ciavarella and Macina [48] is,

$$q_S(x; a, b) = \frac{2}{\pi} f p_0 \frac{x}{a} \sqrt{\frac{b^2 - x^2}{a^2}} \left[\Pi\left(\sqrt{\frac{a^2 - b^2}{a^2 - x^2}}, \sqrt{1 - \frac{b^2}{a^2}} \right) - K\left(\sqrt{1 - \frac{b^2}{a^2}} \right) \right]; \quad |x| \leq b, \tag{4.15}$$

where $\Pi(m, n)$ is the complete elliptic integral of the third kind. Note that the term outside the square brackets is the fundamental function for a square root bounded solution, and which clearly goes to zero at either end of the interval, whilst the terms within the

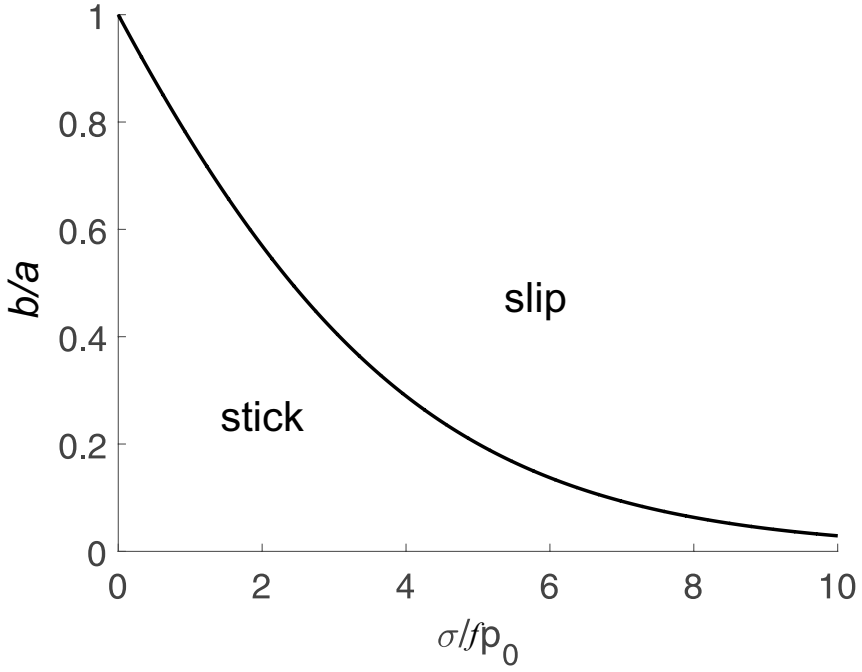


Figure 4.3: Slip and stick regions for a Hertzian contact with bulk stress

square bracket show local square root singular behaviour at the ends of the interval, such that the product of the two is finite.

Expanding the elliptic integral for points near $x = \pm b$ and taking the limit of the resulting shear traction as these points are approached, it is found that the value tends to a constant which is continuous with the shear traction in $|x| > b$,

$$q_S(b; a, b) = \frac{2}{\pi a} f p_0 \frac{b}{a} \sqrt{b^2 - x^2} \left[\frac{\pi}{2} \frac{a}{b} \frac{\sqrt{a^2 - b^2}}{\sqrt{b^2 - x^2}} + ... \right] \approx \pm f p_0 \sqrt{1 - \frac{b^2}{a^2}}; \quad |x| \to b^-. \quad (4.16)$$

4.5 Periodic loading

The process outlined in the following sections is an extension to the method developed by Barber et al. [50]. This method considers incomplete contacts under varying normal and shear loads but in the absence of differential bulk tensions. In this case, the process is straightforward as the Ciavarella-Jäger theorem [45, 46] is applied. The size of the stick zone is found by drawing a straight line of gradient $\pm f$ from the current load state, until it intersects a previous point in the load cycle. In the case of bulk tension, curvilinear lines

must be drawn where the equation of the line depends on the geometry of the contact. A general elliptic loading path in $a - \sigma$ space is considered, which is centered on a point (a_0, σ_0). The initial loading to get to the ellipse ensures full stick. Thus it must not violate the inequality given in Equation 4.7.

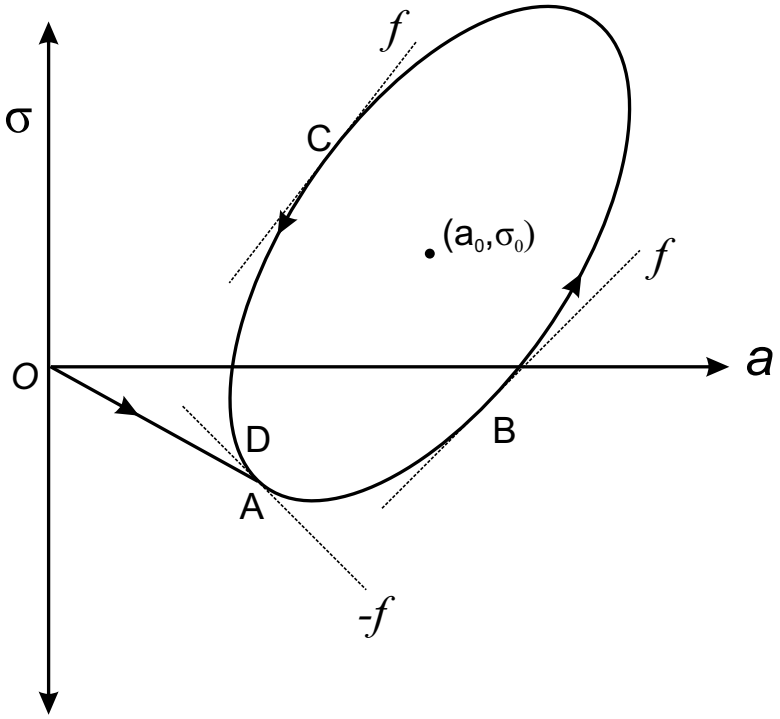


Figure 4.4: The loading cycle

The general parametric equation of an ellipse is,

$$a = a_0 + a_c sin(t), \quad \sigma = \sigma_0 + \sigma_c sin(t - \phi). \tag{4.17}$$

When the phase lag, ϕ, is zero, the ellipse collapses to a straight line. In this instance, the gradient of the line will determine if there is slip during the cycle. If there is a non zero phase lag, there will certainly be slip present during the cycle, at least when the gradient is negative and $dP < 0$ and so $da < 0$.

Either a or P can be used as the variable representing the normal loading:

$$P(t) = \frac{\pi E^*}{4R}(a_0 + a_c sin(t))^2. \tag{4.18}$$

Throughout the solution procedure, X represents the point on the load cycle (a_X, σ_X)

for which a solution is required. The point Y (a_Y, σ_Y) denotes the point during the immediately preceding loading cycle at which the contact area is equal to the instantaneous stick zone at loading point X.

4.6 Transient cycle

The letters correspond to salient points in the loading trajectory.

4.6.1 Full stick $O \rightarrow B$

The initial loading and the sector of the ellipse from A to B is fully stuck as can be seen in Figure 4.4. To find the shear traction distribution incorporated during this loading, the contribution from an increment of bulk loading is first considered,

$$\Delta q = \frac{-x\Delta\sigma}{4\sqrt{a^2 - x^2}}. \tag{4.19}$$

Assuming the increment is small, a derivative with respect to a can be taken,

$$\frac{dq}{da} = \frac{-x}{4\sqrt{a^2 - x^2}} \frac{d\sigma}{da}(a). \tag{4.20}$$

Integrating Equation 4.20 gives the fully stuck traction distribution at a general point X which lies between $O \rightarrow B$,

$$q_X(x) = \int_0^{a_X} \left[\frac{-x}{4\sqrt{a^2 - x^2}} \frac{d\sigma}{da}(a) \right] da. \tag{4.21}$$

4.6.2 Forward slip $B \rightarrow C$

The contact enters a state of partial slip from point B (see Figure 4.5), when the gradient of the cycle crosses, f, violating the full stick condition. The addition of bulk tension will cause slip zones of opposite sign at the edges of the contact with a central stick zone. Since the normal traction is known, the shear traction distribution for a point X (see Figure 4.5), in the slip zones can be written,

$$q_X(x) = f p_X(x) sgn(x); \quad b \leq |x| \leq a_X, \tag{4.22}$$

where, b is the size of the stick zone. To find the size of the stick zone, a line is drawn,

$$\sigma(a) = \sigma_X - \frac{2 f a_X}{\pi}\left[K\left(\sqrt{1-\left(\frac{a}{a_X}\right)^2}\right) - E\left(\sqrt{1-\left(\frac{a}{a_X}\right)^2}\right)\right], \tag{4.23}$$

from X on the load cycle to locate a previous point in the load cycle, Y, which is fully stuck. This equation comes from a re-arrangement of Equation 4.13, instead of going from zero to σ, the change in bulk tension is from σ_Y to σ_X. An example line of this kind, marked in red can be seen in Figure 4.5.

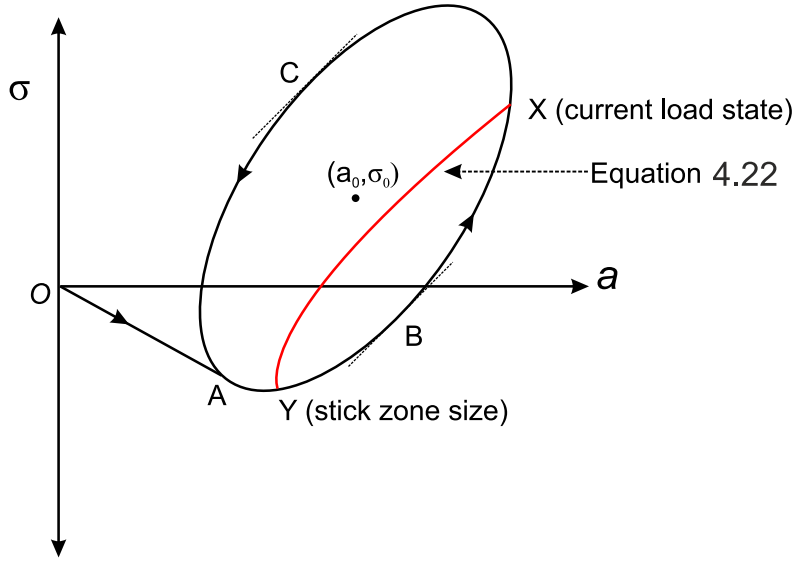


Figure 4.5: Finding the size of the stick zone

As X moves along the cycle between B and C, the predicted size of Y becomes smaller, so throughout this phase the absolute size of the stick zone recedes. This is despite the fact that the contact becomes initially larger, then smaller. Initially, the point Y will be mapped onto the cycle itself, but as Y becomes smaller than A, it intersects the initial loading (OA). Therefore, in the first cycle, the size of the stick zone depends on the initial loading. For all subsequent cycles, the initial loading affects only the locked in shear traction in regions that have never slipped. The traction distribution within the stick zone at a general point X between B and C, Figure 4.5 is given by,

$$q_X(x) = \int_0^{a_Y} \left[\frac{-x}{4\sqrt{a^2 - x^2}} \frac{d\sigma}{da}(a) \right] da + q_S(x; a_X, a_Y); \quad |x| \leq a_Y, \tag{4.24}$$

where $q_S(x; a, b)$ is defined by Equation 4.15. The shear traction is made up of two parts, which originates from the way the loading has been segmented. First, the fully stuck traction from the initial loading stage (up to point Y) which locks in displacements in the zone which will remain stuck. The next stage introduces a shear traction that ensures that the locked in displacements are preserved.

The point C is where slip no longer advances, where the gradient of the line used to determine Y is equal to the gradient of the cycle, i.e.,

$$\left. \frac{d\sigma(a)}{da} \right|_{a=a_C} = \frac{2f}{\pi} K(0) = f, \tag{4.25}$$

which shows that C may be found when the gradient of the cycle is equal to the coefficient of friction. At C, the contact becomes instantaneously stuck.

4.6.3 Reverse slip $C \to D$

Reverse slip begins as soon as X is past C. The notation that X is a point on the cycle where the solution is required and Y is the location of the point determining the size of the stick zone (and the shear traction distribution within it) is retained. The location of Y is determined by drawing a line from X given by,

$$\sigma(a) = \sigma_X + \frac{2f a_X}{\pi} \left[K\left(\sqrt{1 - \frac{a^2}{a_X^2}} \right) - E\left(\sqrt{1 - \frac{a^2}{a_X^2}} \right) \right] \tag{4.26}$$

(Note the change in sign from Equation 4.23) and finding its intersection with Equation 4.23 when $X \to C$. Figure 4.6 shows the line used to find the size of the stick zone. The method is the same as in the forward slip case, except now it is the intersection with the line from YC to C and not the load cycle or initial path, as shown in Figure 4.6. The aim is to conserve the locked in displacements in the stick region defined by a new point Y, which can again be done with the same form of solution as the sequential loading case. The shear traction is a superposition of the traction at Y and the equivalent sequential

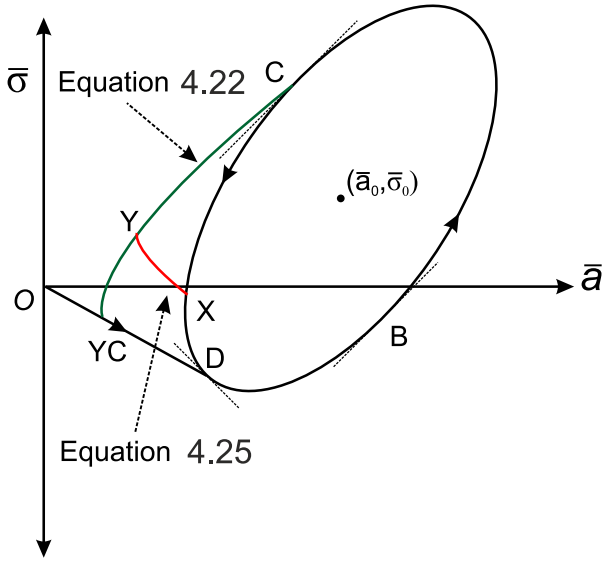


Figure 4.6: Finding the size of the stick zone in reverse slip

loading from Y to X. The shear traction at Y is found from unloading along the line $C \rightarrow YC$, this ensures that in the new stick zone, the tangential strains locked in at C are preserved. The shear traction in the slip zone is,

$$q_X(x) = -fp_X(x)sgn(x); \quad a_Y \leq |x| \leq a_X. \tag{4.27}$$

Moving inwards from the edges, in the region which is now stuck but has experienced forward slip just before C, the traction is given by,

$$q_X(x) = fp_Y(x)sgn(x) - q_S(x; a_X, a_Y); \quad a_{YC} \leq |x| \leq a_Y. \tag{4.28}$$

If the current stick zone becomes smaller or equal to the size of the stick zone just before C, the size will be zero. Moving closer to the center of the contact, in the region which has always remained stuck, the traction due to the fully stuck initial loading is preserved:

$$q_X(x) = -q_S(x; a_X, a_Y) + q_S(x; a_Y, a_{YC}) + \int_0^{a_{YC}} \left[\frac{-x}{4\sqrt{a^2 - x^2}} \frac{d\sigma}{da}(a) \right] da; \quad |x| \leq a_{YC}. \tag{4.29}$$

Reverse slip continues until D, where the contact becomes fully stuck, because the cycle

no longer violates the full stick inequality given by Equation 4.7. Thus, D is found as the point when the gradient of the cycle is $-f$.

4.7 The second cycle

Much like the first cycle, the contact starts off fully stuck, until the point B is reached. The traction distribution at a general point, X, between D and B is given by,

$$q_X(x) = q_D(x) + \int_{a_D}^{a_X} \left[\frac{-x}{4\sqrt{a^2 - x^2}} \frac{d\sigma}{da}(a) \right] da. \tag{4.30}$$

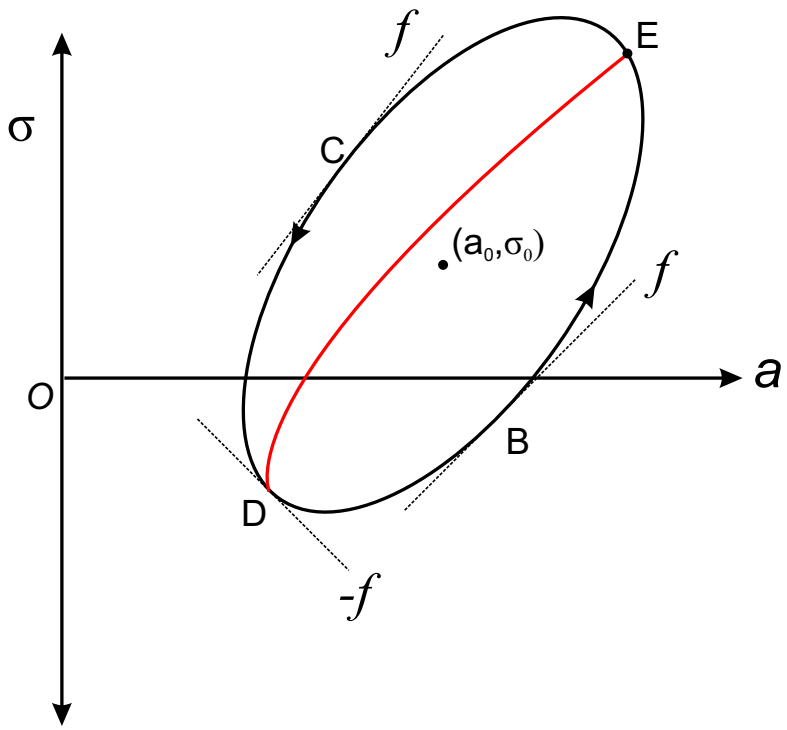


Figure 4.7: The second cycle

Forward slip begins from point B where the gradient of the cycle crosses f. The size of the stick zone is given by the same procedure as in the first cycle. The traction distributions in the second cycle may also be found in an identical fashion to the first cycle, the superposition of the shear traction at Y and the sequential loading from Y to X.

This continues until point E (see Figure 4.7), where the size of the stick zone is equal to

that defined by point D. Beyond the point E, the stick zone becomes smaller than D, and so there is no longer an obvious corrective solution as the cycle was accumulating reverse slip before D. Once the point E is passed on the second cycle, the slip zone starts to erase the reverse slip shear traction locked in at D and a new solution is necessary.

4.7.1 The phase $E \rightarrow C$

The intersection of Equation 4.23 with the initial load path (which has now been erased) or the loop itself no longer gives the size of the stick zone. The point where it intersects the line, used to find the size of the stick zone from point D (when the contact was in reverse slip) is required. This is given by Equation 4.26 as $a_X \rightarrow D$. This can be seen in Figure 4.8 as the intersection of the red and green lines denoted by the point Y.

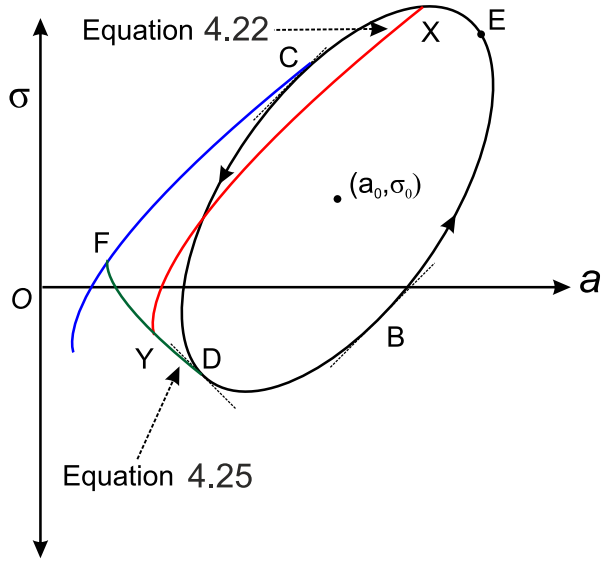


Figure 4.8: Stick zone size in the second cycle

At point C, the contact again becomes instantaneously stuck. Just before point C, the size of the stick zone is given by point F (the intersection of green and blue lines in Figure 4.8). Moving beyond C, the reverse slip solution is found in an identical fashion to the first cycle until D. All further cycles will follow the same solution and so steady state has been attained after one cycle of loading.

4.8 The permanent stick zone

The permanent stick zone size is defined by the point denoted F in Figure 4.8. It is found from the intersection of Equation 4.23 where $X \to C$ and Equation 4.26 where $X \to D$. The size of the permanent stick zone is dependent wholly on the steady state loading cycle and is independent of the initial loading. The locked in tangential strains in the stick zone are, however, from the initial loading. In the steady state, the locked in tangential strains have no effect on the size of the slip zone. It is also known that this shear traction has no effect on the slip displacements in the steady state [60]. This is a very useful result for fretting fatigue calculations. The transient problem is not important when looking at the steady state behaviour.

4.9 Example

To illustrate the procedure an example loading cycle, defined by,

$$a = 0.5 + 0.07sin(t), \quad \sigma = 0.05 + 0.1sin(t - 0.9) \tag{4.31}$$

is considered. Figure 4.9 shows the size of the contact and the slip-stick boundary around the cycle. There are four different types of behaviour that may be seen for a particle in the contact region.

1. Near the edge, particles experience only forward slip, they lift off and move back to their original positions when not in contact.

2. Moving closer to the center, some particles experience a combination of forward slip, some reverse slip and lift off and return to their original location.

3. Closer still, the particles are subject to equal amounts of forward and reverse slip.

4. The innermost region is in a state of full stick throughout the loading cycle.

The normalised shear traction at significant points in the load cycle are given in Figure 4.10 for the transient cycle and Figure 4.11 for the steady state. a_0 is taken to be the contact

half width when the contact is at its widest. The blue dashed line is the normalised normal traction $(sgn(x)p(x)/p_0(a_0))$ at the respective point. It is clear that the transient loading has locked in tangential strains in the stick zone which are preserved in subsequent cycles.

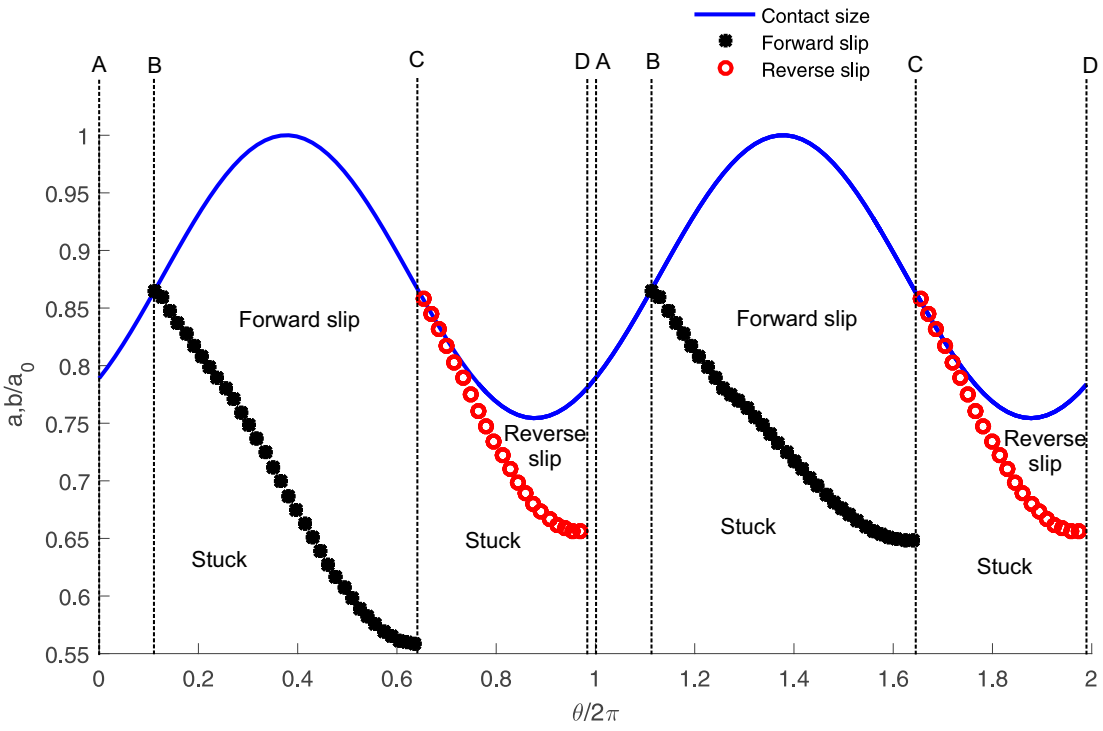
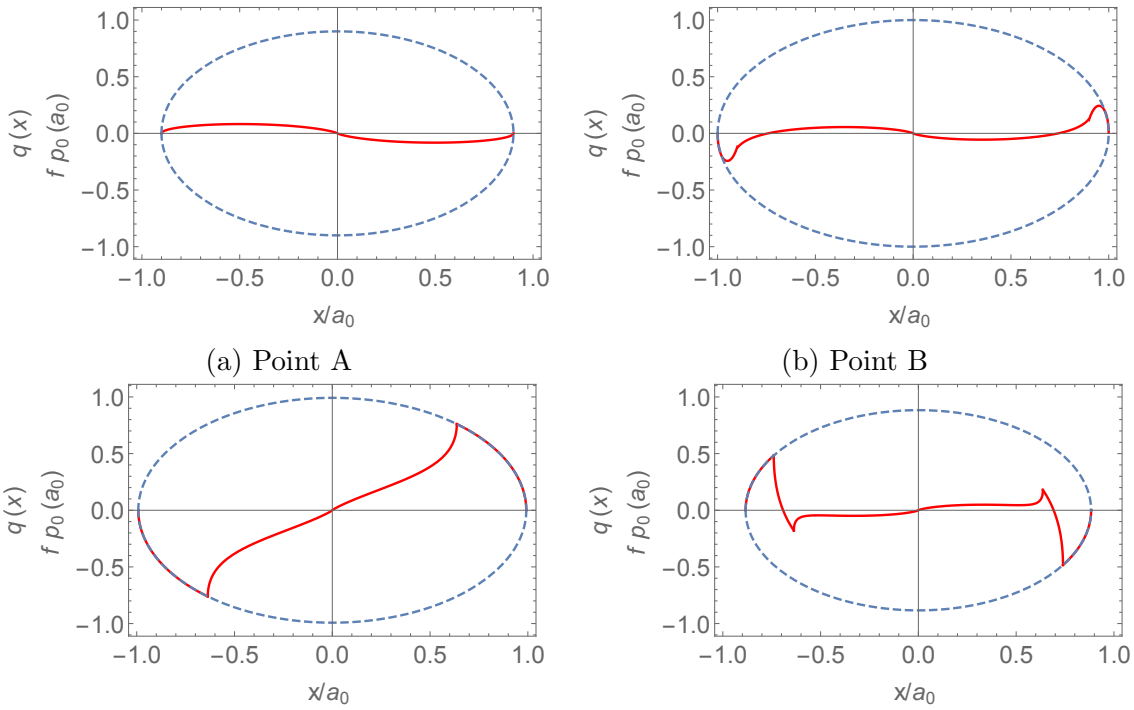


Figure 4.9: Size of contact and slip-stick boundary ($f = 0.8$)

4.10 Summary

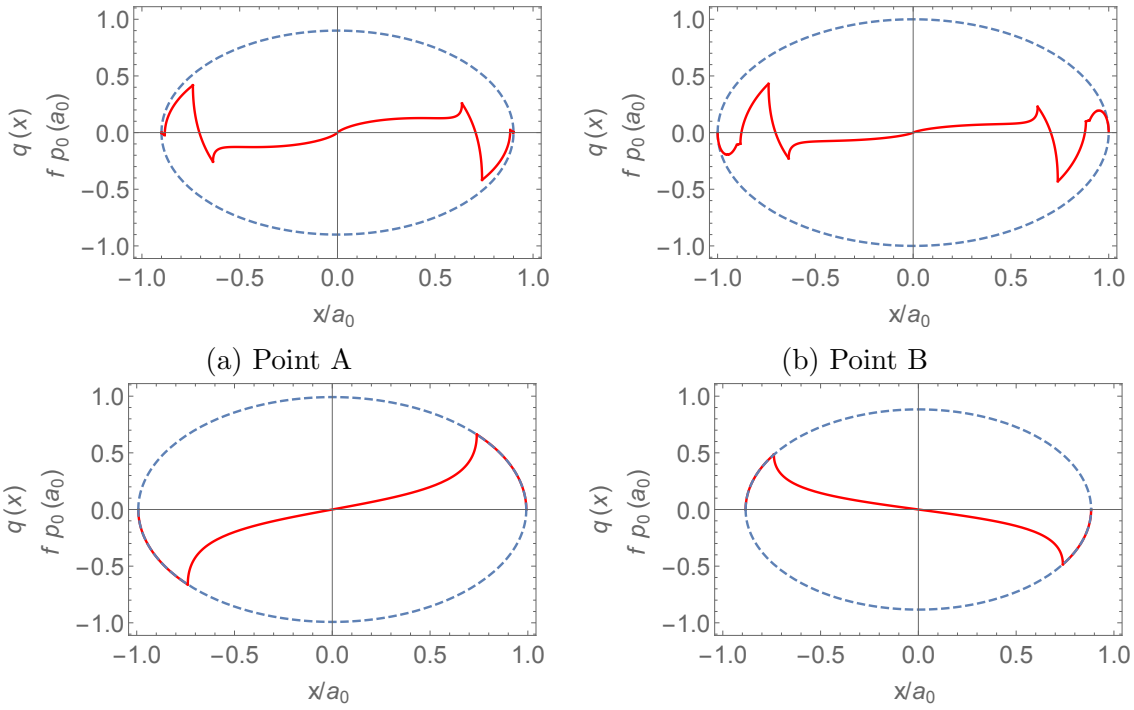
The shear traction and the size of stick zone in an incomplete contact subject to a varying normal load and bulk tension solution may be found using the superposition procedure outlined above. The procedure is illustrated for a Hertzian contact taken around an elliptic load path in $a - \sigma$ space. There are four distinct regions in the contact interface moving around a loading cycle. It is not obvious which region will have the greatest energy dissipation. The size of the permanent stick zone is independent of the initial loading trajectory, which is also true for the case for the $P - Q$ problem. The limitation of the method is that it cannot be extended to problems that include a shear force.



(a) Point A (b) Point B

(c) Point C (d) Point D

Figure 4.10: Tractions in the first cycle



(a) Point A (b) Point B

(c) Point C (d) Point D

Figure 4.11: Tractions in the steady state cycle

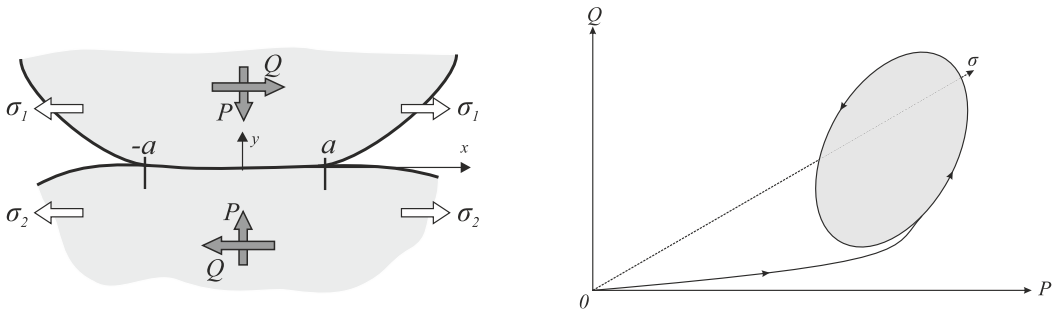
5 Varying normal load with a shear force and bulk tension

Chapter 4 showed a graphical method of solving the varying normal load and bulk tension problem. The limitation of the method is that it cannot be extended to problems that also include a shear force. This chapter extends the method developed in Chapter 3 to solve problems where the normal load varies along with both a shear force and bulk tension.

5.1 Introduction

The study of incomplete contact problems with a varying normal load began with Mindlin and Deresiewicz [61] who looked at the effect of proportional loading on the shear traction. More than half a century later, further progress was made on the subject by Barber et al. [50], who noted that the Ciavarella-Jäger theorem continues to apply in problems where the normal load, $P(t)$, and shear force, $Q(t)$, vary with time. Although the problem is quasi-static so that rates of change are not important, the influence of time is significant as it determines the sequence of loading. Using the same underlying method, Chapter 4 solves a similar problem with a varying normal load and bulk tension [51].

In chapter 2, it was shown that partial slip problems can be solved by starting with a fully stuck solution and introducing a dislocation correction [62]. In chapter 3 the method was extended to problems with both a shear force and bulk tension [63]. Here the method is further extended to handle a varying normal load. The desired output is the size and location of the stick zone, as well as the strain in the slip zone for any contact capable of idealisation as two half-planes, and where the loading trajectory is fully defined. An



(a) (b)

Figure 5.1: (a) Incomplete contact with loading, (b) Loading trajectory in $P - Q - \sigma$ space

example geometry with the loading applied is shown in Figure 5.1a and an example loading trajectory is shown in Figure 5.1b.

The procedure is shown first for the problem of a varying normal load and shear force, before extending to the more general problem of a varying normal load, shear force and bulk tension.

5.2 Normal load and shear force

Figure 5.2 shows an example loading trajectory in $P - Q$ space. The condition for the contact to remain fully stuck is,

$$\frac{dQ}{dP} < f. \tag{5.1}$$

The salient points to note are, point B where the gradient of loading is sufficient to cause slip and point D when the contact becomes instantaneously stuck and slip begins in the reverse direction.

The proposed method starts from the fully stuck solution and introduces slip through distributed dislocations in the slip zone. The following conditions must be satisfied by the correction,

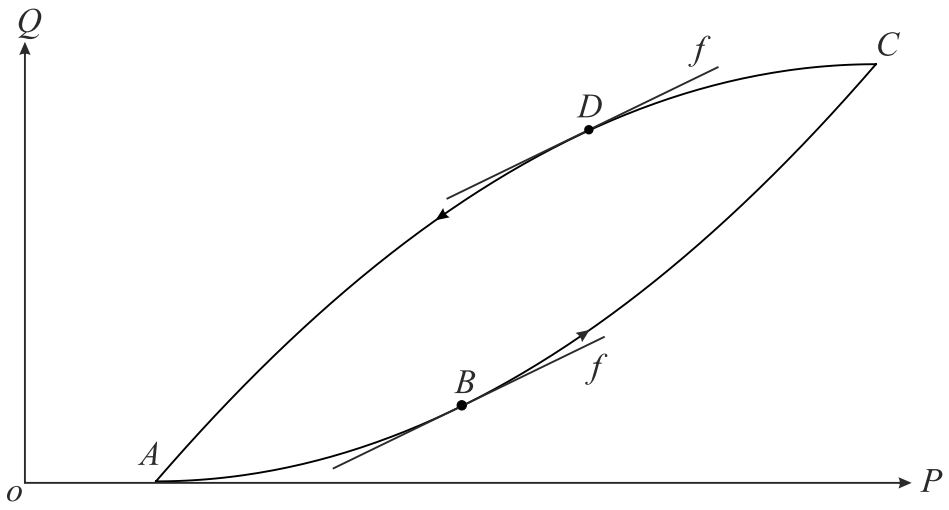


Figure 5.2: Loading trajectory in $P - Q$ space

$$\left.\frac{du}{dx}\right|_c = 0; \quad |x| \leq b, \tag{5.2}$$

$$q_c(x) = 0; \quad |x| > a. \tag{5.3}$$

The first condition comes from the fact that the fully stuck traction contains the correct strain in the stick zone. The second condition states that the corrective traction should be zero outside of the contact interface. The shear traction is the sum of the fully stuck traction and the corrective term,

$$q(x) = q_{st}(x) + q_c(x). \tag{5.4}$$

5.2.1 Increasing normal load $A \rightarrow C$

The fully stuck solution is found by superimposing flat ended punches [52],

$$q_{st}(x) = \frac{1}{\pi}\int_{|x|}^{a} \frac{dQ}{ds}\frac{ds}{\sqrt{s^2 - x^2}}; \quad |x| \leq a, \tag{5.5}$$

where the gradient of loading is lower than the coefficient of friction ($A \rightarrow B$), there is no slip. From B to C, there is slip at both edges of the contact. Substituting $q(x) = fp(x)$

into Equation 5.4 in the slip zone results in,

$$q_c(x) = fp(x) - \frac{1}{\pi}\int_{|x|}^{a} \frac{dQ}{ds}\frac{ds}{\sqrt{s^2 - x^2}}; \quad b \leq |x| \leq a. \tag{5.6}$$

An integral equation can be formed where the displacement density, $B_x(x)$, is the primary unknown,

$$q_c(x) = \frac{E^*}{2\pi\sqrt{a^2 - x^2}}\left[\int_b^a \frac{\sqrt{a^2 - \xi^2}B_x(\xi)}{\xi - x}d\xi + \int_{-a}^{-b} \frac{\sqrt{a^2 - \xi^2}B_x(\xi)}{\xi - x}d\xi\right]. \tag{5.7}$$

It can be inverted using the method developed by Moore et al. [63],

$$B_x(x) = \frac{-2Sign(x)}{E^*\pi}\sqrt{x^2 - b^2}\left[\int_b^a \frac{q_c(\xi)d\xi}{\sqrt{\xi^2 - b^2}(\xi - x)} - \int_{-a}^{-b} \frac{q_c(\xi)d\xi}{\sqrt{\xi^2 - b^2}(\xi - x)}\right]; \quad b \leq |x| \leq a. \tag{5.8}$$

The side condition from the inversion must be evaluated to find b,

$$\int_b^a \frac{sq_c(s)ds}{\sqrt{s^2 - b^2}} = 0. \tag{5.9}$$

The overall slip displacement is the sum of $B_x(x)$ with the displacements accumulated in the fully stuck phase,

$$\frac{du}{dx} = \left.\frac{du}{dx}\right|_{st} + B_x(x); \quad |x| \leq a. \tag{5.10}$$

Where [52],

$$\left.\frac{du}{dx}\right|_{st} = \frac{(\kappa + 1)Sign(x)}{2\pi\mu}\int_0^{|x|} \frac{dQ}{ds}\frac{ds}{\sqrt{x^2 - s^2}}. \tag{5.11}$$

5.2.2 Decreasing normal load $C \rightarrow D$

At a typical point, X, when the normal load is decreasing but the gradient is less than f, the fully stuck traction is given by,

$$q_{st}(x) = \frac{1}{\pi}\int_{|x|}^{a} \frac{dQ}{ds}\frac{ds}{\sqrt{s^2 - x^2}} + \frac{Q_X - Q_Z}{\pi\sqrt{a^2 - x^2}}. \tag{5.12}$$

The first term is the fully stuck shear traction at point Z (see Figure 5.3). Any further material that is laid down beyond a_Z is also removed. The point Z is a previous point in the load path with the same normal load. This means that the locked in strain at X is the same as Z. To account for the additional shear force at X an additional term is required, which does not change the locked in displacements. This is achieved by the second term. The same procedure as in the increasing normal load problem is used to find the slip stick boundary and the strain in the contact interface.

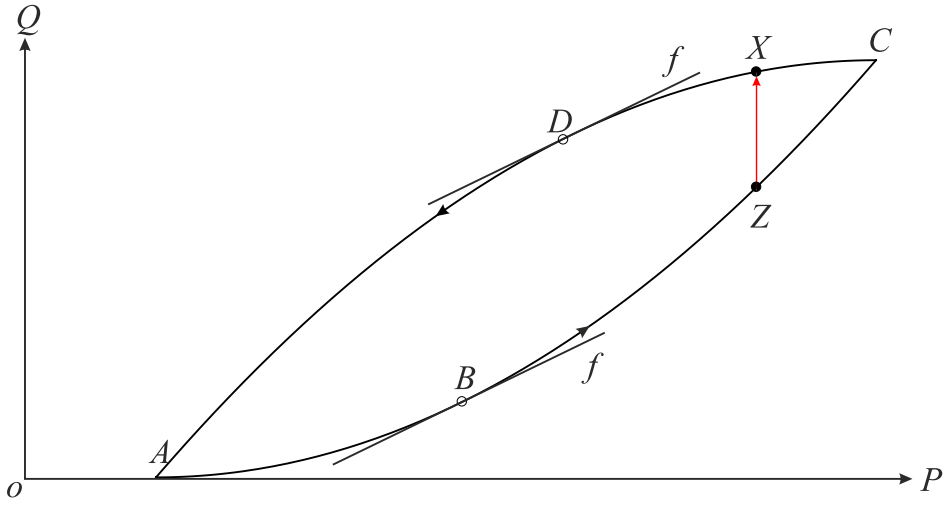


Figure 5.3: Loading trajectory - reversing normal load

The slip is in a forward direction until the gradient of loading reaches f, as denoted by the point D in Figure 5.3. At this point the whole contact becomes instantaneously stuck.

5.2.3 Decreasing normal load $D \to A$

The displacements accumulated up to point D, due to slip, are locked in. The dislocations that have been inserted to model slip are now considered to be part of the fully stuck solution. This can be seen in Figure 5.4 which shows the state of the contact just before it reaches the point D, where dislocations are inserted into the two slip zones. As the normal load continues to decrease, some of these locked in dislocations are erased. At a general point X, the corrective dislocations (opposite in direction) must be applied. The

fully stuck displacement at a general point X (Figure 5.5) which lies between D and A is given by,

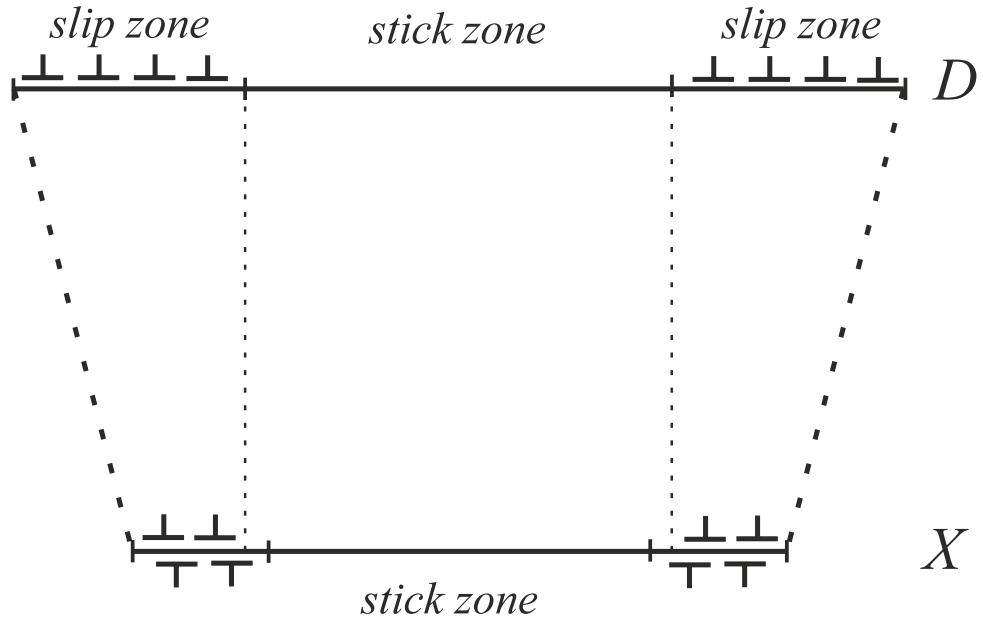


Figure 5.4: Dislocation correction between $D \rightarrow A$

$$\left.\frac{du}{dx}\right|_{st}^{X} = \left.\frac{du}{dx}\right|_{st}^{Z} + B_x^D(x). \tag{5.13}$$

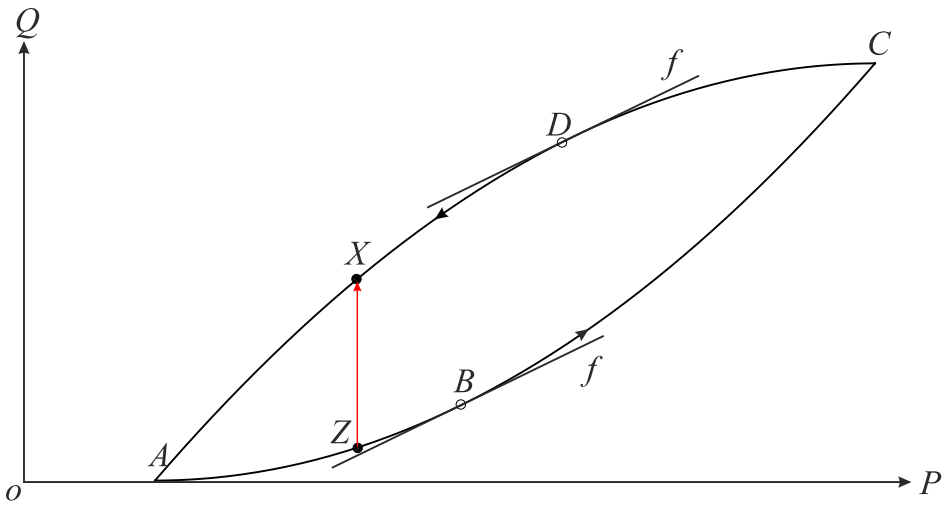


Figure 5.5: Reversing normal load - reverse slip

Analogously, the fully stuck traction is,

$$q_{st}(x) = q_{st}^{Z}(x) + \frac{E^*}{\pi\sqrt{a^2-x^2}}\int_{b_D}^{a} \frac{\sqrt{a^2-\xi^2}B_x^D(\xi)\xi}{\xi^2-x^2}d\xi + \frac{Q_X - Q_Z}{\pi\sqrt{a^2-x^2}}. \tag{5.14}$$

The first term is the fully stuck traction at the point Z as defined in Figure 5.5. The second term is the contribution from the forward slip that has been accumulated up to the point D. The slip up to this point gets locked in as the contact becomes instantaneously stuck at D. The final term is the additional shear force between point Z and point X, which has no effect on the fully stuck strain in the contact interface. Since the slip is in the opposite direction, the sliding solution is of the opposite sign, so the corrective shear traction required is,

$$q_c(x) = -fp(x) - q_{st}(x); \quad b \leq |x| \leq a. \tag{5.15}$$

5.2.4 Example problem

To illustrate the method in detail, an example loading trajectory is applied to a Hertzian contact,

$$Q(P) = \frac{(P-85)^2}{40}; \quad 85 \leq P \leq 115 \quad (A \to C), \tag{5.16}$$

$$Q(P) = -\frac{(P-115)^2}{40} + \frac{45}{2}; \quad 85 \leq P \leq 115 \quad (C \to A). \tag{5.17}$$

Equation 5.5 can be specialised to a Hertzian contact with the substitution,

$$\frac{dQ}{ds} = \frac{dQ}{dP}\frac{dP}{ds} = \frac{dQ}{dP}\frac{\pi E^* s}{2R}, \tag{5.18}$$

to get,

$$q_{st}(x) = \frac{E^*}{2R}\int_{a_A}^{a} \frac{P-85}{20}\frac{sds}{\sqrt{s^2-x^2}}; \quad |x| \leq a. \tag{5.19}$$

It is relatively straightforward to evaluate this integral,

$$q_{st}(x) = \frac{E^*}{240R^2}\sqrt{a^2-x^2}\Big[x^2\pi E^* + 2PR - 510R\Big] \\ -\frac{E^*}{240R^2}\sqrt{a_A^2-x^2}\Big[x^2\pi E^* + 2P_A R - 510R\Big]; \quad |x| \le a. \tag{5.20}$$

The corrective term is now,

$$q_c(x) = fp_0\sqrt{1-\left(\frac{x}{a}\right)^2} - \frac{E^*}{240R^2}\sqrt{a^2-x^2}\Big[x^2\pi E^* + 2PR - 510R\Big] \\ -\frac{E^*}{240R^2}\sqrt{a_A^2-x^2}\Big[x^2\pi E^* + 2P_A R - 510R\Big]; \quad b \le |x| \le a. \tag{5.21}$$

Substituting this into Equation 5.8 reveals the dislocation density,

$$B_x(x) = \frac{2fp_0\ Sign(x)}{aE^*}\sqrt{x^2-b^2} - \frac{Sign(x)}{120R^2}\sqrt{x^2-a_A^2}\Big[E^*\pi x^2 + \frac{\pi E^* a_A^2}{2} - 510R\Big]; \quad |x| \le a. \tag{5.22}$$

In order to find the strain, the locked in displacements from the fully stuck solution must be added to the dislocation density,

$$\left.\frac{du}{dx}\right|_{st} = \frac{(\kappa+1)Sign(x)}{2\pi\mu}\frac{\pi E^*}{2R}\int_{a_A}^{|x|}\frac{P-85}{20}\frac{sds}{\sqrt{x^2-s^2}}. \tag{5.23}$$

It is straightforward to evaluate this integral,

$$\left.\frac{du}{dx}\right|_{st} = \frac{Sign(x)}{120R^2}\sqrt{x^2-a_A^2}\Big[E^*\pi x^2 + \frac{\pi E^* a_A^2}{2} - 510R\Big]. \tag{5.24}$$

When Equation 5.22 is added to Equation 5.24,

$$\frac{du}{dx} = \frac{2fp_0\ Sign(x)}{aE^*}\sqrt{x^2-b^2}; \quad |x| \le a. \tag{5.25}$$

Figure 5.6 shows the size of the contact and also the estimated stick zone size, b/a over the loading trajectory. The blue stars are the solution obtained from the Barber method [50]. The letters above the black line correspond to the salient points in the loading cycle

(Figure 5.2).

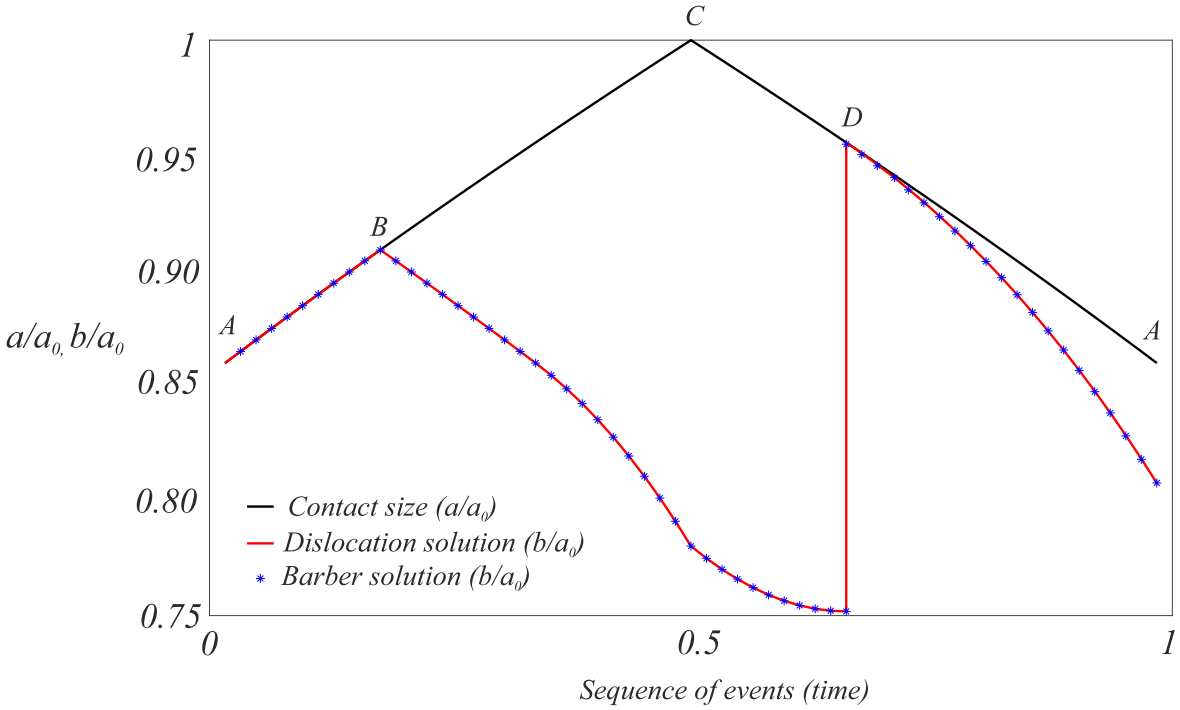


Figure 5.6: Slip-stick boundary

5.3 General loading loop

This section looks at the most general loading scenario where the normal load is varying with the presence of both a shear force and differential bulk tension. This problem cannot be solved using any of the existing analytical techniques. The method developed by Barber hinges on finding a previous point in the load history where the strain across the whole contact interface is equal to that which is locked in stick zone. As the stick zone is no longer centered, so a previous point satisfying this condition does not exist.

5.3.1 Salient points

The point B (Figure 5.2) is now two points as can be seen in Figure 5.7. This is because the condition for slip is different at each edge of the contact,

$$\frac{dQ}{dP} \pm \frac{\pi a}{4}\frac{d\sigma}{dP} < f. \tag{5.26}$$

This arises because a shear force gives rise to a symmetric shear traction, and bulk tension gives rise to an anti-symmetric shear traction. The first end to slip, B_1 is where the effect of the shear force and bulk tension are additive. At this end, slip moves inwards as the contact size increases. At the other end, the contact size increases by the same amount but all the material laid down is stuck. At point B_2 the slip condition is violated at the other edge also, and so slip moves inwards from both.

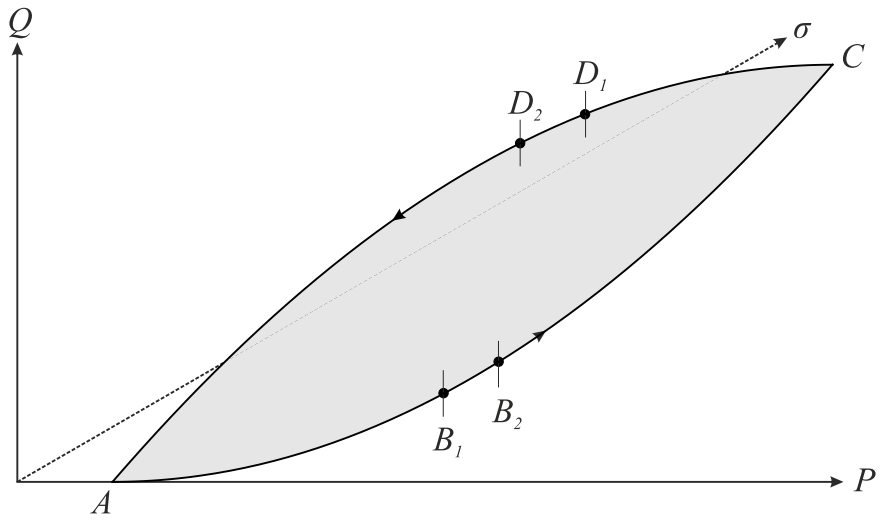


Figure 5.7: Loading trajectory - salient points

An analogous phenomenon occurs at points D_1 and D_2 where the transition from forward slip to reverse slip occurs over two points. Also note that these transitions can occur multiple times through a cycle depending on the variation in shear force and bulk tension.

5.3.2 Increasing normal load

The fully stuck shear traction can be found from superimposing flat ended punches,

$$q_{st}(x) = \frac{1}{\pi}\int_{|x|}^{a} \frac{dQ}{ds}\frac{ds}{\sqrt{s^2-x^2}} + \frac{x}{4}\int_{|x|}^{a} \frac{d\sigma}{ds}\frac{ds}{\sqrt{s^2-x^2}}; \quad |x| \leq a. \tag{5.27}$$

Before the point B_1 is reached, there is no slip. At the point B_1, slip begins at the end of the contact where the effect of the shear force and bulk tension are additive ($\frac{dQ}{dP} + \frac{\pi a}{4}\frac{d\sigma}{dP}$).

If dQ/dP, $d\sigma/dP$ and σ are positive, then it is at the right edge of the contact. The slip zone increases in size at this edge of the contact, whilst the other edge remains fully stuck. At the point B_2 the slip condition is violated at the other edge ($\frac{dQ}{dP} - \frac{\pi a}{4}\frac{d\sigma}{dP}$), so now slip occurs at both edges of the contact. The corrective traction required in the slip zones is given by,

$$q_c(x) = fp(x) - \frac{1}{\pi}\int_{|x|}^{a} \frac{dQ}{ds}\frac{ds}{\sqrt{s^2 - x^2}} - \frac{x}{4}\int_{|x|}^{a} \frac{d\sigma}{ds}\frac{ds}{\sqrt{s^2 - x^2}}; \quad b \leq |x| \leq a. \tag{5.28}$$

As in the $P - Q$ problem, dislocations are introduced in the slip zones, and an integral equation may be formed where the dislocation density is the primary unknown. Note however, that the slip zones are not symmetric. The right hand slip zone size is denoted by b_1 and the left hand slip zone is given by b_2,

$$q_c(x) = \frac{E^*}{2\pi\sqrt{a^2 - x^2}}\left[\int_{b_1}^{a} \frac{\sqrt{a^2 - \xi^2}B_x(\xi)}{\xi - x}d\xi + \int_{-a}^{-b_2} \frac{\sqrt{a^2 - \xi^2}B_x(\xi)}{\xi - x}d\xi\right]. \tag{5.29}$$

It can be inverted using the method developed by Moore et al. [63],

$$B_x(x) = \frac{-2}{E^*\pi}\sqrt{(x - b_1)(x + b_2)}\left[\int_{b_1}^{a} \frac{q_c(\xi)d\xi}{\sqrt{(\xi - b_1)(\xi + b_2)}(\xi - x)} - \int_{-a}^{-b_2} \frac{q_c(\xi)d\xi}{\sqrt{(\xi - b_1)(\xi + b_2)}(\xi - x)}\right]; \quad b_1 \leq x \leq a, \tag{5.30}$$

$$B_x(x) = \frac{2}{E^*\pi}\sqrt{(x - b_1)(x + b_2)}\left[\int_{b_1}^{a} \frac{q_c(\xi)d\xi}{\sqrt{(\xi - b_1)(\xi + b_2)}(\xi - x)} - \int_{-a}^{-b_2} \frac{q_c(\xi)d\xi}{\sqrt{(\xi - b_1)(\xi + b_2)}(\xi - x)}\right]; \quad -a \leq x \leq -b_2. \tag{5.31}$$

The two side conditions generated from the inversion determine the slip-stick boundaries, and they are

$$\int_{-a}^{-b_2} \frac{q_c(s)ds}{\sqrt{(s - b_1)(s + b_2)}} - \int_{b_1}^{a} \frac{q_c(s)ds}{\sqrt{(s - b_1)(s + b_2)}} = 0, \tag{5.32}$$

$$\int_{-a}^{-b_2} \frac{q_c(s)sds}{\sqrt{(s-b_1)(s+b_2)}} - \int_{b_1}^{a} \frac{q_c(s)sds}{\sqrt{(s-b_1)(s+b_2)}} = 0. \tag{5.33}$$

The overall slip displacement is the sum of the dislocation density with the displacements accumulated in the fully stuck phase,

$$\frac{du}{dx} = \left.\frac{du}{dx}\right|_{st} + B_x(x); \quad |x| \leq a. \tag{5.34}$$

as given by Hills et al. [52],

$$\left.\frac{du}{dx}\right|_{st} = \frac{(\kappa+1)Sign(x)}{2\pi\mu} \int_0^{|x|} \frac{dQ}{ds} \frac{ds}{\sqrt{x^2-s^2}} + \frac{(\kappa+1)|x|}{8\mu} \int_0^{|x|} \frac{d\sigma}{ds} \frac{ds}{\sqrt{x^2-s^2}}. \tag{5.35}$$

5.3.3 Decreasing normal load $C \rightarrow D_1$

The method for this part of the loading is identical to the $P-Q$ problem except now the fully stuck traction is given by,

$$q_{st}(x) = \frac{1}{\pi} \int_{|x|}^{a} \frac{dQ}{ds} \frac{ds}{\sqrt{s^2-x^2}} + \frac{x}{4} \int_{|x|}^{a} \frac{d\sigma}{ds} \frac{ds}{\sqrt{s^2-x^2}} + \frac{Q_X - Q_Z}{\pi\sqrt{a^2-x^2}} + x\frac{\sigma_X - \sigma_Z}{4\sqrt{a^2-x^2}}. \tag{5.36}$$

5.3.4 Decreasing normal load $D_1 \rightarrow D_2$

At the point D_1, the *right hand* edge of the contact becomes instantaneously stuck. Reverse slip begins at this edge, whilst the left hand edge continues to slip in the forwards direction. As shown in Figure 5.8, the dislocations that are inserted at the point D_1 become locked in, and further dislocations must be included to introduce the slip that occurs after this point. The dislocations inserted on the right hand side of the contact are opposite in sign from the existing dislocations, because the slip is in the opposite direction.

The fully stuck traction is given by,

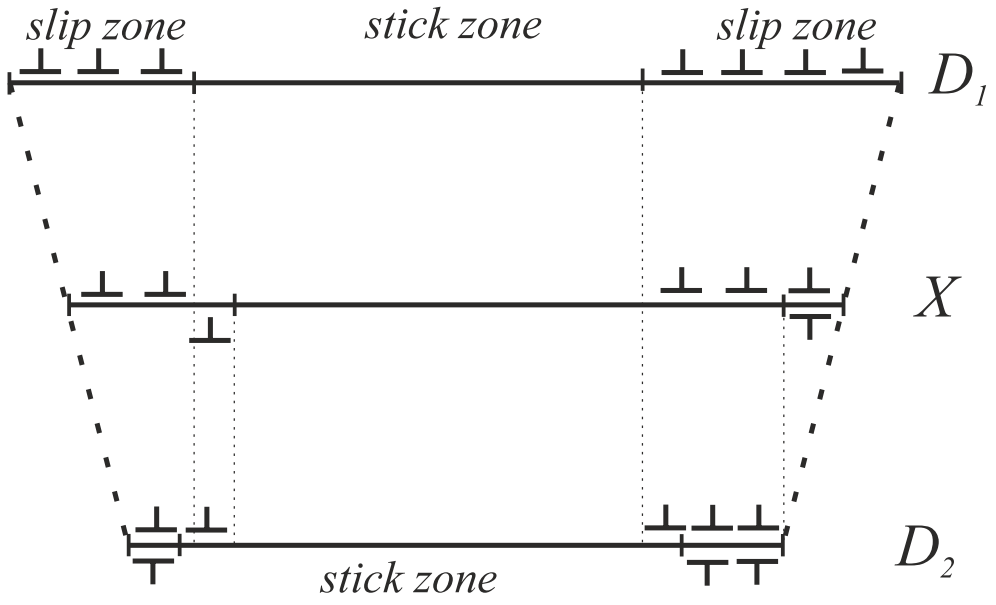


Figure 5.8: Dislocation correction $D_1 \rightarrow D_2$

$$q_{st}(x) = q_{st}^{Z}(x) + \frac{E^*}{2\pi\sqrt{a^2-x^2}}\int_{b_1^D}^{a} \frac{\sqrt{a^2-\xi^2}B_x(\xi)}{\xi - x}d\xi + \frac{Q_X - Q_Z}{\pi\sqrt{a^2-x^2}} + x\frac{\sigma_X - \sigma_Z}{4\sqrt{a^2-x^2}}, \quad (5.37)$$

where the point Z is defined as a previous point in the load space with the same normal load. The second term is from the dislocations locked in at D_1, and hence the lower limit on the integral corresponds to the stick zone size at D_1. The final two terms correct for the difference in shear force and bulk tension between the points Z and X, but they have no effect on the differential strain. Since the slip is in the opposite direction at each edge of the contact, the corrective shear traction required is,

$$q_c(x) = -Sign(x)fp(x) - q_{st}(x); \quad b \leq |x| \leq a. \quad (5.38)$$

5.3.5 Decreasing normal load $D_2 \rightarrow A$

At the point D_2, the left hand edge of the contact becomes instantaneously stuck and slip begins in the reverse direction. The right hand edge continues to slip in the reverse direction, as it has been doing since the point D_1. In this region, the fully stuck traction

is given by,

$$q_{st}(x) = q_{st}^{Z}(x) + \frac{E^*}{2\pi\sqrt{a^2-x^2}}\left[\int_{b_1^{D_1}}^{a} \frac{\sqrt{a^2-\xi^2}B_x(\xi)}{\xi - x}d\xi + \int_{-a}^{-b_2^{D_2}} \frac{\sqrt{a^2-\xi^2}B_x(\xi)}{\xi - x}d\xi\right] + \frac{Q_X - Q_Z}{\pi\sqrt{a^2-x^2}} + x\frac{\sigma_X - \sigma_Z}{4\sqrt{a^2-x^2}}. \tag{5.39}$$

There is now reverse slip in both directions and so the corrective traction is given by,

$$q_c(x) = -fp(x) - q_{st}(x); \quad b \leq |x| \leq a. \tag{5.40}$$

5.4 Example problem

To illustrate the method in greater depth, a simple example problem is considered, a straight line loading trajectory in $P - Q - \sigma$ space (Figure 5.9),

$$Q(P) = \frac{3P}{4}; \quad 85 \leq P \leq 115, \tag{5.41}$$

$$\sigma(P) = \frac{3P}{4}; \quad 85 \leq P \leq 115. \tag{5.42}$$

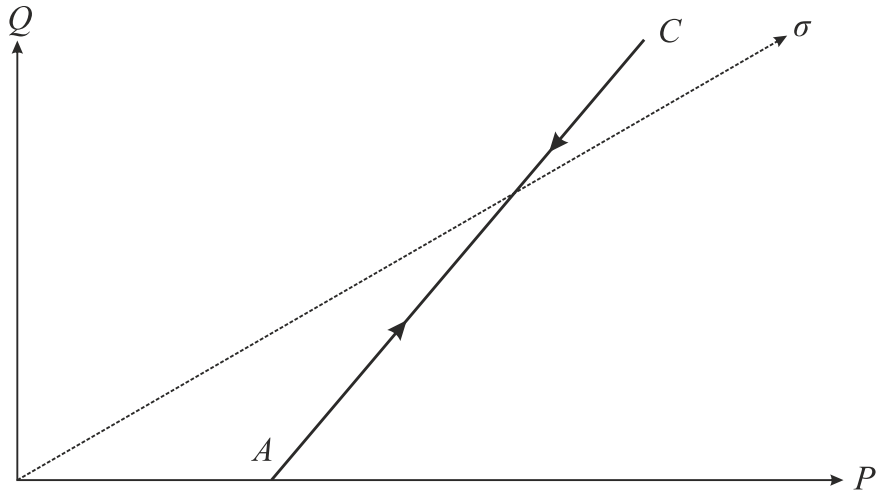


Figure 5.9: Example loading trajectory

Many real problems have a straight line loading trajectory or have loops that can be readily approximated as a straight line. Slip starts from the same point, A, and changes direction at the same point, C. Equation 5.5 can be specialised to a Hertzian contact by substituting Equation 5.18 to get,

$$q_{st}(x) = \frac{3E^*}{8R}\int_{a_A}^{a}\frac{sds}{\sqrt{s^2-x^2}} + \frac{3x\pi E^*}{32R}\int_{a_A}^{a}\frac{sds}{\sqrt{s^2-x^2}}; \quad |x| \leq a. \tag{5.43}$$

It is relatively straightforward to evaluate this integral,

$$q_{st}(x) = \frac{3E^*}{8R}\left(\sqrt{a^2-x^2}-\sqrt{a_A^2-x^2}\right)+\frac{3x\pi E^*}{32R}\left(\sqrt{a^2-x^2}-\sqrt{a_A^2-x^2}\right); \quad |x| \leq a. \tag{5.44}$$

The corrective term is now,

$$\begin{aligned} q_c(x) = fp_0\sqrt{1-\left(\frac{x}{a}\right)^2} - \frac{3E^*}{8R}\left(\sqrt{a^2-x^2}-\sqrt{a_A^2-x^2}\right) \\ -\frac{3x\pi E^*}{32R}\left(\sqrt{a^2-x^2}-\sqrt{a_A^2-x^2}\right); \quad b \leq |x| \leq a. \end{aligned} \tag{5.45}$$

Substituting this into Equations 5.30 and 5.31 reveals the dislocation density,

$$B_x(x) = \frac{2fp_0\ Sign(x)}{aE^*}\sqrt{(x-b_1)(x+b_2)}-\frac{3Sign(x)}{4R}\sqrt{x^2-a_A^2}-\frac{3|x|\pi}{16R}\sqrt{x^2-a_A^2}; \quad |x| \leq a. \tag{5.46}$$

In order to find the strain, the locked in displacements from the fully stuck solution must be added to the dislocation density,

$$\left.\frac{du}{dx}\right|_{st} = \frac{3(\kappa+1)Sign(x)}{8\pi\mu}\frac{\pi E^*}{2R}\int_{a_A}^{|x|}\frac{sds}{\sqrt{x^2-s^2}} + \frac{3(\kappa+1)|x|}{32\mu}\frac{\pi E^*}{2R}\int_{a_A}^{|x|}\frac{sds}{\sqrt{x^2-s^2}}. \tag{5.47}$$

It is straightforward to evaluate this integral,

$$\left.\frac{du}{dx}\right|_{st} = \frac{3Sign(x)}{4R}\sqrt{x^2 - a_A^2} + \frac{3|x|\pi}{16R}\sqrt{x^2 - a_A^2}. \tag{5.48}$$

When Equation 5.46 is added to Equation 5.24, the strain is,

$$\frac{du}{dx} = \frac{2fp_0\ Sign(x)}{aE^*}\sqrt{(x - b_1)(x + b_2)} \quad |x| \leq a. \tag{5.49}$$

Figure 5.10 shows the size of the contact and also the estimated stick zone size, b_1/a and b_2/a over the loading trajectory.

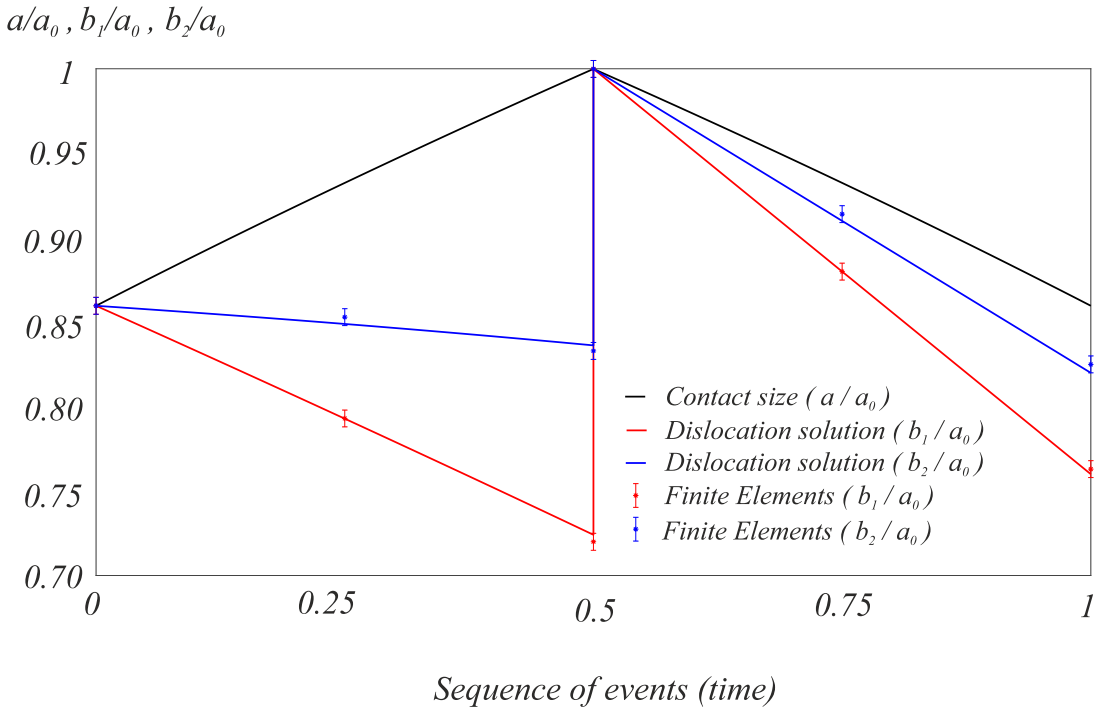


Figure 5.10: Slip-stick boundary

The dislocation solution is compared to results from a finite element model shown by the data points with error bars in Figure 5.10. The finite element simulation was carried out in Abaqus. The contacting bodies in the model are one hundred times larger than the contact patch so they approximate a half-plane as closely as possible. The material is assumed to be linear elastic and despite regions of high stress, plasticity is not modelled. The mesh elements are one hundredth of the contact patch to give accuracy in finding the slip-stick interface. The contact uses a Lagrange contact algorithm which has been proven to give greater accuracy compared to other algorithms such as Penalty.

5.5 Numerical challenges

The examples given in this thesis are all for a Hertzian contact with load paths that allow for a fully analytical solution. However, there are many instances where a numerical solution is required. This may be if the contact geometry does not have a closed form normal traction or contact law. It may also be because the loading trajectory is complex and the integrals for the fully stuck traction cannot be evaluated in closed form. In these cases, numerical schemes can be used to find the solution to the problem. The optimal scheme for evaluating the Cauchy Principal Value problems is the Gauss-Chebychev scheme used by Erdogan [59].

The scheme reduces the integral equation to a set of algebraic equations. The solution is evaluated at a finite number of points, N, over the region of interest. The scheme is accurate for values of N greater than 20. A limitation of the scheme is that the end point behaviour must be known a priori, which can either be singular or bounded.

For problems where both ends are singular, the number of equations is equal to the number of unknown variables. The end points are fixed, and the solution can be found from solving the equations. However, in problems where both the ends are bounded, the end points must be determined. In such problems there an extra equation and solving it independently determines the end points. Further details can be found in the book by Hills et al. [53].

The method works well when the normal load is increasing but during the part of the load cycle where the normal load is decreasing, problems will arise due to the layering of dislocations on top of each other. The challenge with the numerical schema is that there are fixed evaluation points. The next layer of dislocations is unlikely to correspond to those exact points. The interpolation formulation by Krenk [64] must be used to correctly evaluate the numerical solutions when layering them.

5.6 Summary

This chapter outlines how the dislocation method can be used to solve partial slip problems with a varying normal and shear load with a bulk tension. A simple example problem is given for a Hertzian contact which shows good agreement with the finite element method. The slip zone is always larger on the side of the contact where the shear force and bulk tension are additive.

6 Conclusions

The motivation for this thesis is to model better the effect of the loads experienced by contacts. The new method studied in this thesis allows for a much more realistic model of these problems which should improve the lifing prediction of components.

There are three main conclusions that can be drawn from this thesis: there are four different methods to solve incomplete contact problems in partial slip; a problem with a varying normal load and bulk tension may be solved by using a corrective traction to the sliding solution; a problem with a varying normal load, bulk tension and shear force may be solved using a dislocation correction to the fully stuck solution.

6.1 Methods to solve incomplete contact problems in partial slip

Historically, partial slip contact problems have been solved by using a shear traction correction to the sliding solution. The sliding solution ensures that the shear traction in the slip zones is correct and the corrective term must ensure that the displacements in the stick zone are correct. In this thesis, three other methods are found which use either a sliding or fully stuck solution as the starting point and use either a traction or dislocation correction. The most promising method is using a dislocation correction to the fully stuck solution. This method does not rely on symmetry (or anti-symmetry) of the shear traction and so may be applied to a problem where both bulk tension and shear force are varying.

The advantage with the dislocation correction to the fully stuck solution (4) is that it can

handle problems where the shear traction is not symmetric. It is more difficult to apply compared to the graphical methods developed. Finding the distribution of dislocations involves the solution to some complex integrals. However, the simpler graphical methods cannot handle the cases where both the shear force and bulk tension vary with the normal load. The two methods discussed briefly (2,3) have the disadvantage that two sets of corrections are required and these corrections need to be made over the entire contact area.

6.2 Varying normal load and bulk tension

Barber et al. [50] developed a graphical procedure to solve problems where both the normal load and shear force are varying with time. In this thesis, a similar solution is found for a varying normal load and bulk tension but in the absence of a shear force. It makes use of a similar technique where a corrective traction to the sliding solution is sought. It is found that there is a permanent stick zone, much like in the $P-Q$ problem. The solution is strongly dependent on the contact geometry unlike in the $P-Q$ problem. This method has the advantage of being very simple to implement for any load trajectory, since it is graphical. The downside is that the solution for the sequential loading problem must be known. The line used to find the size of the stick zone depends strongly on the contact geometry. This method cannot be extended to problems that also include a shear force hence why the dislocation method is so appealing despite the increased complexity.

6.3 Varying normal load, bulk tension and shear force

The method of using a traction correction to the sliding solution cannot handle problems where the normal load, bulk tension and shear force are varying. The varying normal load means that the displacement that must be preserved in the stick zone is non-trivial. For problems where only the shear force or bulk tension is present, the stick zone is centred on the origin; and so a previous point in the load trajectory can be found where the whole contact interface is equal to the stick zone size. However, the presence of both a shear

force and bulk tension means that the stick zone is no longer centred around the origin, and there may not be a previous point in the load trajectory which is equal to the stick zone.

The problem is solved by starting with the fully stuck solution, which automatically preserves the displacement in the stick zone. Dislocations are inserted in the slip zone to ensure the correct shear traction is present in the slip zones.

7 Further work

The new method developed in this thesis to solve incomplete contact problems has the potential to be expanded in a number of ways:

1. **Unsymmetric geometry:** The method has been shown to be able to handle an unsymmetric shear traction that arises due to mixed tangential loading. It is obvious that there exist other scenarios where the contacting body may itself not be symmetric - this gives rise to an unsymmetric normal and shear traction.

2. **Moment:** Similar to an unsymmetric contact profile, if a moment is introduced (rolling), the shear and normal traction will not be symmetric. It should be possible to use the method presented in this thesis to consider such problems. The challenge lies in finding the fully stuck traction for such loading.

These extensions allow for more accurate modeling of engineering contacts which will help to better estimate fretting fatigue and therefore improve lifing predictions.
The results obtained in this thesis also need to be experimentally verified through fretting fatigue tests. The challenge with both of these extensions to the work lies in finding a fully stuck contact solution for unsymmetric geometries. This involves generalising the Mossakovski solution that is currently being used to find the fully stuck solution.
The purpose of the tests is to show that the predicted shear tractions match test results. However there are a number of challenges:

1. The stress may not be directly measured but must be done through strain measurements.

2. These measurements must be made in-situ as stopping the experiment will cause a relaxation of the contact.

3. The displacements are very small and so to get a meaningful measurement the contact must be made very large. This means that very large actuators are required to produce the forces needed to cause partial slip.

4. The measurements cannot be made at the ends as the calculations assume plane-strain so either one of the bodies must be transparent or x-ray techniques must be used to see into the material.

Another way to test the predictions is to run thousands of load cycles and look for the development of cracks and study if the origin of the cracks is where the analytical result predicts: the point of maximum energy dissipation. There are two challenges, the first is that crack nucleation is complicated, and it is difficult to see exactly where it originated; the second is that repeated loading will cause a change in the surface, altering the coefficient of friction. It is not obvious which coefficient of friction should be used in the analytical model.

Bibliography

[1] R. Rajasekaran. *Analysis of dovetails for fretting fatigue*. PhD thesis, University of Oxford, 2005.

[2] Fan blade hub cfm56-5b. `https://www.flickr.com/photos/keleivis/2378036305`. Accessed: 2018-03-03.

[3] M. Varenberg. Towards a unified classification of wear. *Friction*, 1(4):333–340, 2013.

[4] D. A Hills and D. Nowell. *Mechanics of Fretting Fatigue*. Kulwer academic publishers, 1994.

[5] L. Ma and A. M. Korsunsky. Vector j-integral analysis of crack initiation at the edge of complete sliding contact. *Proceedings of the Royal Society A: Mathematical, Physical and Engineering Sciences*, 462:1805 – 1820, 2006.

[6] N. Pugno, M. Ciavarella, P. Cornetti, and A. Carpinteri. Generalized paris law for fatigue crack growth. *Journal of the Mechanics and Physics of Solids*, 54:1333 – 1349, 2005.

[7] F. P. E. Dunne, A. J. Wilkinson, and R. Allen. Experimental and computational studies of low cycle fatigue crack and nucleation in a polycrystal. *International Journal of Plasticity*, 23(2):273 – 295, 2007.

[8] M. Sabsabi, E. Giner, and F. J. Fuenmayor. Experimental fatigue testing of a fretting complete contact and numerical life correlation using x-fem. *International Journal of Fatigue*, 33:811 – 822, 2010.

[9] A. Mugadu, D. A. Hills, and L. Limmer. An asymptotic approach to crack initiation in fretting fatigue of complete contacts. *Journal of the Mechanics and Physics of Solids*, 50:531 – 547, 2000.

[10] D. A. Hills, A. Thaitirarot, J. R. Barber, and D. Dini. Correlation of fretting fatigue experimental results using an asymptotic approach. *International Journal of Fatigue*, 43:62 – 75, 2012.

[11] J. Dundurs. Discussion: "edge-bonded dissimilar orthogonal elastic wedges under normal and shear loading". *ASME Journal of Applied Mechanics*, 36(3):650 – 652, 1969.

[12] Cylindrical roller bearing. `http://www.wychbearings.co.uk/nu205-e-tvp3_nke.html`. Accessed: 2018-03-03.

[13] H. Deresiewicz. *R. D. Mindlin and Applied Mechanics*. New York: Pergamon Press, Inc., 1974.

[14] D. A. Spence. The hertz contact problem with finite friction. *Journal of Elasticity*, 5(3-4):297–319, 1975.

[15] C. Cattaneo. Sul contatto di due corpi elastici. *Atti Accad. naz. Lincei Rc*, 27: 342–348, 434–436, 474–478, 1938.

[16] R. D. Mindlin. Compliance of elasic bodies in contact. *ASME Journal of Applied Mechanics*, 16:249 – 268, 1949.

[17] J. R. Barber. *Elasticity*. Dordrecht, 3rd Ed., 2010.

[18] D. Dini and D. A. Hills. Bounded asymptotic solutions for incomplete contacts in partial slip. *International Journal of Solids and Structures*, 41:7049 – 7062, 2004.

[19] D. Dini, A. Sackfield, and D. A. Hills. Comprehensive bounded asymptotic solutions for incomplete contacts in partial slip. *Journal of the Mechanics and Physics of Solids*, 53(2):437 – 454, 2005.

[20] D. A. Hills, R. M. N Fleury, and D. Dini. Partial slip incomplete contacts under constant normal load and subject to periodic loading. *International Journal of Mechanical Sciences*, 108-109:115 – 121, 2016.

[21] D.A. Hills and D. Dini. What level of friction guarantees adhesion in a complete contact? *Journal of Strain Analysis*, 39(5):549–551, 2004.

[22] C.M. Churchman and D.A. Hills. General results for complete contacts subject to oscillatory shear. *Journal of the Mechanics and Physics of Solids*, 54(6):1186–1205, 2006.

[23] C.M. Churchman and D.A. Hills. Slip zone length at the edge of a complete contact. *International Journal of Solids and Structures*, 43:2037–2049, 2006.

[24] S. Karuppanan. *Analysis of Incomplete and Complete Contacts in Sliding and Partial Slip*. PhD thesis, University of Oxford, 2007.

[25] S. Karuppanan and D.A. Hills. Frictional complete contacts between elastically similar bodies subject to normal and shear load. *International Journal of Solids and Structures*, 45(17):4662 – 4675, 2008.

[26] R.C. Flicek, R. Ramesh, and D.A. Hills. A complete frictional contact: The transition from normal load to sliding. *International Journal of Engineering Science*, 92(0):18–27, 2015.

[27] R. M. N. Fleury, D. A. Hills, and J. R. Barber. A corrective solution for finding the effects of edge rounding on complete contact between elastically similar bodies. part i: Contact law and normal contact considerations. *International Journal of Solids and Structures*, 85 - 86:89 – 96, 2016.

[28] R. M. N. Fleury, D. A. Hills, and J. R. Barber. A corrective solution for finding the effects of edge rounding on complete contact between elastically similar bodies. part ii: Near-edge asymptotes and the effect of shear. *International Journal of Solids and Structures*, 85-86:97 – 104, 2016.

[29] Flanged joint. https://www.gptindustries.com/en/products/electroflange-pre-fabricated-isolating-flanges. Accessed: 2018-03-03.

[30] L. M. Keer, J. Dundurs, and K. C. Tsai. Problems involving a receding contact between a layer and a half-space. *ASME Journal of Applied Mechanics*, 39:1115 – 1120, 1972.

[31] L. M. Keer and M. A. G. Silva. Two mixed problems for a semi-infinite layer. *ASME Journal of Applied Mechanics*, 39:1121 – 1124, 1972.

[32] J. Dundurs. *Properties of elastic bodies in contact - Mechanics of contact between deformable bodies*. Delft University Press, 1975.

[33] T. Chaise, R. J. H. Paynter, and D. A. Hills. Contact analysis of a semi-infinite strip pressed into a half plane by a line force. *International Journal of Mechanical Sciences*, 81:60 – 64, 2014.

[34] Y. J. Ahn and J. R. Barber. Response of frictional receding contact problems to cyclic loading. *International Journal of Mechanical Sciences*, 50:1519 – 1525, 2008.

[35] K. S. Parel and D. A. Hills. Frictional receding contact analysis of a layer on a half-plane subjected to semi-infinite surface pressure. *International Journal of Mechanical Sciences*, 108 - 109:137 – 143, 2016.

[36] D.A. Hills, R. Ramesh, R. M. N. Fleury, and K. Parel. A unified approach for representing fretting and damage at the edges of incomplete and receding contacts. *Tribology International*, 108:16–22, 2017.

[37] M.E. Kartal, J.R. Barber, D. A. Hills, and D. Nowell. Partial slip problem for two semi-infinite strips in contact. *International Journal of Mechanical Sciences*, 49: 203–211, 2011.

[38] R. Ramesh and D. A. Hills. The condition for first slip in a common edge contact subject to in-plane & anti-plane loading. *Journal of Strain Analysis*, 50(6):386 – 390, 2015.

[39] Connecting rod. https://www.aeroflon.com/crank_shaft.html. Accessed: 2018-03-03.

[40] D. A. Hills and D. Dini. Common edge contacts: effect of interface line orientation. *International Journal of Mechanical Sciences*, 81:73–76, 2014.

[41] Z. Clark, R. Ramesh, and D. A. Hills. Edge slip zone size of misaligned common edge contacts. *Journal of Strain Analysis*, 52:450–454, 2017.

[42] A. Flamant. Sur la répartition des pressions dans un solide rectangulaire chargé transversalement. *Compte. Rendu. Acad. Sci. Paris*, 114:1465, 1892.

[43] I. N. Sneddon. *Fourier Transforms*. McGraw-Hill, 1951.

[44] M. Ciavarella, D. A. Hills, and G. Monno. The influence of rounded edges on indentation by a flat punch. *Proceedings of the Institution of Mechanical Engineers Part C – Journal of Mechanical Engineering Science*, 212:319–327, 1998.

[45] M. Ciavarella. The generalized Cattaneo partial slip plane contact problem. i - theory. *International Journal of Solids and Structures*, 35(18):2349 – 2362, 1998.

[46] J. Jäger. A new principle in contact mechanics. *ASME Journal of Tribology*, 120(4): 677 – 684, 1998.

[47] D. Nowell and D. A. Hills. Mechanics of fretting fatigue tests. *International Journal of Mechanical Sciences*, 29(5):335 – 365, 1987.

[48] M. Ciavarella and G. Macina. New results for the fretting-induced stress concentration on hertzian and flat rounded contacts. *International Journal of Mechanical Sciences*, 45:449– 467, 2003.

[49] J. Vázquez, C. Navarro, and J. Domínguez. Analytical solution for a cylindrical contact with reverse slip. *Journal of Strain Analysis*, 48(3):189–197, 2013.

[50] J. R. Barber, M. Davies, and D. A. Hills. Frictional elastic contact with periodic loading. *International Journal of Solids and Structures*, 48:2041 – 2047, 2011.

[51] R. Ramesh, J. R. Barber, and D. A. Hills. Plane incomplete contact problems subject to bulk stress with a varying normal load. *International Journal of Mechanical Sciences*, 122:228–234, 2017.

[52] D. A. Hills, M. Davies, and J. R. Barber. An incremental formulation for half-plane contact problems subject to varying normal load, shear and tension. *Journal of Strain Analysis*, 46(6):436 – 443, 2011.

[53] D.A. Hills, P.A. Kelly, D.N. Dai, and A.M. Korsunsky. *Solution of crack problems: The distributed dislocation method*. Kluwer, 1996.

[54] J. R. Rice. Limitations to the small scale yielding approximation for crack tip plasticity. *Journal of the Mechanics and Physics of Solids*, 22:17 – 26, 1974.

[55] J. A. Greenwood and P. Williamson, J. B. Contact of nominally flat surfaces. *Proceedings of the Royal Society A: Mathematical, Physical and Engineering Sciences*, 295:300–319, 1966.

[56] D. A. Hills, D. Nowell, and J. J. O'Connor. On the mechanics of fretting fatigue. *Wear*, 125:129–146, 1988.

[57] L. Gorbatikh, B. Nuller, and M. Kachanov. Sliding on cracks with non-uniform frictional characteristics. *International Journal of Solids and Structures*, 38:42–43, 2001.

[58] D. A. Hills, D. Nowell, and A. Sackfield. *Mechanics of Elastic Contacts*. Butterworth Heinemann, Jordan Hill, Oxford, 1993.

[59] F. Erdogan and G.D. Gupta. On the numerical solution of singular integral equations. *Q. Appl. Math*, 30:525–534, 1972.

[60] L. E. Andersson, J. R. Barber, and A. R. S. Ponter. Existence and uniqueness of attractors in frictional systems with uncoupled tangential displacements and normal tractions. *International Journal of Solids and Structures*, 51:3710 – 3714, 2014.

[61] R. D. Mindlin and H. Deresiewicz. Elastic spheres in contact under varying oblique forces. *ASME Journal of Applied Mechanics*, 20:327–344, 1953.

[62] D. A. Hills, R. Ramesh, J. R. Barber, and M. R. Moore. Methods to solve half-plane partial slip contact problems. *International Journal of Solids and Structures*, Accepted, 2018.

[63] M. R. Moore, R. Ramesh, D. A. Hills, and J. R. Barber. Half-plane partial slip contact problems with a constant normal load subject to a shear force and differential bulk tension. *Journal of the Mechanics and Physics of Solids*, 118:245 – 253, 2018.

[64] S. Krenk. On the use of the interpolation polynomial for solutions of singular integral equations. *Quarterly of Applied Mathematics*, 32(4):479–484, 1975.

[65] D.A. Hills and D. Dini. Characteristics of the process zone at sharp notch roots. *International Journal of Solids and Structures*, 48(14-15):2177–2183, 2011.

[66] M.L. Williams. Stress singularities resulting from various boundary conditions in angular corners of plates in extension. *ASME Journal of Applied Mechanics*, 19: 526–528, 1952.

[67] M. Costabel and M. Dauge. General edge asymptotics of solutions of second order elliptic boundary value problems *i*, *ii*. *Proceedings of Royal Society of Edinburgh*, 123A:109–155, 1993.

[68] M. Dauge. Elliptic boundary value problems in corner domains – smoothness and asymptotics of solutions. *Lecture Notes in Mathematics*, 1341, 1988.

[69] V. G. Maz'ya, S. A. Nazarov, and B. A. Plamenvskii. Evaluation of the asymptotic form of the intensity coefficient on approaching corner or conical points. *U.S.S.R computational mathematics and mathematical physics*, 23:50–58, 1983.

[70] A. Carpinteri, P. Cornetti, N. Pugno, and A. Sapora. A finite fracture mechanics approach to structures with sharp v-notches. *Engineering Fracture Mechanics*, 75(7): 1736–1752, 2008.

[71] A. Carpinteri, P. Cornetti, N. Pugno, and A. Sapora. On the most dangerous v-notch. *International Journal of Solids and Structures*, 47(7-8):887–893, 2010.

[72] S. Harding, A. Kotousov, P. Lazzarin, and F. Berto. Transverse singular effects in v-shaped notches stressed in mode ii. *International Journal of Fracture*, 164(1):1–14, 2010.

[73] G. B. Sinclair. Stress singularities in classical elasticity-i: removal, interpretation, and analysis. *Applied Mechanics Reviews*, 57:251–297, 2004.

[74] A. Carpinteri, M. Paggi, and N. Pugno. Numerical evaluation of generalized stress-intensity factors in multi-layered composites. *International Journal of Solids and Structures*, 43(3-4):627–641, 2006.

[75] B. Atzori, P. Lazzarin, and G. Meneghetti. A unified treatment of the mode i fatigue limit of components containing notches or defects. *International Journal of Fracture*, 133(1):61–87, 2005.

[76] B. Atzori, P. Lazzarin, G. Meneghetti, and M. Ricotta. Fatigue design of complex welded structures. *International Journal of Fatigue*, 31(1):59–69, 2009.

[77] D. Leguillon. A criterion for crack nucleation at a notch in homogeneous materials. *Comptes Rendus De L'Academie Des Sciences Serie II Fascicule B-Mechanique*, 329 (2):97–102, 2001.

[78] D. Leguillon. Strength or toughness? a criterion for crack onset at a notch. *European Journal of Mechanics - A/Solids*, 21(1):61–72, 2002.

[79] P. Lazzarin and S. Filippi. A generalized stress intensity factor to be applied to round v-shaped notches. *International Journal of Solids and Structures*, 43(9):2461–2478, 2006.

[80] D.B. Bogy. Two edge-bonded elastic wedges of different materials and wedge angles under surface tractions. *ASME Journal of Applied Mechanics*, 38:377–386, 1971.

[81] D.B. Bogy and K.C. Wang. Stress singularities at interface corners in bonded dissimilar isotropic elastic materials. *International Journal of Solids and Structures*, 7: 993–1005, 1971.

[82] C.C. Ma and B.L. Hour. Analysis of dissimilar anisotropic wedges subjected to antiplane shear deformation. *International Journal of Solids and Structures*, 25(11): 1295–1309, 1989.

[83] P.E.W. Labossiere and M.L. Dunn. Calculation of stress intensities at interface corners in anisotropic media. *Engineering Fracture Mechanics*, 61(5-6):635–654, 1998.

[84] M. Paggi and A. Carpinteri. On the stress singularities at multimaterial interfaces and related analogies with fluid dynamics and diffusion. *Applied Mechanics Reviews*, 61(2), 2008.

[85] R.C. Flicek, D.A. Hills, and D. Dini. Refinements in the characterisation of mode-mixity and small scale yielding at sharp notch roots. *Engineering Fracture Mechanics*, 126:73–86, 2014.

[86] D. Dini and D.A. Hills. Asymptotic characterisation of nearly-sharp notch root stress fields. *International Journal of Fracture*, 130(3):651–666, 2004.

[87] M. R. Ayatollahi, M. Dehghany, and M. Nejati. Fracture analysis of v-notched components - effects of first non-singular stress term. *International Journal of Solids and Structures*, 48(10):1579 – 1589, 2011.

[88] F. D. Gakhov. *Boundary Value Problems*. Pergamon, 1966.

A An alternative normalisation of sharp notch roots

This appendix extends the normalisation used by Hills and Dini [65] for the state of stress near sharp notch roots to include mode III loading. Sharp notches are of interest because of the stress intensification effect, which means they are likely to nucleate cracks. This work can be applied to study the edges of complete contacts.

A.1 Introduction

Figure A.1 shows a semi-infinite notch of angle 2α, with a cylindrical coordinate set r, θ, z. The state of stress in the neighbourhood of the root is written using an appropriate series representation. The classical Williams solution [66], together with the corresponding anti-plane component, emerges as the solution. The former has been built upon by many researchers (see [67, 68, 69]), and has been used extensively for estimating the plastic process zones (see [70, 71, 72, 73]) of notches and cracks. A great deal of work has also been done on evaluating stress intensity factors in increasingly complex geometries [74]. Stress intensity factors are particularly useful when determining the fatigue limit [75, 76]. Some analysis has also been carried out to determine a suitable criterion for crack nucleation, since the fatigue life of many components will be determined by crack nucleation and propagation [77, 78]. An area of special interest that has been probed is that of rounding, since no real notch can be perfectly sharp [79]. There have been many extensions, including bonded elastically dissimilar wedges [80, 81], and the effect of elastic anisotropy [82, 83, 84].

A.2 Formulation

The starting point is the representation of the stress state,

$$\sigma_{ij}(r,\theta,z) = K_I r^{\lambda_I - 1} f_{ij}^I(r,\theta,z) + K_{II} r^{\lambda_{II} - 1} f_{ij}^{II}(r,\theta,z) + K_{III} r^{\lambda_{III} - 1} f_{ij}^{III}(r,\theta,z), \quad \text{(A.1)}$$

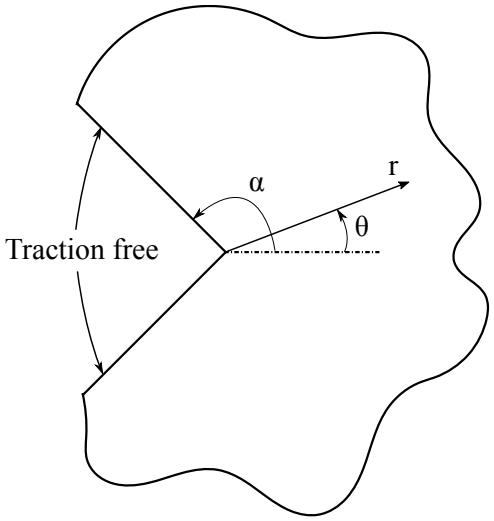


Figure A.1: Semi-infinite wedge

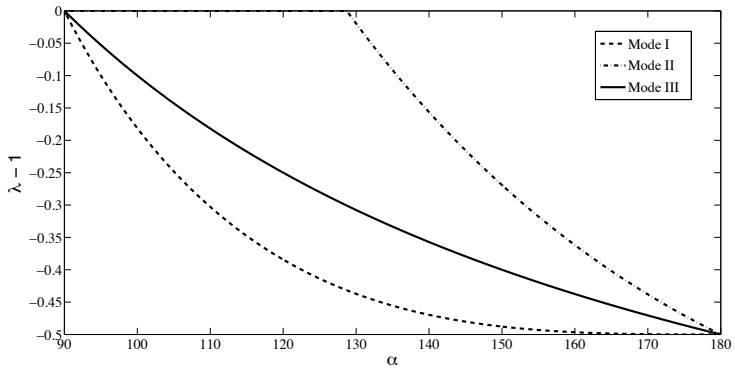


Figure A.2: Williams solution eigenvalues

where the eigenvalues $\lambda_I, \lambda_{II}, \lambda_{III}$, are known functions of α (see Figure A.2) and the eigenfunctions f_{ij}^k (given in Appendix G) are also established. Note that, excluding the solution for a crack (2α=2π), it is known that $\lambda_I < \lambda_{II} < \lambda_{III}$. It follows that there will always be some plasticity present at the notch root. If the loading is light enough and

the material is strong enough, it is always possible to establish a regime under which the process zone is mode I in character. The question arises, when under combined modes loading, under what conditions is the plasticity zone strongly mode I in character, and when is it either mixed mode or strongly dominated by one of the other eigensolutions. The geometry is a semi-infinite wedge so the results found are universal in nature. They can be applied to any finite problem and the results for mode mixity employed without further work. For the case of a notch subject only to in-plane loading, the solution has been found [65, 85]. The intention, here, is to extend this solution to the case where mode III (anti-plane) loading is present, together with at least one of the two in-plane forms of excitation. To form a consistent notation, superscripts in Arabic numerals are added to the variables d_0, G_0. So, starting with a re-iteration of the in-plane loading solution, the first two terms of Equation A.1 may be re-written in the form,

$$\frac{\sigma_{ij}(r,\theta)}{G_0^{12}} = \left(\frac{r}{d_0^{12}}\right)^{\lambda_I - 1} f_{ij}^{I}(\theta) + \left(\frac{r}{d_0^{12}}\right)^{\lambda_{II} - 1} f_{ij}^{II}(\theta), \tag{A.2}$$

where,

$$d_0^{12} = \left|\frac{K_{II}}{K_I}\right|^{\frac{1}{\lambda_I - \lambda_{II}}}, \tag{A.3}$$

$$G_0^{12} = |K_I|^{\frac{\lambda_{II}-1}{\lambda_{II}-\lambda_I}} \, |K_{II}|^{\frac{\lambda_I - 1}{\lambda_I - \lambda_{II}}} . \tag{A.4}$$

The distance d_0^{12} represents the characteristic length scale separating mode I dominant behaviour ($r << d_0^{12}$) and mode II dominant behaviour ($r >> d_0^{12}$). A quantitative way of expressing closeness to either kind of asymptotic form was found by Hills et al. [65] and later refined by Flicek and Hills [85].

Very close to the notch tip, the semi-infinite sharp notch solution dominates the stress field [86]. All practical notches will posses a finite radius; however, the statements made here remain valid at distances which are large compared to the notch radius and small compared to the nearest feature. Another point to consider is the sensitivity to the sign of the stress intensity factors. This of course practically only applies to K_I, the first mode of loading. It has been shown by Churchman et. al. [22] that closure caused by a negative

mode one stress intensity factor does not alter the geometry of the problem greatly.

So far only the singular terms have been considered in the Williams solution. This is because the stress very close to the the notch root is dominated by this term. However, it can be seen in the work by Ayatollahi [87] that the second term does have an effect on the solution. Since only distances of $r/a < 0.01$ are considered (where a is the distance to the nearest feature), it has been shown that the approximation is good.

A.2.1 Extension of formulation to mode III behaviour

By analogy with the definitions of the new parameters G_0^{12}, expressing the magnitude of loading, and d_0^{12}, giving the internal length scale:

$$d_0^{13} = \left| \frac{K_{III}}{K_I} \right|^{\frac{1}{\lambda_I - \lambda_{III}}}, \tag{A.5}$$

$$G_0^{13} = |K_I|^{\frac{\lambda_{III}-1}{\lambda_{III}-\lambda_I}} |K_{III}|^{\frac{\lambda_I - 1}{\lambda_I - \lambda_{III}}}. \tag{A.6}$$

These parameters can be used for problems with mode I and III loading. If mode I loading is absent but mode II is present, the definitions for mode II and III loading are:

$$d_0^{23} = \left| \frac{K_{III}}{K_{II}} \right|^{\frac{1}{\lambda_{II} - \lambda_{III}}}, \tag{A.7}$$

$$G_0^{23} = |K_{II}|^{\frac{\lambda_{III}-1}{\lambda_{III}-\lambda_{II}}} |K_{III}|^{\frac{\lambda_{II} - 1}{\lambda_{II} - \lambda_{III}}}. \tag{A.8}$$

By eliminating the stress intensity factors from the d_0^{ij} definitions, a relationship can be found between these characteristic lengths,

$$(d_0^{23})^{\lambda_{II}-\lambda_{III}} = \frac{(d_0^{13})^{\lambda_I - \lambda_{III}}}{(d_0^{12})^{\lambda_I - \lambda_{II}}}. \tag{A.9}$$

The relationship means that the three variables are not independent. If two of the d_0 values are known, the third is fixed. A number of interesting conclusions can be drawn from this relationship:

1. d_0^{12} always lies between d_0^{13} and d_0^{23}. Thus, all loading regimens can be classified into one of the cases $d_0^{13} < d_0^{23}$ or $d_0^{23} < d_0^{13}$.

2. For the case $d_0^{13} < d_0^{23}$, it is possible to have mode III dominance for distances that lie between d_0^{13} and d_0^{23}. When $d_0^{23} < d_0^{13}$, mode III dominance is not possible.

3. If two of the d_0 values are equal then the third must also equal this value.

4. For both categories (note 1), very close to the notch root there is mode I dominance. This is because it is the fastest decaying of the three modes.

5. For both categories (note 1), distant from the notch root there is mode II dominance. This is because it is the slowest decaying of the three modes.

Looking at the definition of d_0^{13}, it is clear that when $r < d_0^{13}$ mode I is stronger relative to mode III and the converse is true for $r > d_0^{13}$. Figures A.3 and A.4 show how single mode dominance can be deduced from these properties.

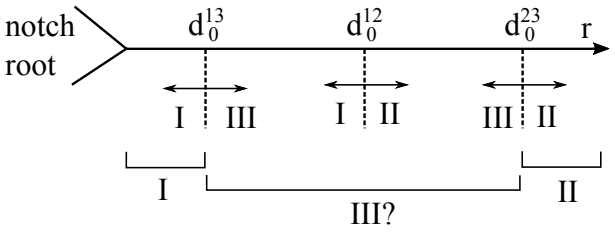


Figure A.3: Regions of single mode dominance: $d_0^{13} < d_0^{23}$

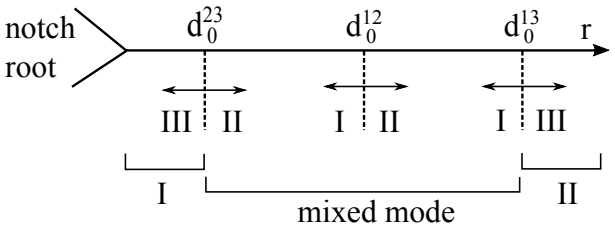


Figure A.4: Regions of single mode dominance: $d_0^{23} < d_0^{13}$

A.2.2 Characterisation of the plasticity zone

The dominance of a single mode can be found by looking at the shape of the plastic zone. This can be obtained by considering countours of the Von Mises yield criterion for

extended elastic behaviour at the notch root. The shape of these fronts can be compared to the solution for the separately excited individual modes of loading, and it is easy to determine which mode the loading is closer to. The yield condition is given by,

$$3k^2 = J_2 = \frac{1}{3}(\sigma_{11} + \sigma_{22} + \sigma_{33})^2 - \sigma_{11}\sigma_{22} - \sigma_{22}\sigma_{33} - \sigma_{11}\sigma_{33} + \sigma_{12}^2 + \sigma_{13}^2 + \sigma_{23}^2. \quad \text{(A.10)}$$

Where J_2 is the second deviatoric invariant and k is the yield stress in pure shear.

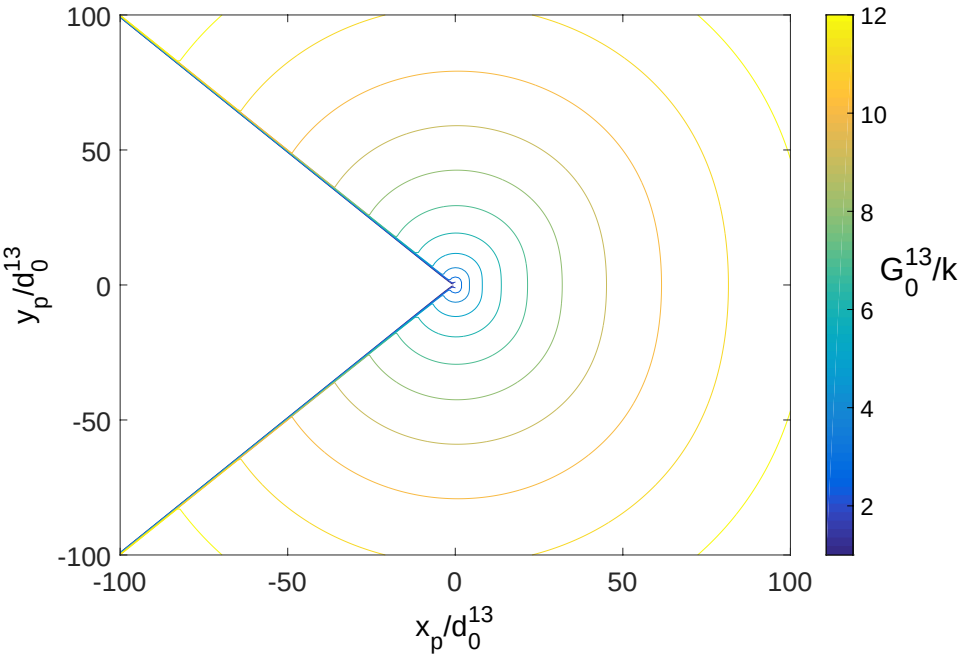
A.3 Mode I and III loading

In many ways it is easier to carry out an analysis of the proximity of the solution to mode III than it is to either mode I or mode II, simply because the implied shape of the plasticity zone is a circle. In much of what follows, an example geometry where $2\alpha = 3\pi/2$ is used to provide illustrative results. With this notch angle, $\lambda_I = 0.544484$ and $\lambda_{III} = 0.666667$ so that, at light loads the solution is mode I dominant and at high loads it is mode III dominant. The solution studied assumes tranverse plane strain, with a Poisson's ratio of 0.3.

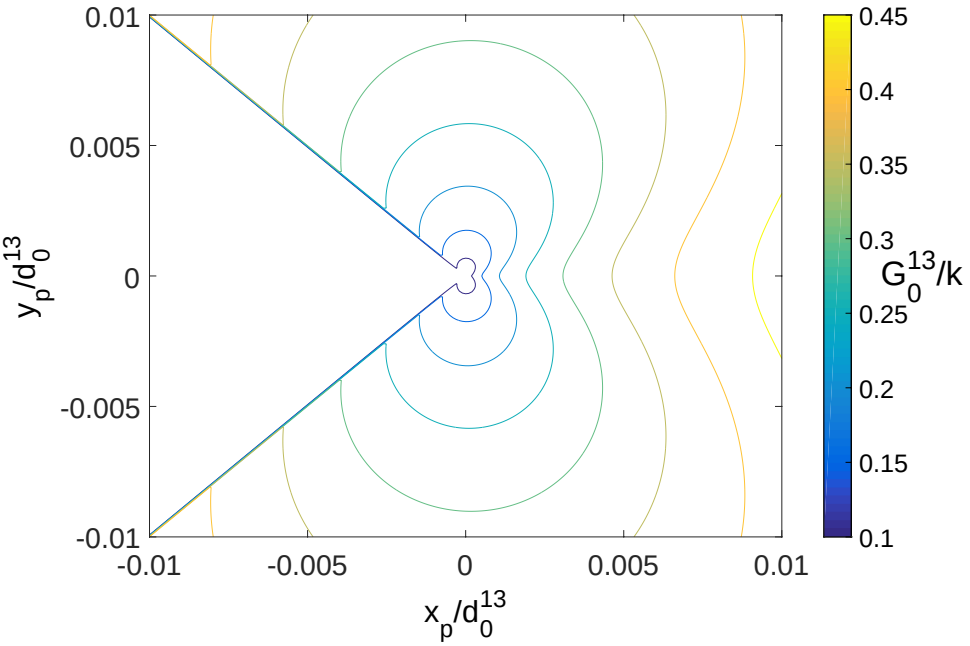
Figure A.5 shows plots which show two extreme cases of the plastic radius where there is dominance of mode III (Figure A.5a) and mode I (Figure A.5b) respectively. It can be seen that high values of G_0^{13} give rise to mode III dominance and low values give mode I dominance. This is illustrated more explicitly in Figure A.6, where the ratio of the plastic radius along $\theta = 0$ to that along $\theta = \pi/2$ is given.

For the case of pure mode III loading, $r_p(0) = r_p(\pi/2)$ whereas for mode I loading, $r_p(0) = 0.1708 r_p(\pi/2)$. Thus, the ratio $r_p(0)/r_p(\pi/2)$ would seem to be a good, simple measure of the closeness of the notch root plastic zone to either the mode I or mode III solution.

An improved estimate of mode dominance can be found by looking at the whole field rather than just at $\theta = 0$ & $\pi/2$. The percentage error is found by looking at the sum of all the squares of the error between the plastic radius of the mixed mode compared to



(a) Mode III dominance



(b) Mode I dominance

Figure A.5: Plastic radius of mixed mode loading

the pure mode normalised by the pure mode ($k = I, III$),

$$\text{fractional difference} = \frac{\int (r_p^{mm}(\theta) - r_p^k(\theta))^2 d\theta}{\int r_p^k(\theta)^2 d\theta}. \tag{A.11}$$

The difference in magnitude is quantified by the average of the mixed mode solution

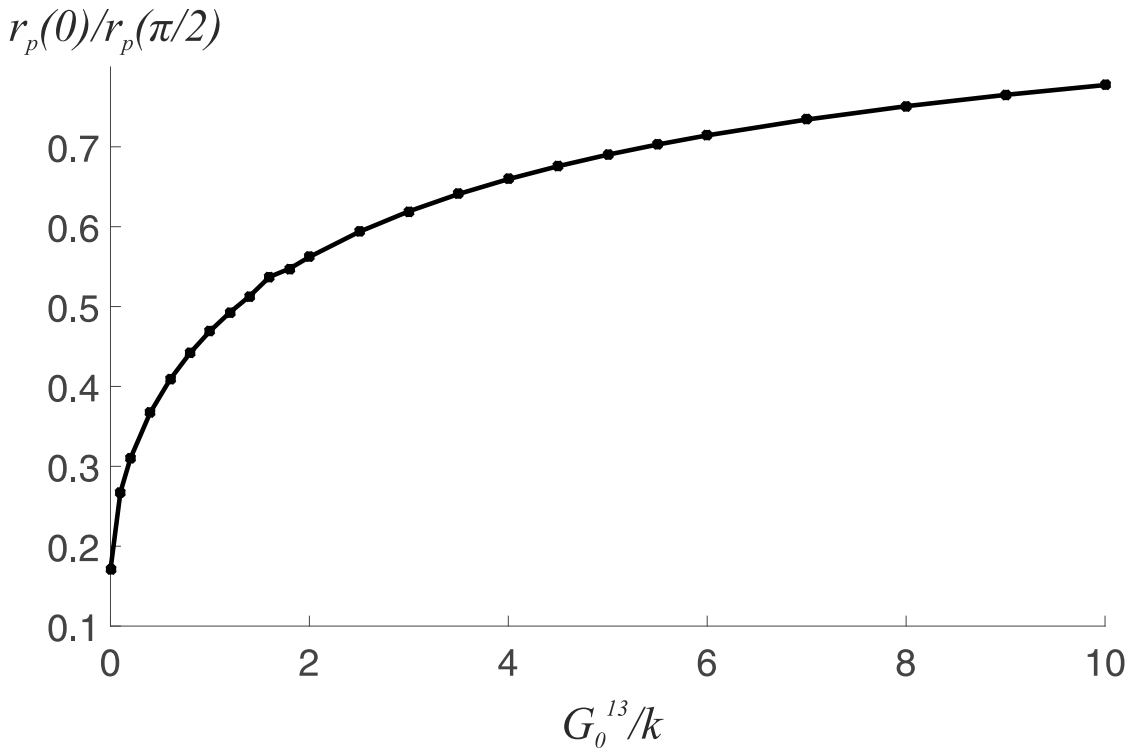


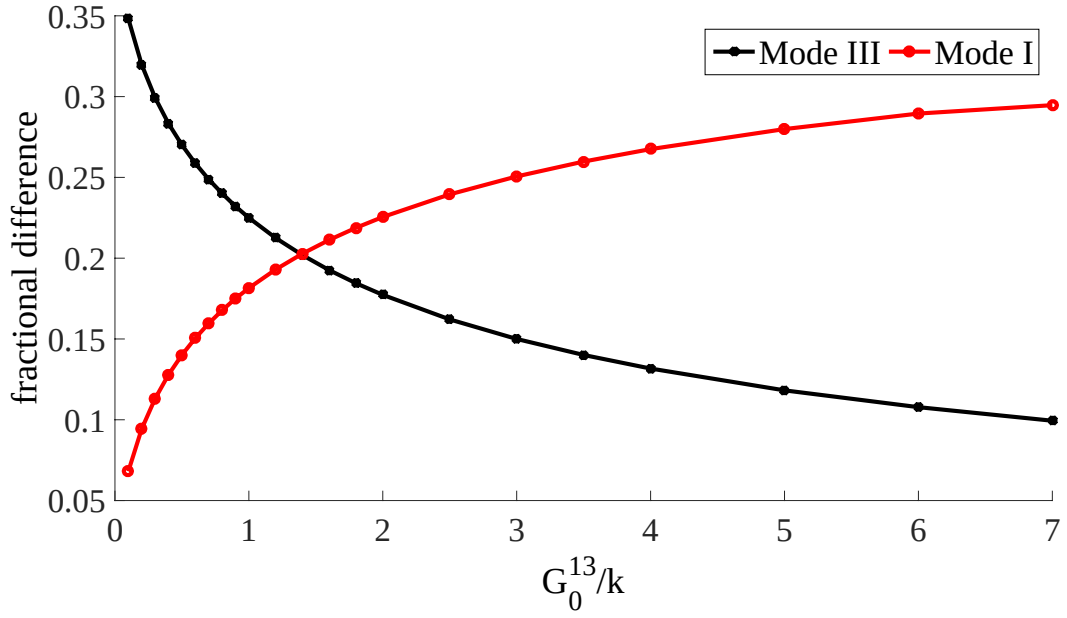
Figure A.6: Mode I and III

normalised by the average of the pure mode solution. Figure A.7 quantifies how close the mixed mode loading is to pure modes of loading (I,III).

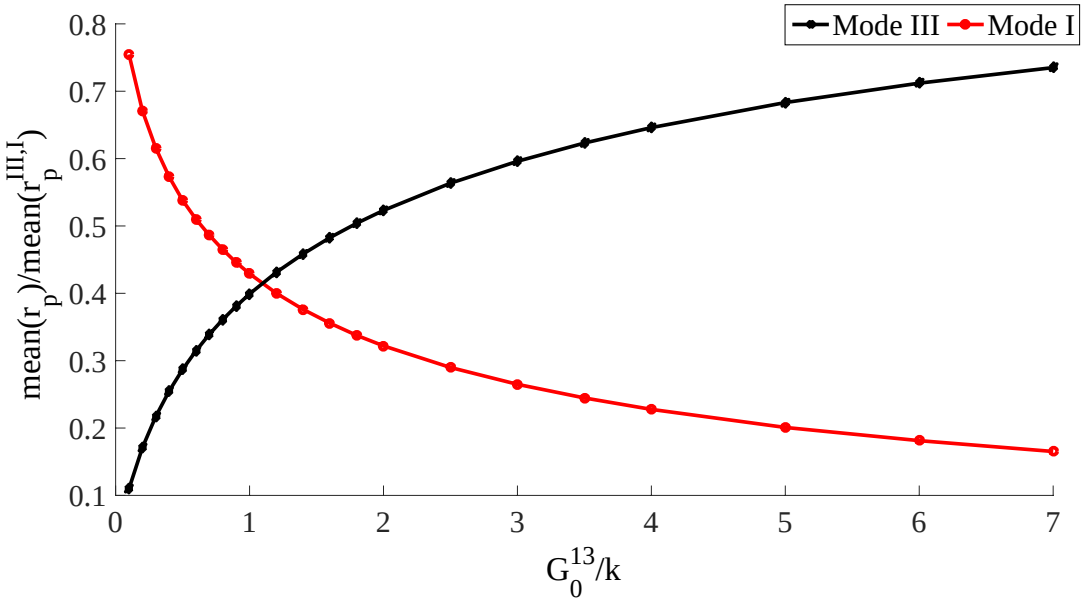
A.4 Mode II and III loading

When only mode II and III loading are present and for the example case $2\alpha = 3\pi/2$, the value of $\lambda_{II} = 0.90853$. Light loads give rise to mode III dominance and heavy loads mode II dominance. Figure A.8 shows the implied plastic zone sizes and shapes at light and heavy loads. The ratio $r_p(\pi/2)/r_p(0)$ (inverse of the ratio used before) provides a good measure of the similarity between the plastic zone shape and to pure mode III loading or pure mode II loading. The results of these calculations are summarised in Figure A.9.

Figure A.10 compares the full fields of the mixed loading problem with the pure mode solutions. There is good agreement with the comparison when only $r_p(0)$ and $r_p(\pi/2)$ are considered. A low G_0^{23}/k gives rise to mode III dominance and there is mode II



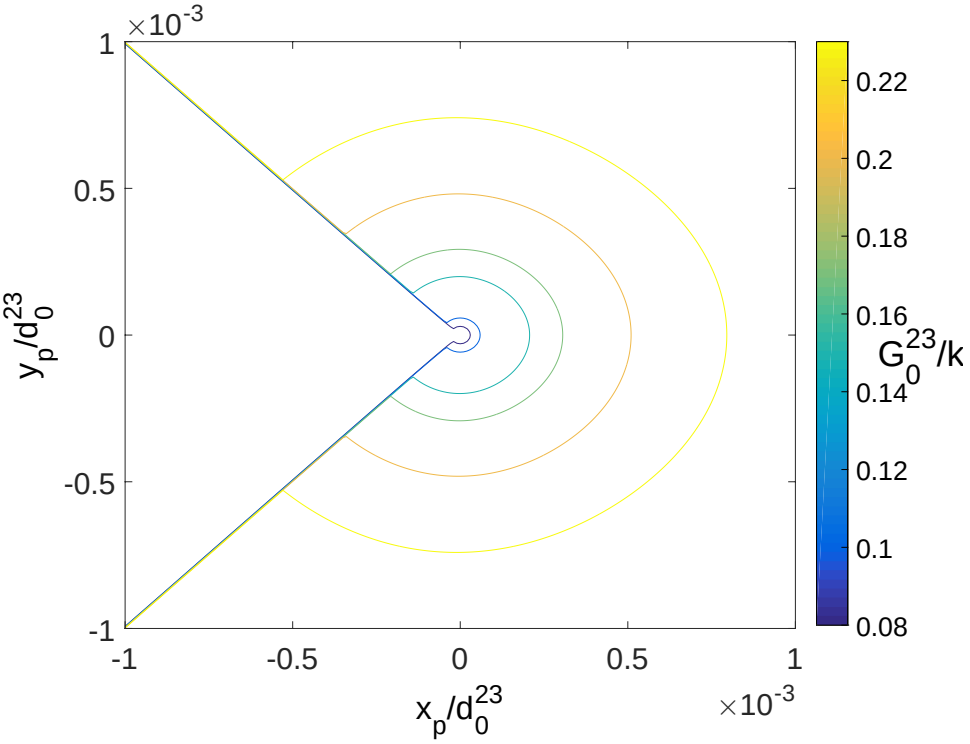
(a) Comparison of the **shape** of mixed loading to pure mode loading



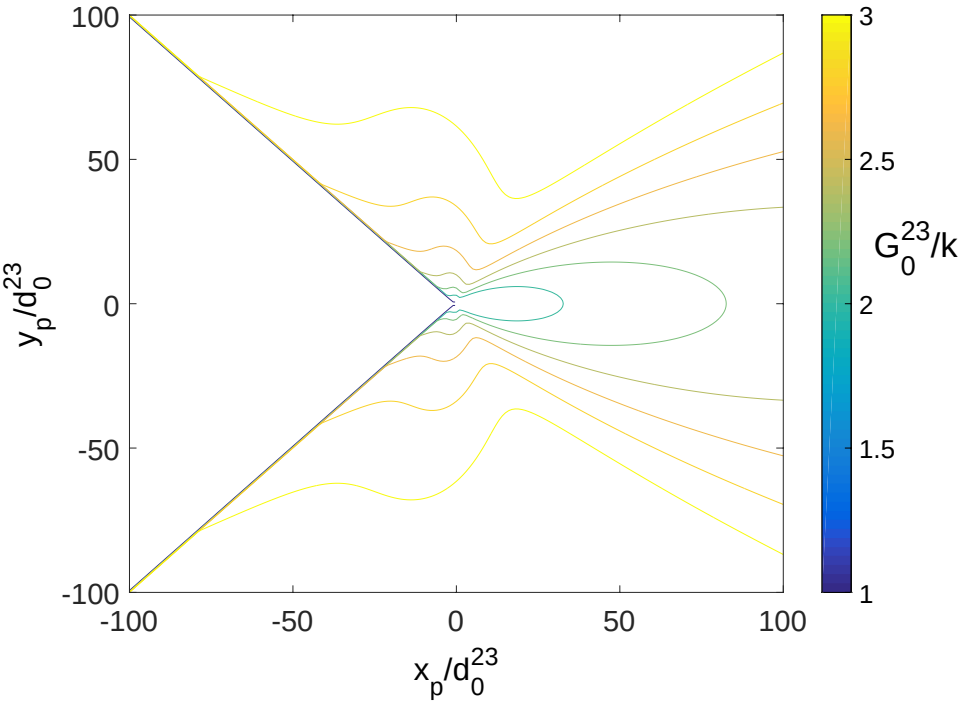
(b) Comparison of the **size** of mixed loading to pure mode loading

Figure A.7: Comparison of mode dominance

dominance for large values of G_0^{23}/k.



(a) Mode III dominance



(b) Mode II dominance

Figure A.8: Plastic radius of mixed mode loading

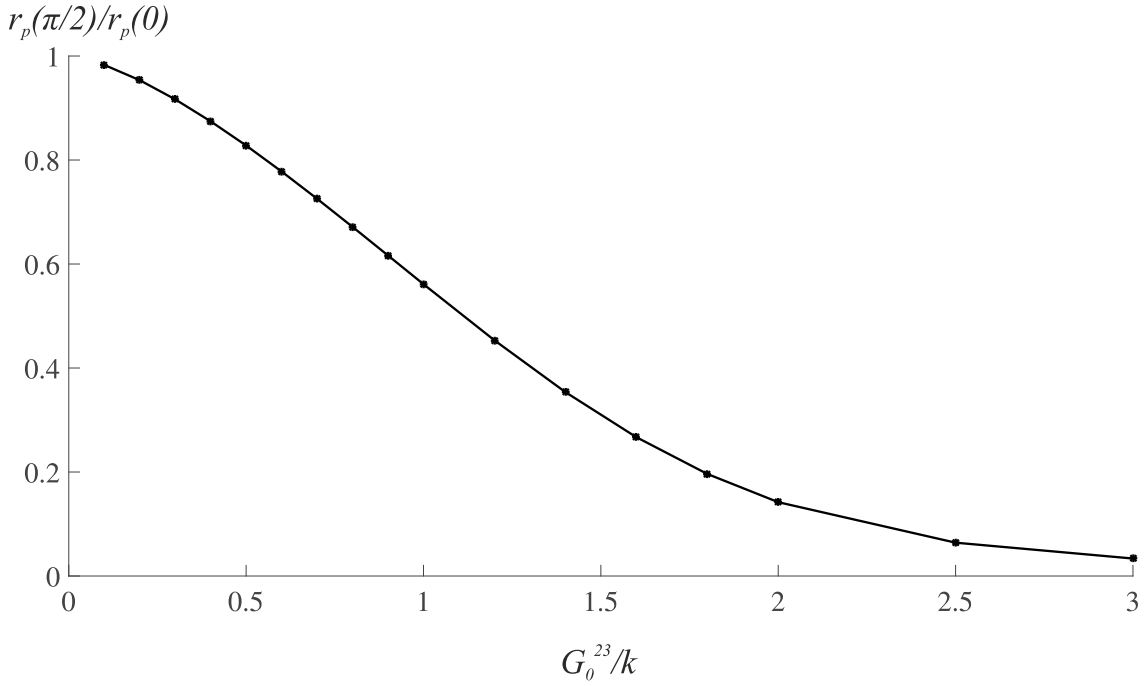


Figure A.9: Mode II and III

A.5 General loading

There is a clear underlying framework to each pair of loading cases. To understand this further, the G_0's are combined into a single variable,

$$G = G_0^{12} + G_0^{13} + G_0^{23}. \tag{A.12}$$

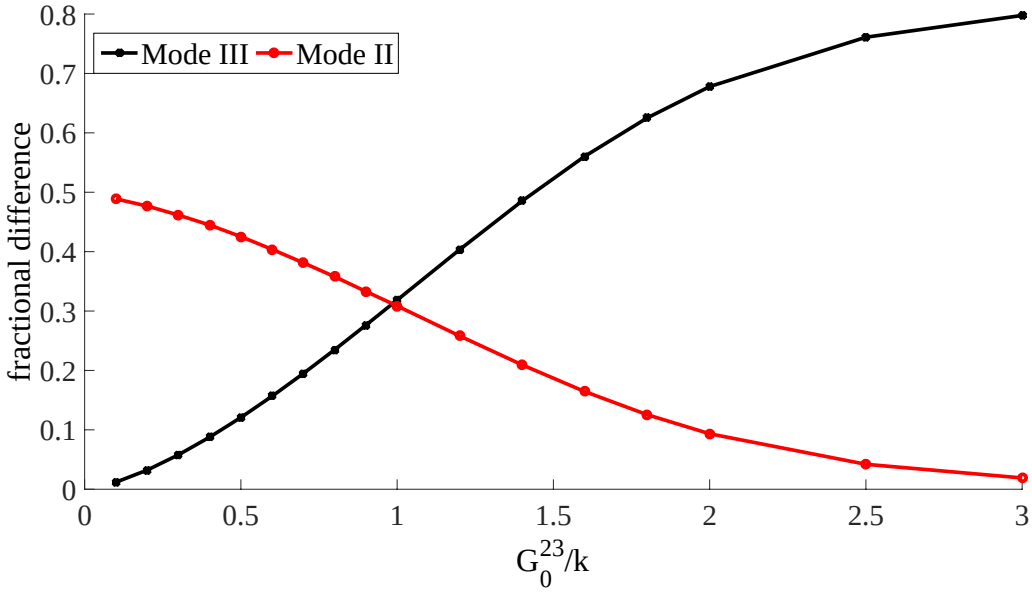
After some algebraic manipulation, this leads to the following statement of the stress state under general three modes loading,

$$\frac{\sigma_{ij}(r,\theta)}{G} = \frac{r^{\lambda_I - 1}}{a} f_{ij}^{I}(\theta) + \frac{r^{\lambda_{II} - 1}}{b} f_{ij}^{II}(\theta) + \frac{r^{\lambda_{III} - 1}}{c} f_{ij}^{III}(\theta). \tag{A.13}$$

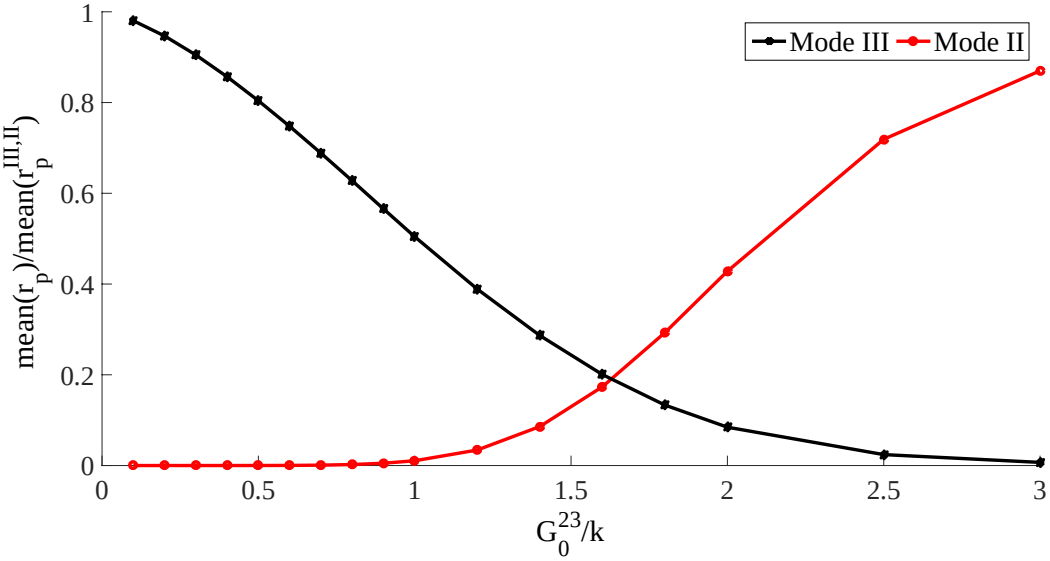
Where the intermediate variables are defined as:

$$a = (d_0^{12})^{\lambda_1 - 1} + (d_0^{13})^{\lambda_I - 1} + (d_0^{12})^{\lambda_I - \lambda_{II}} (d_0^{23})^{\lambda_{II} - 1}, \tag{A.14}$$

or,



(a) Comparison of the **shape** of mixed loading to pure mode loading



(b) Comparison of the **size** of mixed loading to pure mode loading

Figure A.10: Comparison of mode dominance

$$a = (d_0^{12})^{\lambda_1 - 1} + (d_0^{13})^{\lambda_I - 1} + (d_0^{12})^{\frac{(\lambda_I - \lambda_{II})(1-\lambda_{III})}{\lambda_{II} - \lambda_{III}}} (d_0^{13})^{\frac{(\lambda_1 - \lambda_{III})(\lambda_{II}-1)}{\lambda_{II} - \lambda_{III}}}, \tag{A.15}$$

and,

$$b = (d_0^{12})^{\lambda_{II} - 1} + (d_0^{12})^{\lambda_{II} - \lambda_1} (d_0^{23})^{\lambda_1 - 1} + (d_0^{23})^{\lambda_{II} - 1}, \tag{A.16}$$

and,

$$c = (d_0^{12})^{\lambda_I - 1}(d_0^{13})^{\lambda_{III} - \lambda_I} + (d_0^{13})^{\lambda_{III} - 1} + (d_0^{23})^{\lambda_{III} - 1}, \tag{A.17}$$

or,

$$c = (d_0^{13})^{\lambda_{III} - 1} + (d_0^{23})^{\lambda_{III} - 1} + (d_0^{23})^{\frac{(\lambda_I - 1)(\lambda_{III} - \lambda_{II})}{\lambda_I - \lambda_{II}}}(d_0^{13})^{\frac{(\lambda_{III} - \lambda_I)(1 - \lambda_{II})}{\lambda_I - \lambda_{II}}}. \tag{A.18}$$

The first form given is useful because it is easy to see that the dimensions are consistent. G has the dimension of stress and a, b and c have the dimensions of distance to the power of $\lambda_I - 1, \lambda_{II} - 1$ and $\lambda_{III} - 1$ respectively, thus making each term on the right hand side of Equation A.13 dimensionless. The second form explicitly shows the symmetry that can be seen in the equation.

This framework in its current form can be applied to physical problems but is more useful when only two modes of loading are present.

A.6 Finite example problems

The derived solutions are applied to example problems. The finite element method is used to calibrate the stress intensity factors, K_k. The calibrations of the different modes are defined as,

$$K_k = \Lambda_k \sigma_0 c^{1 - \lambda_k}, \tag{A.19}$$

where the stress along the bisector (such that $\theta = 0$) is given by,

$$\sigma_{ij}(r, 0) = K_k r^{\lambda_i - 1} f_{ij}^k(0); \quad k = I, II, III, \tag{A.20}$$

where c is the distance to the nearest feature and σ_0 is the reference stress. The eigenvectors have a value of one when $\theta = 0$ ($f_{ij}^k(0) = 1$), thus Equation A.20 is used to find K_k and substitute it into Equation A.19 to find Λ_k.

A.6.1 Notched cylinder under tension and torsion (Mode I and III)

The example problem considered is a notched cylinder (Figure A.11) of length L and diameter D, the notch is small compared to the overall dimensions of the cylinder.

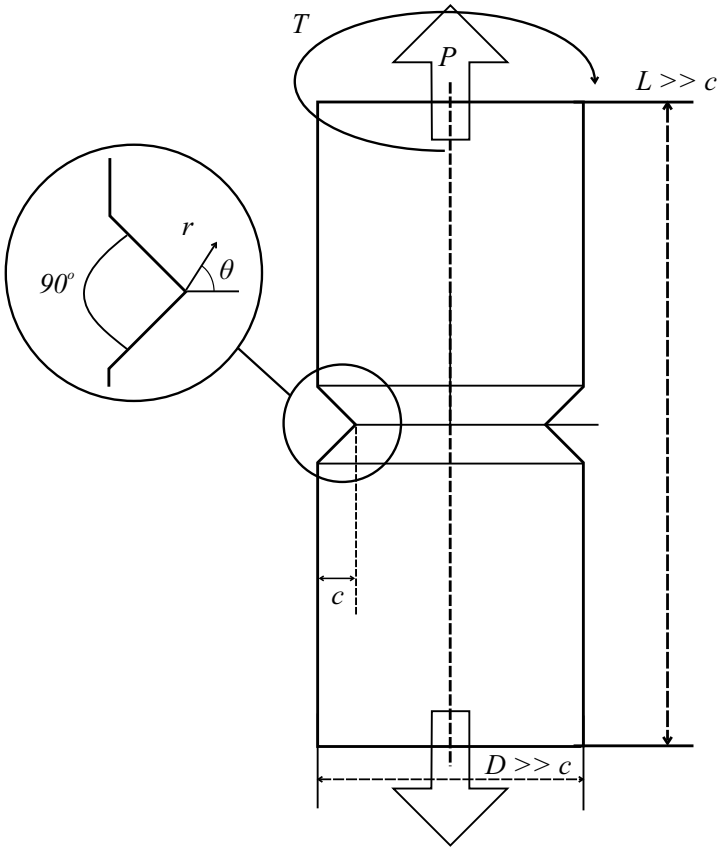


Figure A.11: Mode I and III

$$\begin{bmatrix} K_I c^{\lambda_I - 1} \\ K_{III} c^{\lambda_{III} - 1} \end{bmatrix} = \begin{bmatrix} 0.97786 & 0 \\ 0 & 1.0873 \end{bmatrix} \begin{bmatrix} \sigma_0 \\ \tau_T \end{bmatrix} \tag{A.21}$$

σ_0 is the stress due to the axial load, P, and τ_T is the shear stress induced by a torque, T, at the edge of the rod of diameter, D. Let,

$$\sigma_0 = \frac{4P}{\pi D^2}, \tag{A.22}$$

$$\tau_T = 16TD^3. \tag{A.23}$$

Using the definition of d_0^{13},

$$\frac{r}{c} = \frac{r}{d_0^{13}}\frac{1}{c}\left|\frac{K_{III}}{K_I}\right|^{\frac{1}{\lambda_I - \lambda_{III}}} = \frac{r}{d_0^{13}}\left|\frac{1.0873\tau_T}{0.97786\sigma_0}\right|^{-8.184}. \tag{A.24}$$

Therefore, the dimensionless variables σ_0/k and τ_T/k required to give a plastic radius r_p/c is,

$$\frac{r_p}{c} = 0.4196\frac{r_p}{d_0^{13}}\left[\frac{\sigma_0/k}{\tau_T/k}\right]^{8.184}. \tag{A.25}$$

It should be noted here that the exponents are very large. Small changes in the loading will produce large differences in the plastic radius. Similarly, the magnitude of loading, G_0^{13}, is given by Equation A.6. In non dimensionalised terms,

$$\frac{G_0^{13}}{k} = 1.4511\left(\frac{\tau_T}{k}\right)^{3.7275}\left(\frac{k}{\sigma_0}\right)^{2.7275}. \tag{A.26}$$

If $d_0^{13}/c > 1$ the solution cannot have mode III dominance, and, from Equation A.24 this occurs when,

$$\tau_T \leq 1.1119\sigma_0. \tag{A.27}$$

Considering Figure A.7a, the variation from the pure mode solution can be chosen. For example, if a 10% error is chosen, the corresponding values of G_0^{13}/k are found by reading off the plot at 0.1. So $G_0^{13}/k < 0.2$ implies almost true mode I and $G_0^{13}/k > 5.6$ implies almost true mode III. Figure A.12 shows the load space and the regions of single mode dominance.

For mode I and III loading, the maximum plastic radius will always lie at $\theta = \pi/2$. It is important to ensure that the plastic radius is not large enough to feel the effects of the nearest boundary, this is defined as the Small Scale Yielding (SSY) limit.

It is conservative to define SSY to be when the plastic radius, r_p, normalised by the

characteristic length of the problem c reaches 1%. When it crosses this value, the boundary will begin to affect the solution and the analysis using an infinite plane is no longer valid.

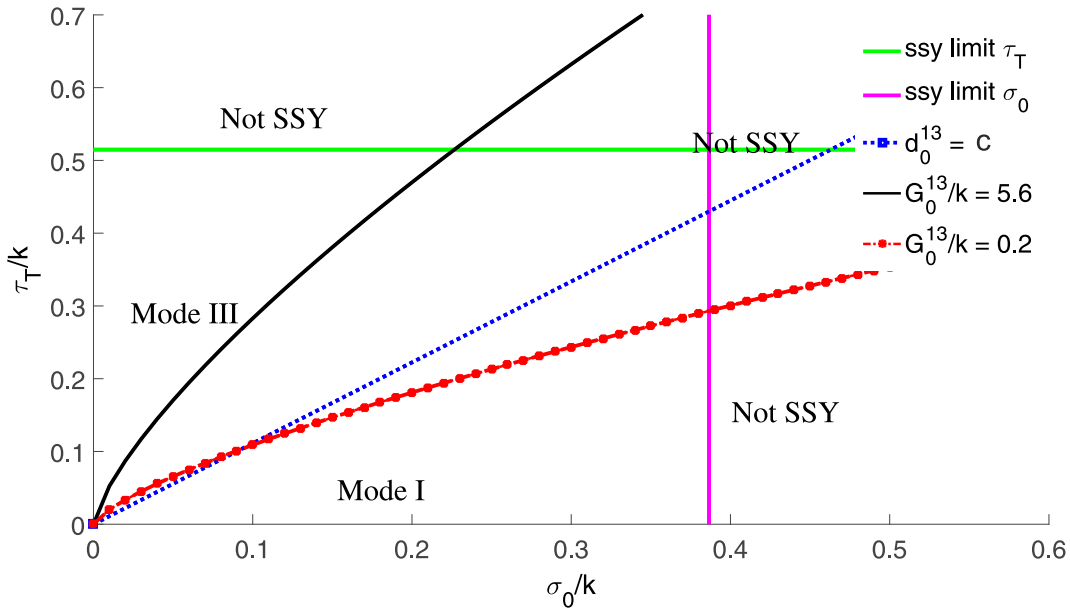
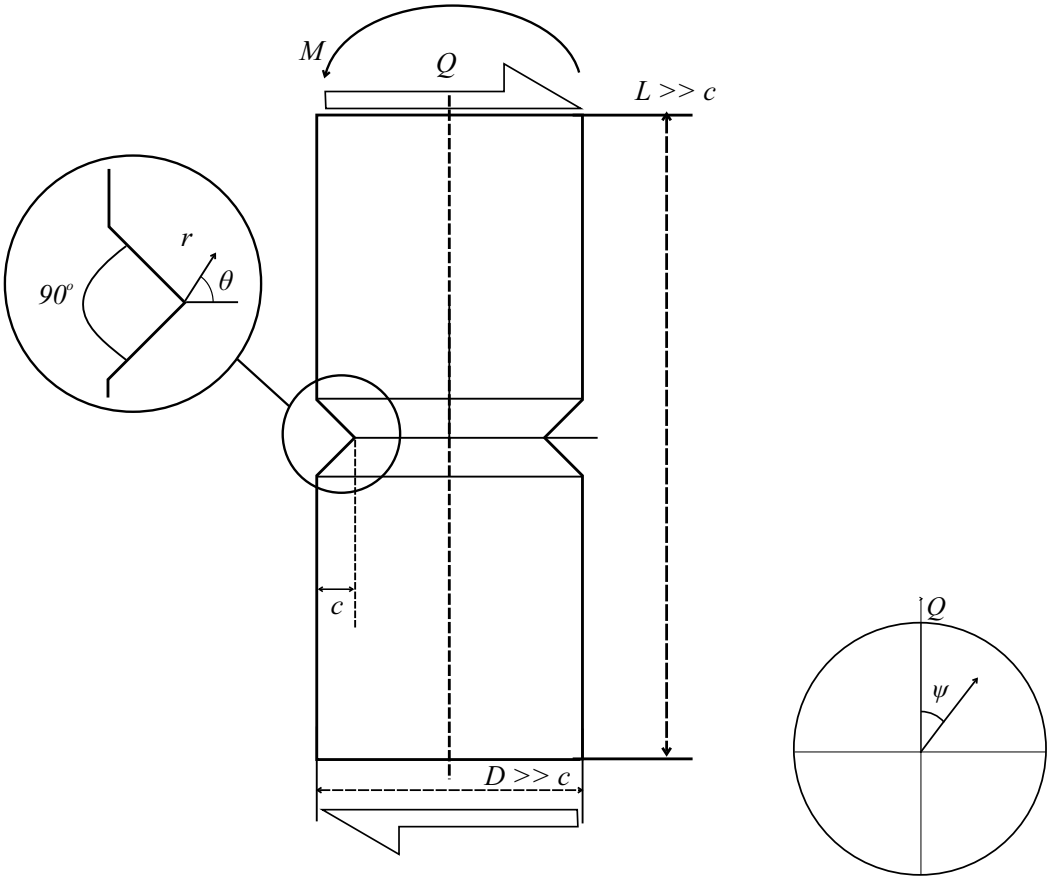


Figure A.12: Dominance of modes along with SSY limits

A.6.2 Notched cylinder under shear (Mode II and III)

To explore the mode II and III loading combination the same geometry can be used, but with a transverse shear force, as shown in Figure A.13a. To maintain overall equilibrium, a bending moment is applied such that the shear force is acting in the plane of the notch. The shear force will generate pure mode II notch loading along the diameter in the direction of shear ($\psi = 0$), and pure mode III along the diameter perpendicular to the shear direction ($\psi = \pi/2$). In all other locations, there is a mix of the two modes. The angle ψ is defined on the plane, and zero is defined to be in the direction of the shear force as shown in Figure A.13b.

The calibrations for mode II and III are calculated in the same way as for mode I and III. This leads to



(a) Mode II and III (b) Notch plane

Figure A.13: Geometry of cylinder under shear

$$\begin{bmatrix} K_{II}c^{\lambda_{II}-1} \\ K_{III}c^{\lambda_{III}-1} \end{bmatrix} = \begin{bmatrix} 0.3875cos(\psi) \\ 1.4283sin(\psi) \end{bmatrix} \tau_0 \tag{A.28}$$

where,

$$\tau_0 = \frac{Q}{\pi(D/2)^2}. \tag{A.29}$$

From Equation A.8, for this geometry, the magnitude of the loading, $G_0^{23}(\psi)$ varies around the notch in the form,

$$\frac{G_0^{23}}{\tau_0} = 2.3393cos(\psi)(cot(\psi))^{0.3782}. \tag{A.30}$$

The values of G_0^{23}/k decide the transition between mode II and III dominance. Considering the definition of d_0^{23}, it is straightforward to eliminate a region of the graph which

cannot have mode II dominance ($d_0^{23}/c > 1$),

$$d_0^{23} = \left(\frac{1.4283\tau_0 sin(\psi) c^{\lambda_{III}-1}}{0.3875\tau_0 cos(\psi) c^{\lambda_{II}-1}} \right)^{\frac{1}{\lambda_{II}-\lambda_{III}}}. \tag{A.31}$$

This can be rearranged to obtain the inequality,

$$\frac{d_0^{23}}{a} > 220.005(tan(\psi))^{4.1348}, \tag{A.32}$$

to ensure that mode II dominance cannot arise. Figure A.14 shows that at very small angles, moderate levels of load give rise to mode II dominance and heavy loads give rise to mode III dominance. The $d_0^{23} = c$ line signifies that beyond this angle, mode II dominance is not possible. In this instance, the loading and geometry will have violated SSY before this comes into effect.

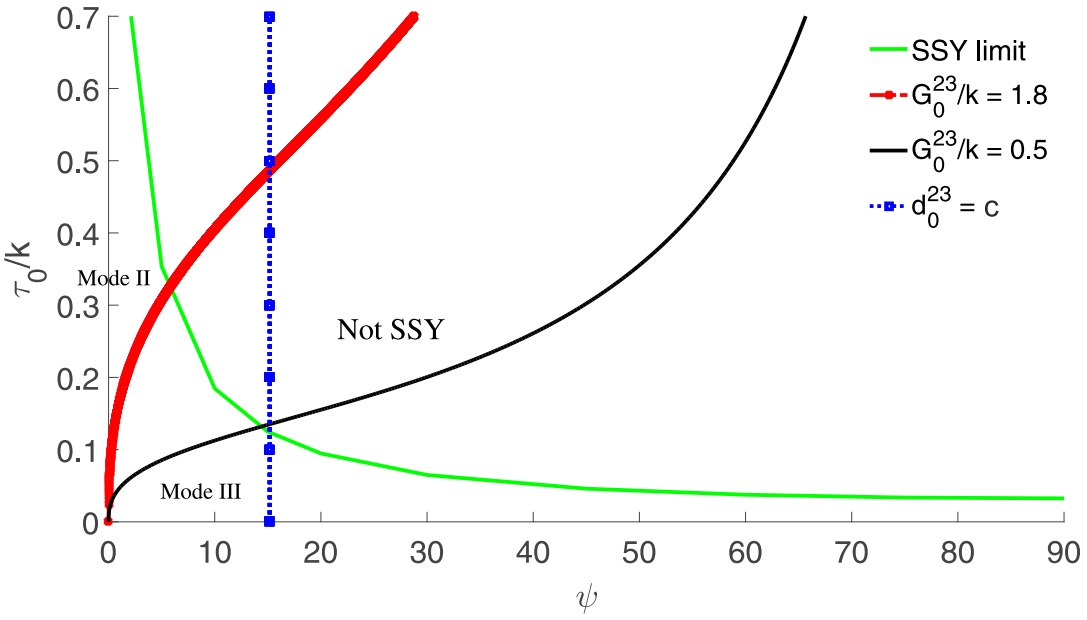


Figure A.14: Dominance of modes with SSY limits

A.7 Summary

It is shown that a new set of parameters d_0^{ij}, G_0^{ij} are more informative than the three stress intensity factors, when characterizing the state of stress near the root of a sharp notch. The d_0^{ij} parameters give information on the mode mixity. They also have units of length and serve as a partition between the two respective eigensolutions. The G_0^{ij} parameters give information on the magnitude of the loading. It has been shown under the most general loading that mode I will dominate very close to the notch root and mode II will dominate far away. The order of the d_0^{ij} values reveals if it is possible to have mode III dominance. It should be noted that there has been a transformation from three variables (K_I, K_{II}, K_{III}) to six variables. This implies that there are three equations which should connect the variables. Equation A.9 is the first and most enlightening link between the six variables. A framework is established to apply these results to a finite problem without further work and determine if they fall within the scope of small scale yielding.

B Analytical inversion of singular integral equations

This procedure is given in full in the Mechanics of Elastic contacts book by Hills et al. [58]. The equation to be solved is,

$$\frac{1}{\pi}\fint_{-a}^{a}\frac{f(s)}{s-x}ds = g(x); \quad |x| \leq a. \tag{B.1}$$

The solution is given by,

$$f(x) = -\frac{w(x)}{\pi}\fint_{-a}^{a}\frac{g(s)ds}{w(s)(s-x)} + Cw(x), \tag{B.2}$$

where the function $w(x)$ depends on the behaviour of the solution at the end points. If the solution is singular at both ends,

$$w(x) = \frac{1}{\sqrt{a^2-x^2}}. \tag{B.3}$$

On the other had, if the solution is bounded at both ends,

$$w(x) = \sqrt{a^2-x^2}. \tag{B.4}$$

It also requires that the following consistency condition is satisfied,

$$\int_{-a}^{a}\frac{g(s)}{w(s)}ds = 0. \tag{B.5}$$

Similarly, when the limits of the integral are different,

$$\frac{1}{\pi}\int\!\!\!\!\!\!-_b^a \frac{f(s)}{s-x}ds = g(x), \quad b \leq |x| \leq a. \tag{B.6}$$

The solution, when it is bounded at both ends is given by,

$$f(x) = -\frac{1}{\pi}\sqrt{(x-b)(a-x)}\int\!\!\!\!\!\!-_b^a \frac{g(s)}{\sqrt{(s-b)(a-s)}}\frac{ds}{s-x}, \tag{B.7}$$

with the associated side condition,

$$\int_b^a \frac{g(s)ds}{\sqrt{(s-b)(a-s)}} = 0. \tag{B.8}$$

C Dislocations between partially bonded half-planes

Two elastically similar half planes are bonded together over the line segment $-a \leq x \leq a$, but devoid of surface tractions outside this interval ($|x| \leq a$). Suppose that the half-planes are bonded with a relative shift between corresponding points on the surfaces of the half-planes, $u(x) = u_1(x) - u_2(x)$. The corresponding interface shearing traction present, $q(x)$ is given by,

$$\frac{du}{dx} = \frac{2}{\pi E^*} \int_{-a}^{a} \frac{q(\xi) d\xi}{\xi - x}, \tag{C.1}$$

and the inversion of this equation when the end points are fixed and (hence the singular solution), is

$$q(x) = \frac{1}{\pi\sqrt{a^2 - x^2}} \left[C + \frac{E^*}{2} \int_{-a}^{a} \frac{\sqrt{a^2 - \xi^2} u'(\xi) d\xi}{(\xi - x)} \right]; \quad |x| \leq a. \tag{C.2}$$

Suppose that the slip displacement gradient is zero everywhere except at the point $\xi = c$ where a dislocation of Burgers vector b_x is inserted, so that $u'(x) = b_x(c)\delta(x - c)$ where $\delta(\bullet)$ is Dirac's delta function, and hence,

$$q(x) = \frac{E^* b_x}{2\pi\sqrt{a^2 - x^2}} \int_{-a}^{a} \frac{\sqrt{a^2 - \xi^2}\delta(\xi - c) d\xi}{\xi - x} = \frac{E^* b_x(c)}{2\pi\sqrt{a^2 - x^2}} \frac{\sqrt{a^2 - c^2}}{c - x}; \quad |x| \leq a \tag{C.3}$$

where the rigid body term, C, has been dropped. A distribution of dislocations, $B_x(x) = \frac{db_x}{dx}$, therefore gives rise to a shear traction distribution,

$$q(x) = \frac{E^*}{2\pi\sqrt{a^2-x^2}} \int_{-a}^{a} \frac{\sqrt{a^2-\xi^2} B_x(\xi)\, d\xi}{\xi - x}; \quad |x| \leq a. \tag{C.4}$$

C.1 Bounded distribution of dislocations

A slightly different solution arises when a distribution of glide dislocations is needed which does not extend to the ends of the bonded section. The starting point is,

$$\frac{du}{dx} = \frac{2}{\pi E^*} \int_{-b}^{b} \frac{q(\xi) d\xi}{\xi - x}, \tag{C.5}$$

but now the solution for the shear traction is required where the distribution is bounded at both ends. This is appropriate when the edges of the stick zone are not pre-determined, and find,

$$q(x) = \frac{E^*\sqrt{b^2-x^2}}{2\pi} \int_{-b}^{b} \frac{u'(\xi) d\xi}{\sqrt{b^2-\xi^2}(\xi - x)} = \frac{E^*\sqrt{b^2-x^2}}{2\pi} \int_{-b}^{b} \frac{B_x(\xi) d\xi}{\sqrt{b^2-\xi^2}(\xi - x)}. \tag{C.6}$$

Where a distribution of dislocations, $B_x(x) = \frac{du}{dx}$, gives rise to a shear traction distribution along with the consistency condition, which is automatically satisfied as $u'(x)$ is an odd function.

D Side condition - bulk tension

The integral equation to be solved, rearranging Equation 2.25, and substituting the relevant equations for a Hertzian contact,

$$\frac{1}{\pi}\fint_b^a \left[\frac{\sqrt{a^2-\xi^2}B_x(\xi)}{\xi^2-x^2}\right]d\xi = \frac{sgn(x)fp_0(a^2-x^2)}{xaE^*} - \frac{\sigma}{4E^*}; \quad b \leq |x| \leq a. \tag{D.1}$$

This is not in the standard form and so the same substitutions must be made as in the pure shear problem (Equation 2.19), leading to

$$\frac{1}{\pi}\fint_e^g \left[\frac{1}{\sqrt{\eta}}\frac{\sqrt{g-\eta}B_x(\eta)}{\eta-y}\right]d\eta = \frac{2fP}{\pi E^*\sqrt{y}}\left(1-\frac{y}{g}\right) - \frac{\sigma}{4E^*}; \quad e \leq |x| \leq g. \tag{D.2}$$

Now, consider the side condition,

$$\frac{2fP}{\pi E^*}\left[\int_e^g \frac{ds}{\sqrt{s}\sqrt{(s-e)(g-s)}} - \frac{1}{g}\int_e^g \frac{\sqrt{s}ds}{\sqrt{(s-e)(g-s)}}\right] = \frac{\sigma}{4E^*}\int_e^g \frac{1}{\sqrt{(s-e)(g-s)}}ds. \tag{D.3}$$

This can be simplified (evaluating the third integral) to give,

$$\int_e^g \frac{1}{\sqrt{s}}\frac{1}{\sqrt{(s-e)(g-s)}}ds - \frac{1}{g}\int_e^g \frac{\sqrt{s}}{\sqrt{(s-e)(g-s)}}ds = \frac{\sigma\pi^2}{8fP}. \tag{D.4}$$

The first two integrals may also be evaluated to give,

$$\frac{2}{\sqrt{g}}K\left(\sqrt{1-\left(\frac{b}{a}\right)^2}\right) - \frac{2}{\sqrt{g}}E\left(\sqrt{1-\left(\frac{b}{a}\right)^2}\right) = \frac{\sigma\pi^2}{8fP}. \tag{D.5}$$

Which can be rearranged to give Equation 2.26.

E Incomplete contact problems with a constant normal load

E.1 Inversion of the integral equation

This section shows the inversion procedure for the following singular integral equation in the two slip zones,

$$q_c(x) = \frac{E^*}{2\pi\sqrt{a^2-x^2}}\left[\int_{b_1}^{a}\frac{\sqrt{a^2-\xi^2}B_x(\xi)d\xi}{\xi-x}+\int_{-a}^{-b_2}\frac{\sqrt{a^2-\xi^2}B_x(\xi)d\xi}{\xi-x}\right]; \quad x\in(-a,-b_2)\cup(b_1,a). \tag{E.1}$$

By scaling variables using the contact size,

$$x=at, \quad \xi=as, \quad B_x(as)=F(s), \quad \frac{2\sqrt{1-t^2}}{E^*}q_c(at)=Q(t). \tag{E.2}$$

EquationE.1 may be reduced to,

$$Q(t)=\frac{1}{\pi}\left[\int_{-1}^{-\beta}\frac{\sqrt{1-s^2}}{s-t}F(s)ds+\int_{\alpha}^{1}\frac{\sqrt{1-s^2}}{s-t}F(s)ds\right]; \quad t\in(-1,-\beta)\cup t(\alpha,1), \tag{E.3}$$

where $\alpha=b_1/a, \quad \beta=b_2/a$. The problem is now to invert the singular integral equation,

$$Q(t)=\frac{1}{\pi}\int_L\frac{\phi(s)}{s-t}ds, \tag{E.4}$$

where $\phi(s)=\sqrt{1-s^2}F(s)$ and L is the union of disjoint contours $(-1,-\beta)$, $(\alpha,1)$. By extending the contour L to a closed contour C, the problem can be reformulated (E.4)

as a Riemann-Hilbert problem with discontinuous coefficients for $\phi(z)$, which is analytic except on C. This may be solved using the method of Gakhov [88], which reduces the problem to one with continuous coefficients by considering functions with the appropriate local behaviour at the end points of L. There are thus different solutions depending on which behaviour for $\phi(z)$ is most physically relevant; here consider two, the solution unbounded at all ends of L and the solution bounded at all ends of L.

E.1.1 Unbounded at all ends

For a solution that is unbounded at $\pm 1, \alpha, -\beta$, the Riemann-Hilbert problem has index 2, and the appropriate inversion gives,

$$\begin{aligned}\phi(t) = \frac{1}{\pi\sqrt{(1-t^2)(t-\alpha)(t+\beta)}}\Big[\int_{-1}^{-\beta} \frac{\sqrt{(1-s^2)(s-\alpha)(s+\beta)}}{s-t} Q(s)ds \\ -\fint_{\alpha}^{1} \frac{\sqrt{(1-s^2)(s-\alpha)(s+\beta)}}{s-t} Q(s)ds + \rho(t)\Big],\end{aligned} \tag{E.5}$$

for $t \in (\alpha, 1)$, where $\rho(t)$ is an arbitrary polynomial of maximum degree 2. In general, physical constraints are used to determine $\rho(t)$. After returning to the unscaled variables, the dislocation density is given by,

$$\begin{aligned}\sqrt{1-\frac{x^2}{a^2}} B_x(x) = \frac{-1}{\pi\sqrt{\left(1-\frac{x^2}{a^2}\right)\left(\frac{(x-b_1)(x+b_2)}{a^2}\right)}}\Bigg[\fint_{b_1}^{a} \frac{\sqrt{(1-\frac{\xi^2}{a^2})(\frac{(\xi-b_1)(\xi-b_2)}{a^2})}}{\xi - x}\left(\frac{2}{E^*}\sqrt{1-\frac{\xi^2}{a^2}} q_c(\xi)\right) d\xi \\ -\int_{-a}^{-b_2} \frac{\sqrt{(1-\frac{\xi^2}{a^2})(\frac{(\xi-b_1)(\xi-b_2)}{a^2})}}{\xi - x}\left(\frac{2}{E^*}\sqrt{1-\frac{\xi^2}{a^2}} q_c(\xi)\right) d\xi + \rho(x)\Bigg],\end{aligned} \tag{E.6}$$

for $x \in (b_1, a)$. A similar expression can be found for $x \in (-a, -b_2)$, but for brevity is omitted here.

E.1.2 Bounded at all ends

In the context of this thesis, the more physically-relevant regime is that in which the function $\phi(z)$ is bounded at $\pm 1, \alpha, -\beta$. In this regime, the Riemann-Hilbert problem has

index -2 and the appropriate solution is given by,

$$\phi(t) = \frac{-\sqrt{(t-\alpha)(t+\beta)(1-t^2)}}{\pi}\Big[\fint_{\alpha}^{1} \frac{Q(s)}{\sqrt{(1-s^2)(s-\alpha)(s+\beta)}(s-t)}ds - \int_{-1}^{-\beta} \frac{Q(s)}{\sqrt{(1-s^2)(s-\alpha)(s+\beta)}(s-t)}ds\Big], \tag{E.7}$$

for $t \in (\alpha, 1)$. Therefore, returning to unscaled variables, the dislocation density for $x \in (b_1, a)$ is,

$$B_x(x) = \frac{-2}{E^*\pi}\sqrt{(x-b_1)(x+b_2)}\left[\int_{b_1}^{a} \frac{q_c(\xi)}{\sqrt{(\xi-b_1)(\xi+b_2)}}\frac{d\xi}{(\xi-x)} - \int_{-a}^{-b_2} \frac{q_c(\xi)}{\sqrt{(\xi-b_1)(\xi+b_2)}}\frac{d\xi}{(\xi-x)}\right]. \tag{E.8}$$

Similarly for $x \in (-a, -b_2)$, the dislocation density is given by,

$$B_x(x) = \frac{2}{E^*\pi}\sqrt{(x-b_1)(x+b_2)}\left[\int_{b_1}^{a} \frac{q_c(\xi)d\xi}{\sqrt{(\xi-b_1)(\xi+b_2)}(\xi-x)} - \int_{-a}^{-b_2} \frac{q_c(\xi)d\xi}{\sqrt{(\xi-b_1)(\xi+b_2)}(\xi-x)}\right]. \tag{E.9}$$

Since the index of the Riemann-Hilbert problem is negative, two consistency conditions must be enforced, which are given by,

$$\int_{-a}^{-b_2} \frac{q_c(s)s^{j-1}ds}{\sqrt{(s-b_1)(s+b_2)}} - \int_{b_1}^{a} \frac{q_c(s)s^{j-1}ds}{\sqrt{(s-b_1)(s+b_2)}} = 0, \tag{E.10}$$

for $j = 1, 2$. In general, for a given $q_c(x)$, (E.10) allows the determination of expressions for b_1 and b_2, which are discussed in further detail in Section E.2.

E.2 Integral evaluation for fully a fully stuck contact with a constant normal load

The function $q_c(x)$ is made up of three terms:

$$q_c(x) = \frac{Q}{\pi}q_c^1(x) + \frac{\sigma}{4}q_c^2(x) + q_c^3(x) = \frac{Q}{\pi\sqrt{a^2-x^2}} + \frac{\sigma x}{4\sqrt{a^2-x^2}} - fp(x), \tag{E.11}$$

where the first two terms are general and the final term is specific to the geometry being considered. The integral constraints are evaluated (E.10), by using contour integration

to evaluate each integral for q_c^i, $i = 1, 2, 3$. In order to facilitate this, the branch of the function $\sqrt{z^2 - a^2}$ that is real, positive and continuous across the real axis for $x > a$ and the branch of the function $\sqrt{(z - b_1)(z - b_2)}$ that is real, positive and continuous across the real axis for $x > b_1$ are considered. The two general parts of the consistency conditions may be calculated directly. Evaluating (E.10) considering only the first term, $q_c^1(x)$,

$$\int_{-a}^{-b_2} \frac{q_c^1(s)s^{j-1}ds}{\sqrt{(s-b_1)(s+b_2)}} - \int_{b_1}^{a} \frac{q_c^1(s)s^{j-1}ds}{\sqrt{(s-b_1)(s+b_2)}} = \begin{cases} 0 & \text{for} \quad j = 1, \\ -\pi & \text{for} \quad j = 2. \end{cases} \tag{E.12}$$

Similarly, evaluating (E.10) considering only the second term, $q_c^2(x)$,

$$\int_{-a}^{-b_2} \frac{q_c^2(s)s^{j-1}ds}{\sqrt{(s-b_1)(s+b_2)}} - \int_{b_1}^{a} \frac{q_c^2(s)s^{j-1}ds}{\sqrt{(s-b_1)(s+b_2)}} = \begin{cases} -\pi & \text{for} \quad j = 1, \\ -\dfrac{(b_1 - b_2)\pi}{2} & \text{for} \quad j = 2. \end{cases} \tag{E.13}$$

E.2.1 Side condition for a Hertzian contact

Finally, the geometry-specific part of the consistency conditions (E.10) for the particular example of a Hertzian contact is considered. For a Hertzian contact, it is known that,

$$q_c^3(x) = -fp(x) = -p_0\sqrt{1 - \left(\frac{x}{a}\right)^2}. \tag{E.14}$$

Thus, an integral of the form needs to be evaluated,

$$I = \int_{-a}^{-b_2} \frac{s^{j-1}\sqrt{a^2 - s^2}ds}{\sqrt{(s-b_1)(s+b_2)}} - \int_{b_1}^{a} \frac{s^{j-1}\sqrt{a^2 - s^2}ds}{\sqrt{(s-b_1)(s+b_2)}}, \tag{E.15}$$

This integral can be evaluated using contour integration, giving

$$I = \begin{cases} \dfrac{(b_1 - b_2)\pi}{2} & \text{for} \quad j = 1, \\ \left(\dfrac{3}{8}(b_2^2 + b_1^2) - \dfrac{b_1 b_2}{4} - \dfrac{a^2}{2}\right)\pi & \text{for} \quad j = 2. \end{cases} \tag{E.16}$$

F Elliptic integrals

The complete elliptic integral of the first kind is defined as,

$$K(k) = \int_0^1 \frac{dt}{\sqrt{(1-t^2)(1-k^2t^2)}}. \tag{F.1}$$

The complete elliptic integral of the second kind is defined as,

$$E(k) = \int_0^1 \frac{\sqrt{1-k^2t^2}}{\sqrt{1-t^2}} dt. \tag{F.2}$$

The complete elliptic integral of the third kind is defined as,

$$\Pi(n,k) = \int_0^{\frac{\pi}{2}} \frac{d\theta}{(1-nsin^2\theta)\sqrt{1-k^2sin^2\theta}}. \tag{F.3}$$

The derivatives of the integrals are given by,

$$\frac{d}{dk}K(k) = \frac{E(k)}{k(1-k^2)} - \frac{K(k)}{k}, \tag{F.4}$$

$$\frac{d}{dk}E(k) = \frac{E(k)-K(k)}{k}. \tag{F.5}$$

G Williams' eigenvectors & mode III

The mode I eigenvectors are,

$$f^{I}_{\theta\theta}(r,\theta) = \frac{cos[(\lambda_I - 1)\alpha]cos[(\lambda_I + 1)\theta] - cos[(\lambda_I + 1)\alpha]cos[(\lambda_I - 1)\theta]}{cos[(\lambda_I - 1)\alpha] - cos[(\lambda_I + 1)\alpha]}, \tag{G.1}$$

$$f^{I}_{r\theta}(r,\theta) = \frac{sin[(\lambda_I - 1)\alpha]sin[(\lambda_I + 1)\theta] - sin[(\lambda_I + 1)\alpha]sin[(\lambda_I - 1)\theta]}{sin[(\lambda_I - 1)\alpha] - \frac{(\lambda_I+1)}{(\lambda_I-1)}sin[(\lambda_I + 1)\alpha]}. \tag{G.2}$$

The mode II eigenvectors are,

$$f^{II}_{\theta\theta}(r,\theta) = \frac{sin[(\lambda_{II} - 1)\alpha]sin[(\lambda_{II} + 1)\theta] - sin[(\lambda_{II} + 1)\alpha]sin[(\lambda_{II} - 1)\theta]}{-sin[(\lambda_{II} - 1)\alpha] + \frac{(\lambda_{II}-1)}{(\lambda_{II}+1)}sin[(\lambda_{II} + 1)\alpha]}, \tag{G.3}$$

$$f^{II}_{r\theta}(r,\theta) = \frac{cos[(\lambda_{II} - 1)\alpha]cos[(\lambda_{II} + 1)\theta] - cos[(\lambda_{II} + 1)\alpha]cos[(\lambda_{II} - 1)\theta]}{cos[(\lambda_{II} - 1)\alpha] - cos[(\lambda_{II} + 1)\alpha]}. \tag{G.4}$$

The mode III eigenvectors are,

$$f^{III}_{rz} = -sin(\lambda_{III}\theta), \tag{G.5}$$

$$f^{III}_{z\theta} = cos(\lambda_{III}\theta). \tag{G.6}$$